

Winter 2011

Digital image correlation as a tool for bridge load rating and long-term evaluation

Jason Thomas Peddle

University of New Hampshire, Durham

Follow this and additional works at: <https://scholars.unh.edu/thesis>

Recommended Citation

Peddle, Jason Thomas, "Digital image correlation as a tool for bridge load rating and long-term evaluation" (2011). *Master's Theses and Capstones*. 691.

<https://scholars.unh.edu/thesis/691>

This Thesis is brought to you for free and open access by the Student Scholarship at University of New Hampshire Scholars' Repository. It has been accepted for inclusion in Master's Theses and Capstones by an authorized administrator of University of New Hampshire Scholars' Repository. For more information, please contact nicole.hentz@unh.edu.

**DIGITAL IMAGE CORRELATION AS A TOOL FOR BRIDGE LOAD RATING AND
LONG-TERM EVALUATION**

BY

JASON THOMAS PEDDLE

B.S., University of New Hampshire, 2010

THESIS

Submitted to the University of New Hampshire
in Partial Fulfillment of
the Requirements for the Degree of

Master of Science

In

Civil Engineering

December, 2011

UMI Number: 1507830

All rights reserved

INFORMATION TO ALL USERS

The quality of this reproduction is dependent upon the quality of the copy submitted.

In the unlikely event that the author did not send a complete manuscript and there are missing pages, these will be noted. Also, if material had to be removed, a note will indicate the deletion.



UMI 1507830

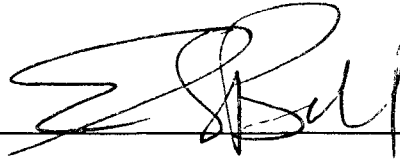
Copyright 2012 by ProQuest LLC.

All rights reserved. This edition of the work is protected against unauthorized copying under Title 17, United States Code.

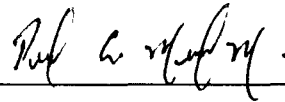


ProQuest LLC
789 East Eisenhower Parkway
P.O. Box 1346
Ann Arbor, MI 48106-1346

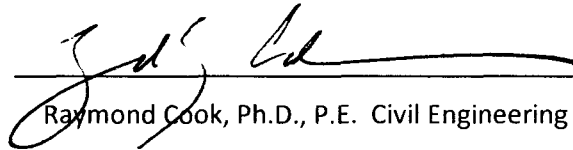
This thesis has been examined and approved.



Thesis Director, Erin Bell, Ph.D., P.E. Civil Engineering



Ricardo Medina, Ph.D., P.E. Civil Engineering



Raymond Cook, Ph.D., P.E. Civil Engineering

12/9/2014

Date

ACKNOWLEDGEMENTS

Funding for this research was provided by the National Science Foundation (NSF) CAREER grant #0644683, “Integrating Structural Health Monitoring, Intelligent Transportation Systems, and Model Updating into a Bridge Condition Assessment”, Major Research Instrumentation (MRI) grant #0821517, “Acquisition of a Digital Image Correlation System to Advance Research, Training, and Education in Engineering”, and Partnership for Innovation (PFI) grant #0650258. This research would not have been possible without support for the National Science Foundation and I am thankful.

I would like to thank all members of the Vernon Avenue Bridge research team, including those from the University of New Hampshire, Tufts University, Fay, Spoffard & Thorndike, and GeoComp Corporation. I’d like to thank Paul Lefebvre and Phillip Brogan for helping me jumpstart my research, Adam Goudreau and Emily Carlson for assisting with digital image correlation testing, and Noah Chinburg, Timothy Foy, Antonio Javier Garcia Palencia, David Gaylord, and Eric Picard for providing assistance any time I may have needed some. Finally, I’d like to thank Dr. Erin Santini-Bell for providing a wealth of guidance and motivation when it was needed most.

In addition to the research team, I’d like to thank my parents and grandparents for all the encouragement and confidence they’ve given me. Finally, I’d like to thank my fiancée Caroline for all of her support and patience while I achieved my goals.

TABLE OF CONTENTS

List of Tables	vii
List of Figures	viii
Abstract	xi
Introduction.....	1
Literature Survey & State of the Art.....	5
2.1 Visual Inspections	5
2.2 Nondestructive Testing.....	7
2.3 Load Rating.....	13
Laboratory & Field Verification of Digital Image Correlation	16
3.1 Laboratory Verification.....	18
3.2 Field Verification.....	23
3.2.1 Vernon Avenue Bridge Verification Experiment	24
3.2.2 Gilford Bridge Verification Experiment	27
3.3 Experimental Techniques Used in DIC Testing.....	30
3.4 Summary	33
Case Study: Vernon Avenue Bridge.....	35
4.1 History.....	36
4.2 Detailed Bridge Description	36
4.3 Instrumentation.....	40

4.4	September 2011 Load Test	42
4.5.1	Model Creation	49
4.5.2	Material Properties and Frame Sections	49
4.5.3	Deck Sections	50
4.5.4	Boundary Conditions	51
4.5.5	Bridge Object Definitions	52
4.5.6	Parametric Variations	52
4.5.7	Diaphragms	53
4.5.8	Update Linked Model	54
4.5.9	Remarks	55
	Integration of Load Test Data with Model	56
5.1	Digital Image Correlation Displacement Results	56
5.2	Model Assessment	59
5.3	Discussion of Model Accuracy	64
	Load Rating of the Vernon Avenue Bridge	67
6.1	Distribution Factor	71
6.2	Load and Resistance Factor Rating	72
6.3	Load Factor Rating	73
6.4	Allowable Stress Rating	74
6.5	Load and Resistance Factor Rating with Structural Model	74
6.6	Load and Resistance Factor Rating with Experimental Distribution Factor	78

6.7 Summary of Rating Factors	80
Conclusions & Future Work	83
7.1 Recommendations for Future Work.....	85
References	87
Appendix A: 2011 VAB Load Test Data	90
Appendix B: Screenshots of Structural Model	106
Appendix C: Calculation of Rating Factors.....	122
C.1 Rating Factors Due to Negative Moment	122
C.2 Rating Factors Due to Positive Moment.....	130

LIST OF TABLES

Table 1 - Hardware And Software Used In This Research	17
Table 2 - Material Properties Entered For Deck Concrete	50
Table 3 – Comparison Of Maximum Negative Displacements On Center Span	60
Table 4 - Comparison Of Maximum Positive Displacements On The Center Span	61
Table 5 – Comparison Of Maximum Negative Displacements On The South Span	61
Table 6 - Comparison Of Maximum Positive Displacements On The South Span	61
Table 7 - Equations And Factors Of The Three Different Load Rating Methodologies	69
Table 8 - Factor Definitions	69
Table 9 – Maximum Positive Moments Due To Live Load And Dead Load From The Structural Model	77
Table 10 – Maximum Negative Moments Due To Live Load And Dead Load From The Structural Model	78
Table 11 - A Summary Of All Interior Beam Rating Factors	80
Table 12 - A Summary Of All Exterior Beam Rating Factors	81

LIST OF FIGURES

Figure 1 - From the Top Left, Clockwise, a Strain Gauge, LVDTs, a Tilt-Meter, and Dye Penetrant	8
Figure 2 - Post Processing Software Tracks The Movement Of Subsets Throughout The Series Of Images (http //www correlatedsolutions com)	11
Figure 3 - LVDTs Were Used During Verification Testing To Ensure The Accuracy Of DIC Measurements	18
Figure 4 - LVDTs Used For Verification Were Calibrated With This Device	18
Figure 5 - Calibration Cards Are Rotated In Front Of The Cameras For Three-Dimensional Analysis	19
Figure 6 - Precision Problems With Three-Dimensional Analysis Can Be Seen In This Graph	20
Figure 7 - A Laboratory Test Measuring Displacement Of A Wide Flange Beam	20
Figure 8 - Comparison Of Vertical Deflection Measurements By DIC And LVDT	21
Figure 9 - A SDOF System On A Shake Table	22
Figure 10 – Dynamic Test Results With A Base Amplitude Of 1-Inch At A Frequency Of 1 Hz	22
Figure 11 – The Newly Constructed Vernon Avenue Bridge	23
Figure 12 – Installation Of LVDT Equipment Underneath The Bridge In Gilford, NH, Post-Renovation	24
Figure 13 - The Setup At The VAB In 2009 Cameras Were Focused On A Point On The Exterior Beam In The South Span	25
Figure 14 – Stop Test Results At Vernon Avenue Bridge Measurements Are Taken At The South Span	27
Figure 15 - View Of The Top Of The Bridge And Load Truck In Gilford, New Hampshire	28
Figure 16 - Gilford Bridge Load Test Layout Plan	29
Figure 17 - Data From A Test At The Bridge In Gilford, NH The DIC Data Is Visibly Noisier Than The LVDT Data At Small Scale Displacements	29
Figure 18 - A Typical Speckle Pattern Created With Chalk On The Web Of A Beam At The VAB	31

Figure 19 - A Rigid Pvc Pipe Attached To The Bottom Flange Of A Girder The Speckle Pattern Translates Vertically With The Beam	32
Figure 20 - A Cut Of Sheet Metal With A Speckle Pattern (Tab) Attached To The Bottom Flange Of A Beam	32
Figure 21 - An Aerial View Of The Vernon Avenue Bridge And Nearby Recycling And Landfill Facilities	35
Figure 22 - Steel Plates Covered The Old Bridge Deck At The Time Of Closure	36
Figure 23 - Deck Cross Section Of The VAB	38
Figure 24 - Plan And Elevation Views Of The Vernon Avenue Bridge	38
Figure 25 - Typical Deck Sections On The VAB	39
Figure 26 - Framing Plan Of The Vernon Avenue Bridge	39
Figure 27 - Bearing Pad Detail (D S Brown)	40
Figure 28 – VAB Instrumentation Plan	41
Figure 29 - The Load Truck Used At The 2011 VAB Bridge Test	43
Figure 30 - Diagram Of The Truck Paths During The 2011 VAB Load Test	44
Figure 31 - Locations Of DIC Measurements During The 2011 VAB Load Test	45
Figure 32 - A View Of The Targets Located At Each POI At The 2011 VAB Load Test	46
Figure 33 - One Of The DIC Cameras At The 2011 VAB Load Test, Capturing Displacements At Station 1	47
Figure 34 - One Of The DIC Cameras At The 2011 VAB Load Test, Capturing Displacements At Stations 8 & 11	47
Figure 35 - Stiffness Values Used For Specification Of The Bearing Pads	51
Figure 36 - An Elevation View Of The Structural Model	52
Figure 37 - Outriggers Cause A Deck Variation In Span 3	53
Figure 38 - The Updated Linked Model	54
Figure 39 - The Updated Linked Model In An Extruded View	55
Figure 40 - Transverse Displacement Measurements Were Taken At 2 Locations Along The Bridge, Indicated By Boxes	57

Figure 41 - Displacements On All 6 Girders At The Midpoint Of Span 2	57
Figure 42 - Displacements On All 6 Girders At The Midpoint Of Span 1	58
Figure 43 - Lane X2 Was Defined In CsiBridge	60
Figure 44 - Displacement Results From Dic And CsiBridge At The Midspan Of Beam 3	62
Figure 45 - Displacement Results From Dic And CsiBridge At The Midspan Of Beam 1	62
Figure 46 - Histogram And Outlier Box Plot Of Error Units Are In Mm	63
Figure 47 - An Ineffective Speckle Pattern (South Span Of Girder 6)	65
Figure 48 - An Effective Speckle Pattern (South Span Of Girder 4)	65
Figure 49 – Flow Chart Of Load Rating Decisions	68
Figure 50 - The HS-20 Design Truck	70
Figure 51 - The Lever Rule As Applied To The VAB	72
Figure 52 - The Three Lanes Can Be Seen In Different Shades	76
Figure 53 - A Screenshot Of The EDM's Enveloped Maximum Deflected Shape Due To Live Load	77
Figure 54 – The Transverse Distribution Of Displacement And Strain During Due To The Truck Travelling Over Beam 3	79
Figure 55 - A Spreadsheet Was Created That Normalized Displacement And Strain Values	79

ABSTRACT

DIGITAL IMAGE CORRELATION AS A TOOL FOR BRIDGE LOAD RATING AND LONG-TERM EVALUATION

by

Jason Thomas Peddle

University of New Hampshire, December 2011

Over 600,000 bridges are currently in service in the United States; one in three is considered either functionally obsolete or structurally deficient. The Federal Highway Administration defines structurally deficient bridge as one with a condition rating less than four on a scale from zero to nine. If a bridge is considered structurally deficient a load rating is determined. A load rating factor indicates the quantity of design live load that can be safely applied to the bridge. Rating factors are often the result of visual inspections and an analytical protocol that accounts for the effects that dead and live loads have on individual structural elements. To more accurately measure these effects there is a need for an easily deployable and objective measurement of bridge performance and condition. Digital image correlation has the potential to be a cost effective technique for collecting displacement measurements at an in-service bridge structure.

This thesis develops rating factors for a recently constructed 3-span steel girder bridge using five different methods. Methods include load and resistance factor rating, load factor rating, allowable stress rating, a rating based on a structural model created in CSiBridge®, and a rating based on experimental displacement results using digital image correlation. The resulting load rating factors are compared and discussed.

CHAPTER 1

INTRODUCTION

1.1 State of the Infrastructure

The United States is home to more than 600,000 bridges, 69,000 of which are classified as structurally deficient (Transportation for America, 2011). The average bridge is approximately 45 years old, a figure that is creeping closer to the typical bridge design life goal of 75 years (American Society of Civil Engineers, 2011). According to the American Society of Civil Engineers' 2011 Report Card for America's Infrastructure, the nation's bridge infrastructure as a whole drew a grade of "C," which is categorized as a fair condition. Bridges located in the state of New Hampshire also received a "C" (American Society of Civil Engineers New Hampshire Section, 2011). To address the nation's bridge infrastructure problem, the Long Term Bridge Performance (LTBP) program was developed in 2005. This research initiative aimed to provide \$100 million to fund research in structural health monitoring and bridge inspection (Federal Highway Administration, 2011).

1.2 Structural Health Monitoring

Structural health monitoring (SHM) can be defined as a system that utilizes one or many types of sensors and/or instruments to capture real-time measurements on a structure or structural element. Data gathered from a SHM system can be used to capture bridge behavior and then to make decisions based on the comparison between predicted and observed behavior. Bridges are increasingly being instrumented with traditional SHM sensors that can objectively assess structural performance and lead to more efficient asset allocation. The implementation of SHM into today's structures is

intended not only to aid in the prevention of catastrophes like the collapse of, the bridge in Minnesota on August 1, 2007, I-35W, but also to take bridge management a step further by deploying instruments that report information such as traffic volume, seismic data, and other statistics that will prove invaluable for total asset management. For example, municipalities can use temperature gauges in bridge decks to decide whether the bridge should be salted during a winter storm, potentially resulting in a savings of tax payer dollars.

An example of SHM being used successfully in bridges can be seen in the new St. Anthony Falls Bridge in Minneapolis, which replaced the I-35 Bridge that collapsed in 2007 (Hamm, 2009). Engineers installed a total of 323 sensors on the bridge including strain gauges, thermistors, potentiometers, and accelerometers. In addition to the SHM sensors, a traffic monitoring system was installed to help inform travelers of delays and accidents. The SHM system on the new Minnesota Bridge came at a cost that was less than 1% of the total bridge cost. Implementation of SHM at such an early stage in design is part of the reason that costs were kept low. Similarly, the Vernon Avenue Bridge, the focus of this research, was instrumented during construction.

It should be noted that SHM is not an entirely new idea. The structural health of bridges has been monitored since the inception of bridge inspections and load ratings. A news article written in 1908, published in the Uxbridge Compendium, describes an analog device that measured bridge deflection that was used to measure the health of the structure (Anon., 1908). Advancements in SHM have certainly occurred since this article was published but the end goal has not changed. Deflection is still being measured as a metric for bridge health, but the data is collected using computers instead of graph paper.

SHM systems are used to augment the primary means of collecting information related to bridge condition: visual inspection. During typical bridge inspection, engineers who are typically contracted by the bridge owner, visually assess and categorize the deck, superstructure, and substructure of the bridge by numerical condition ratings. Section loss and deterioration are visually noted and collectively decrease the available strength of the bridge, and a load rating is developed if deemed necessary. Bridges are normally scheduled to be inspected at intervals not to exceed 24 months or as special circumstances arise (AASHTO, 2011). Among the disadvantages in the bridge inspection process are the discrete nature of collection, the possible subjectivity of the inspector, the enveloped elemental load rating, and the reliability of the nondestructive evaluation (NDE) technique used for hands on inspection (National Cooperative Highway Research Program, 1998).

In addition to visual inspections, there are also numerous instruments that are traditionally used for bridge performance testing. SHM systems include, but are not limited to, linear variable differential transformers (LVDT), string-wire potentiometers (SWP), accelerometers, strain gauges, and temperature sensors, all of which are used to collect performance information during non-destructive tests (NDT). Non-destructive testing can be considered any testing that does not adversely affect the structure (ASNT, 2011). This type of load testing is advantageous because it provides objective performance data but in some situations installation of sensors and data acquisition equipment can be costly and time consuming. The situation is further complicated if the bridge spans a river or active roadway making access to the underside difficult. Another classification of nondestructive instruments is termed non-contact. A non-contact instrument is one that does not have to be in contact with the specimen to collect data about its behavior. Digital image correlation (DIC) is a nondestructive, non-contact

method that will be discussed extensively in this thesis. DIC can be used to capture two or three dimensional displacements, which can be converted into strain and accelerations through post processing.

All types of structural health monitoring can be taken one step further by combining collected data with a structural model created using finite element software. A structural model can augment a SHM system by providing a basis for comparison and interpretation of the system response. Data collected from health monitoring can be used to update a structure's finite element model (FEM). After creating a baseline FEM, a model that represents a structure's behavior the day that construction is finished for instance, data from load tests can be used to update structural parameters such as stiffness, area, or moment of inertia (Santini Bell, et al., 2007). Updating these parameters to match performance testing allows the model to represent the true state of the structure and allow for more accurate load ratings. Because of its non-intrusive nature, DIC may prove to offer a cost effective alternative to traditional instruments in the field of performance based testing.

Major contributions of this thesis expand on four aspects of bridge evaluation: the capabilities of digital image correlation will be highlighted and shown to be a cost-effective tool for measuring deflections on an in-service bridge, an experimental distribution factor for use in load rating will be developed based on displacement data, the creation of a finite element model of the Vernon Avenue Bridge will be outlined and used for load rating, and load rating factors based on displacements and models will be compared to factors calculated using traditional methods.

CHAPTER 2

LITERATURE SURVEY & STATE OF THE ART

It is a goal of Federal Highway Administration's (FHWA) Long Term Bridge Performance Program (LTBPP) to develop "Improved inspection/condition information through non-destructive evaluation and structural health monitoring" (U.S. Department of Transportation, 2011). Standard bridge evaluation and condition rating of in-service bridges is currently accomplished by visual inspection supplemented by nondestructive testing. Although visual inspection is the industry standard, studies have shown that bridge condition assessments may vary widely between inspectors (Graybeal, et al., 2002). Nondestructive testing, such as ground penetrating radar or dye penetrant, does provide a more objective measure of bridge element condition, but still requires a certain degree of user judgment. Digital image correlation as a nondestructive evaluation tool is able to provide displacement data, as a bridge system response that is completely objective. DIC can be used in conjunction with visual inspections to gain a holistic understanding of the structure and derive an accurate bridge load rating. The bridge load rating factor is a numerical measure of a bridge's overall health. Currently, load ratings are primarily based on field observations but this thesis will present new techniques to integrate load test data for a more accurate load rating factor built on state of the art research.

2.1 Visual Inspections

Bridge inspection practices were first established in 1968 according to the National Bridge Inspection Practices (NBIP) which were created by the Federal Highway Administration (FHWA). The creation of the NBIP was in large part a response to the 1967 collapse of the Silver Bridge, which carried U.S. 35 between Point Pleasant, West

Virginia and Gallipolis, Ohio (FHWA, 2011). In 1971 the FHWA created the National Bridge Inspection Standard (NBIS), which forced bridge owners to comply with inventory requirements for all bridges on the federal-aid system, maintain minimum data collection requirements, adhere to minimum inspection training and qualifications, and periodically develop load ratings. The NBIS Bridge inspection legislation has since been periodically amended and many different inspection manuals have been published.

Visual inspections are carried out by bridge inspectors, individuals who are trained in bridge safety, but are not necessarily engineers. Individual requirements for bridge inspector certification vary state to state. In most states inspectors are not required to be professional engineers but have typically achieved NBIS certification. Bridge inspection team leaders must hold a professional engineer's license in the state of the inspection (AASHTO, 2011). Inspectors use a myriad of tools to assess the condition of structural elements including cleaning tools, visual aids, basic measuring equipment, safety equipment, and recording materials (AASHTO, 2011). Section loss on steel members, cracking and spalling of concrete, and condition of bridge bearings are all observations that are made during a routine bridge inspection. While measurements are objective values, whether an inspector sees the deterioration to take the measurement is not certain.

In a study conducted in 2001, a group of 49 practicing bridge inspectors from 25 departments of transportation were brought to a bridge and asked to conduct identical inspections, individually and in teams (Graybeal, et al., 2002). What the researchers found was that 68% of condition ratings were within 1 rating point of the average on a scale from 0 to 9. It was also observed that teams of inspectors were unable to accurately map delaminated areas of a reinforced concrete deck. This study was particularly alarming because load ratings are formulated from visual inspections. The

results of this study prompted many state to establish or re-vamp the visual inspection training program and required skills.

Load rating factors, calculated based on inherently subjective field observations during visual inspections, take into account steel section loss, spalling of concrete, and any other damage that is visually apparent, thus reinforcing the need for more objective inspection procedures. Nondestructive testing offers a more objective look into bridge health and is becoming increasingly popular as the technology and analytical tools for data assessment become more affordable.

2.2 Nondestructive Testing

Advancements and increased affordability in emerging technology in recent years has led to the use of nondestructive testing instruments during routine inspections. A nondestructive testing instrument is one that collects data about a material or element without causing damage to it. Some common nondestructive instruments include, but are not limited to, the following:

- Ground penetrating radar (GPR)
- Dye penetrant inspection (DP) (Figure 1)
- Cross-hole sonic logging (CSL)
- X-ray
- Infrared Imaging (IR)
- Strain gauge (Figure 1)
- Linear variable differential transducer (LVDT) (Figure 1)
- Digital image correlation (DIC)
- Accelerometer
- Tilt-meter (Figure 1)

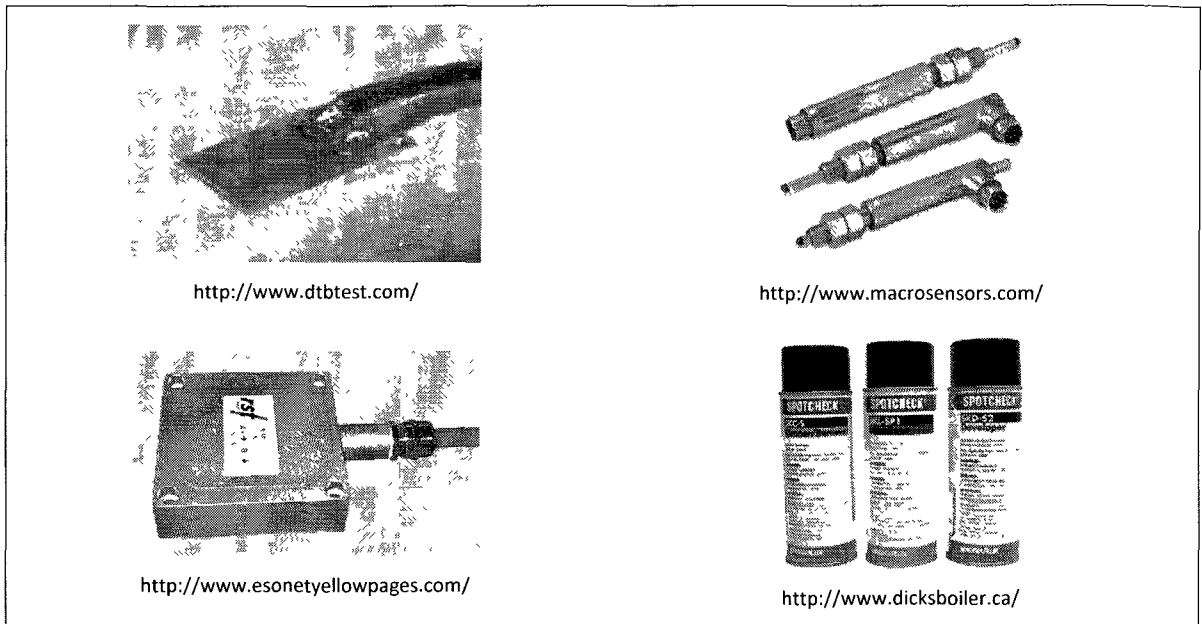


Figure 1 - From the top left, clockwise, a strain gauge, LVDTs, a tilt-meter, and dye penetrant.

GPR, DP, CSL, X-ray, and IR technologies are used in conjunction with visual inspections. Strain gauges, LVDTs, accelerometers, tilt-meters, and DIC measure bridge responses due to loading and are therefore used during load tests, which may or may not include a visual inspection. Bridge load tests use trucks of known weight to induce a bridge response that is measured by instruments. Simultaneous load testing and visual inspection has the potential to offer a better understanding of a bridge's overall structural health.

As an enhancement to traditional inspection methods, researchers have used data from load tests to produce a more accurate rating factor (Chajes, et al., 1997). A load rating procedure in which strain data from a load test conducted on a steel-girder-and-slab bridge in Wilmington, Delaware was used to calibrate a simplified finite element model (FEM) of the bridge. The authors developed an experimental transverse distribution factor, using the moment distribution from the FEM, to calculate live load effect for the rating factor equation. Comparison of the rating factors calculated using the Delaware DOT standard protocol to rating factors based on their finite element

model, showed that the bridge's strength was higher than traditional rating factors had indicated, thus showing the benefits of the experimental procedure.

Another example of using load test data to develop a load rating factor was completed by a group of researchers from the University of New Hampshire and Tufts University under a project funded by a NSF PFI grant called "Whatever Happened to Long-Term Bridge Design." A newly erected three span steel girder bridge was instrumented with over one hundred strain gauges and was load tested using a truck of known weight (Lefebvre, 2010). The strain data from the load test was used to assess a FEM of the bridge that was created using SAP2000® structural analysis software. Available concrete compressive strength and elastomeric bearing pad stiffness data was used to update the model to increase accuracy. A load pattern that used AASHTO lane loads and design trucks was applied to the model and flexural strength output was used to calculate a rating factor. It was found that the rating factor calculated using the AASHTO design specifications was more conservative. The result of this research was a calibrated bridge FEM that can be continuously updated and used for more accurate asset management.

2.3 Structural Health Monitoring Measurements

Strain is only one of the many metrics that can be measured during a bridge load test. Another useful performance based parameter than can be collected is displacement. Displacement is more ideal than strain because it is a more direct measurement of performance. Strain tends to be a local measurement whereas displacement provides a global assessment of a bridge. Although it is more valuable, displacement data can be difficult to collect due to topographical restrictions. Displacement data can be collected using LVDTs or DIC. LVDTs are a contact instrument which means that they need to be in contact with both the structure and

reference point, typically the ground. In contrast, DIC is a non-contact instrument that can collect data from a distance. Although the tripod that holds the cameras still must be in contact with the ground, it is not limited to the ground directly beneath the point of measurement. Being able to collect data without being in contact with a structure is advantageous in situations where the point of interest is inaccessible by ordinary means. LVDTs have been in use for quite some time and are considered a reliable instrument whereas DIC first appeared in experimental mechanics in the 1980s and rose with the popularity and abundance of digital imaging equipment (Chu, et al., 1985).

Digital image correlation uses mathematical algorithms to extract displacement information from a series of photographs (Mahajan, et al., 2000). The post processing software used in this research, developed by Correlated Solutions, Inc., creates blocks within the image, called subsets, which are made up of a square group of pixels, as seen Figure 2. Each subset is assigned a gray value based on the color contents of the pixels. The gray value assigned gives that particular subset a unique identity. The x, y, and z translation and rotation, in units of pixels, of the subsets are tracked and deformation is calculated. The values in pixels are then converted to units of distance through a calibration process in which the user identifies the distance between known reference points in the image. The error associated with measurements and the resolution of measurements that the DIC system is able to capture is a function of the relationship between the magnitude of displacement and pixel size.

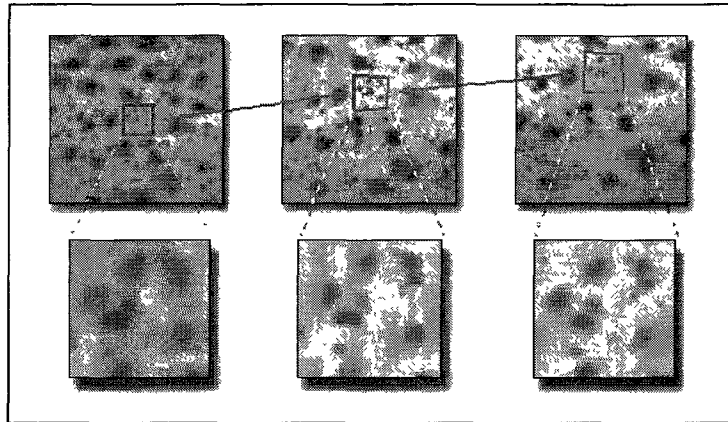


Figure 2 - Post processing software tracks the movement of subsets throughout the series of images (<http://www.correlatedsolutions.com>)

Before post processing can occur, successive images of the specimen under loading must be collected. Required equipment includes a computer with a capable video card, fire wire and/or Ethernet ports, at least one camera that is capable of being connected to the computer, camera lenses, and tripods. Software is also needed to capture and post process images. The University of New Hampshire owns low speed and high speed cameras as part of a NSF Major Research Instrumentation grant. Low speed cameras are capable of taking approximately 3 frames per second (fps) while high speed cameras are capable of 1000+ fps. Low speed cameras are more appropriate for quasi-static testing and high speed cameras work well for capturing dynamic behavior. As seen in Figure 2, it is necessary to apply a random speckle pattern to the specimen to allow subsets to have unique gray values. A speckle pattern can be applied by using a multitude of tools including spray paint, chalk, or magnets, depending on the material of the point of interest.

In 2007, researchers used DIC to capture bridge deflection measurements during a load test in Japan (Yoneyama, et al., 2007). Testing was conducted on a newly built, one span, steel girder bridge and used a 20,000 kg truck to excite the bridge. Cameras were set up to capture the deflected shape of both exterior girders. A speckle pattern was applied to one of the girders but not to the other in order to test the effectiveness of

a specimen without a pattern. The cameras used in this particular experiment had resolutions of 6.3 and 8.2 megapixels. For verification purposes, transducers were also implemented to capture displacements, which ranged from 0 to 3.0 mm. Upon comparison of the results, the standard deviation of the difference between DIC and the transducers was 0.31 mm.

Another article describes a load test on a railroad bridge during which DIC was used to capture horizontal and vertical deflections (Malesa, et al., 2010). DIC testing utilized two cameras, one of which was located within 1 meter of a transverse girder while the other camera was located tens of meters from the bridge. The camera in close proximity to the bridge was a 1 megapixel camera with an 8mm lens. The camera farther from the bridge had a 150mm lens, although the resolution is unknown. Displacements were recorded as trains travelled over the bridge at different speeds and results were compared with a finite element model created by the authors. It was concluded that the model-predicted and DIC measured results matched satisfactorily in the vertical direction and that displacements in the horizontal direction were too small to be properly detected using DIC as configured.

In addition to DIC, there are other methods for measuring displacement that are non-contact and nondestructive in nature. Among these are Global Positioning Systems and Interferometric Radar. Interferometric radar is a unit that can be set up relatively far from the point of interest and has high accuracy, approximately 0.02 mm (Chiara & Morelli, 2010). The system can be set up quickly, is quite portable, and has been used on large bridges such as the Manhattan Bridge in New York City (Mayer, et al., 2010). GPS has been used in long term tests as well. GPS units are easily attached to a bridge and can measure displacements at high or low frequencies for long periods of time with an accuracy of tenths of millimeters (Roberts, et al., 2004). Cost is a factor that cannot

be overlooked when considering any measurement technique. An interferometric radar system costs approximately \$500,000, a GPS system costs approximately \$10,000 per sensor, and a basic DIC system costs approximately \$60,000 (Ha, 2009).

There are many types of nondestructive testing and many ways that the data can be interpreted and used. Chapter 8 in the Manual for Bridge Inspection (AASHTO, 2011) permits bridge owners to consider alternative evaluation techniques to formulate bridge ratings, but does not give a procedure or recommendations.

In 1998 the National Cooperative Highway Research Program (NCHRP) published the “Manual for Bridge Rating through Load Testing” describing the research findings conducted by A.G. Lichtenstein and Associates, Inc. The author points out that “a major aim of diagnostic testing is often to confirm the precise nature of the load distribution” (National Cooperative Highway Research Program, 1998). In a set of load tests referred to as the Ohio Tests, 5 bridges with concrete decks and steel girders underwent testing that measured strain distribution. It was found that 4 of the 5 tests resulted in higher rating factors due to measured distribution and impact factors that were less conservative than AASHTO calculated factors. These findings demonstrate the advantages that nondestructive testing can have on bridge load ratings.

2.3 Load Rating

Three load rating methodologies have historically been used to assess bridge health; allowable stress rating (ASR), load factor rating (LFR), and load and resistance factor rating (LRFR) (Grubb, 1997). Each method is derived from its individual design philosophy; allowable stress design (ASD), load factor design (LFD), and load and resistance factor design (LRFD), respectively. ASD is the oldest of the approaches. When designing using allowable stress, the yield stress of the member is found and then

divided by a factor of safety to give an allowable stress by which the member can be sized.

In 1970 AASHTO adopted LFD as an alternate method for designing structural members (Grubb, 1997). Unlike ASD which considers service conditions and decreases member strength, LFD uses load factors as well as strength reduction factors to calculate member capacities. The factors vary depending on the load levels and uncertainty of the material, and were formulated based on simple calibration and experience. In an effort to eliminate discrepancies and take advantage of recent bridge research, the American Association of State Highway and Transportation Officials (AASHTO) adopted load and resistance factor design (LRFD) in 1993. The largest difference between LFD and LRFD is that the factors used in LRFD were determined through statistical analysis using a reliability index.

Regardless of differences in design methodologies, capacity, dead load, and live load are always taken into account. Dead load is calculated in a relatively typical manner in which permanent components of the bridge are added up and expressed in a weight per length, such as kilo-newton (kN) per linear meter of bridge. The load is then distributed evenly to the beams. Live load is calculated accounting for factors such as impact, multiple presence, lane width, and distribution of loads. Of those factors the distribution factor (DF) might be the most debatable regarding accurately predicting live loads (National Cooperative Highway Research Program, 1998). The distribution factor prescribes a percentage of the live load to be applied to a given stringer, and is typically conservative.

Approximately 25% of bridges in New Hampshire are steel multi-girder with a concrete deck and a length less than 40 meters (Federal Highway Administration, 2011),

a type of bridge for which DIC has provided reliable results. Nondestructive testing, specifically digital image correlation, has potential to be a major contributor towards the goal of more accurate load ratings. DIC is also cost efficient option when compared to other load test options that collect strain and displacement, which tend to be lengthy and cumbersome.

CHAPTER 3

LABORATORY & FIELD VERIFICATION OF DIGITAL IMAGE CORRELATION

Before the digital image correlation system could be used with a high level of confidence, a series of verification experiments were conducted at the University of New Hampshire in a structures laboratory. The purpose of these experiments was both to assess the accuracy and precision of the system and to develop a protocol for field applications of the DIC system. The DIC system is capable of collecting measurements in three dimensions and it was the research team's intention to use this feature. From these experiments, there were significant concerns related to the accuracy of three-dimensional analysis versus two-dimensional analysis for this application. Other factors that influence the accuracy of results are position and orientation of the cameras in reference to the target, low speed and high speed capability, as well as general post processing capabilities. In addition to any laboratory experiment explained here, preliminary uses of DIC in field tests have been investigated for procedure (Santini-Bell, et al., 2011).

The first step to effectively using the DIC equipment was to become familiar with the hardware and software. Table 1 summarizes the hardware and software that were used during this research, most of which was purchased through a collaborative National Science Foundation MRI grant in 2009. Necessary equipment includes a portable computer, digital cameras with lenses, tripods, and applicable cables. Significant time and effort went into reviewing literature provided by Correlated Solutions, Inc. that described the processes involved in successful applications of DIC to measure structural response.

Table 1 - Hardware and software used in this research

Hardware	
Computer	Dell Precision M6400, Intel Core 2 Duo CPU 2.66 GHz, 2GB RAM
Cameras	(2) Point Grey Research Grasshopper 2 Megapixel,
Lenses	(2) Schneider 35mm, (2) Schneider 17mm, (2) Tamron 75mm
Tripod	Manfrotto Carbon Fiber
Cable	6' Belkin 6 to 9 pin firewire cable
LVDT	(2) Macrosensors HSA 750-050
Software	
Operating System	Microsoft Windows 7
Image Capture	Vic-Snap 2010
Post Processing	Vic-2D 2009 & Vic-3D 2009

During all preliminary testing, LVDTs were used as verification instruments (Figure 3). The LVDTs were periodically calibrated to ensure accuracy using an LVDT calibrating device made by GCTS Testing Systems (model #DCD-025) (Figure 4). LVDTs were placed at points of measurement and the data was compared with DIC data. LVDTs are a widely accepted form of linear displacement measurement and are considered extremely accurate.



Figure 3 - LVDTs were used during verification testing to ensure the accuracy of DIC measurements.

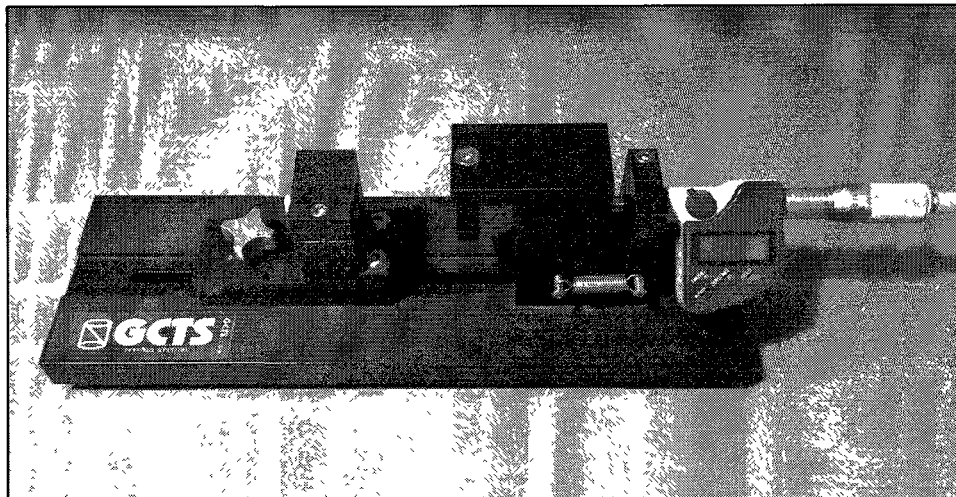


Figure 4 - LVDTs used for verification were calibrated with this device.

3.1 Laboratory Verification

Initial experiments in the laboratory were conducted using a simply supported W10x14 steel beam and loading it at mid-span. Although the primary measurement was vertical displacement, three-dimensional analysis was initially used during these tests and was supplemented by LVDT data. One way in which three-dimensional analysis differs from two-dimensional is in the calibration process. When using three-dimensional analysis, calibration cards with evenly spaced dots are rotated in front of

both cameras for approximately 30 frames so that the post processing software can orient the cameras' axes with respect to each other (Figure 5). The cards are classified by the spacing between the dots; closer spacing works for shorter distances between the cameras and POI while longer spacing is for further distances. After many experiments, data showed that three-dimensional analysis was not accurate on a consistent basis for this range of displacement and the choice was made to primarily use two-dimensional analysis. Figure 6 shows data from a test in which different calibration cards were used to calibrate the same set of images from one single test. The LVDT and two-dimensional analysis results are also shown. The results indicated that the three-dimensional results vary with calibration card size. The variability in this test decreased the reliability of three-dimensional analysis at the scale that is required for this research.

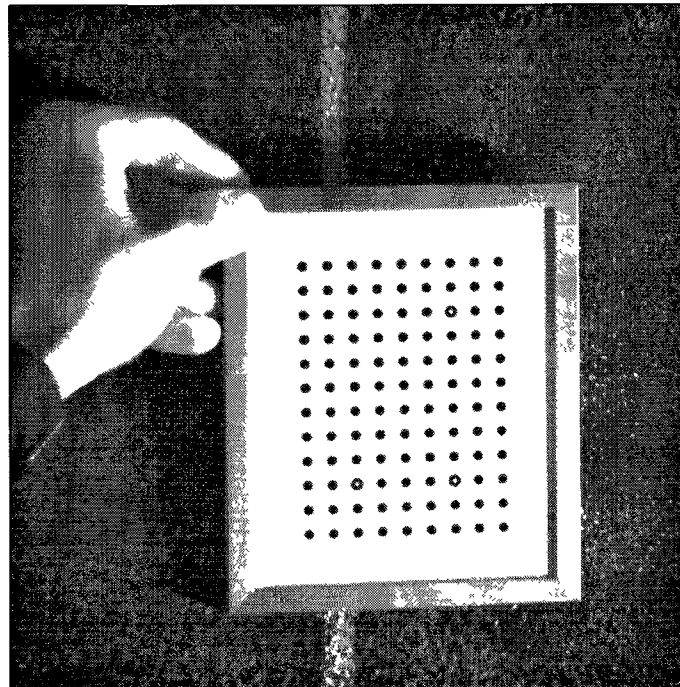


Figure 5 - Calibration cards are rotated in front of the cameras for three-dimensional analysis.

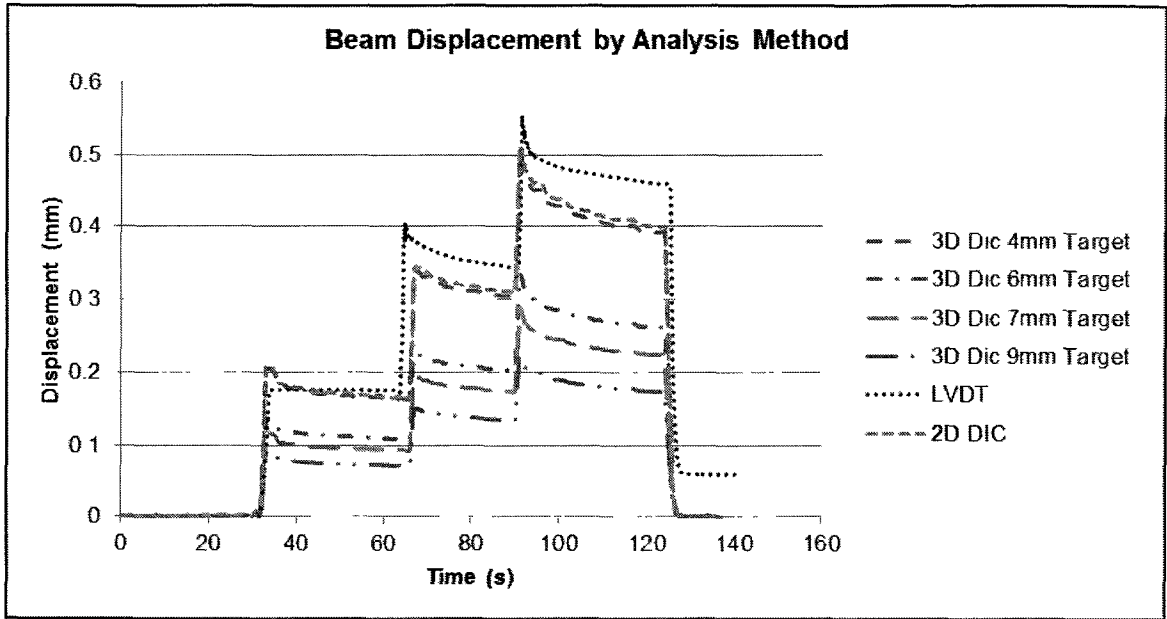


Figure 6 - Precision problems with three-dimensional analysis can be seen in this graph.

Since the decision was made to use two-dimensional analysis exclusively, an additional static load test was conducted in the lab to confirm accuracy (Figure 7). Again, this test was conducted by bending a small steel beam and comparing the DIC and LVDT displacement results. The cameras were placed approximately one meter from the point of interest during this test and a 35mm lens was used. Results, seen in Figure 8, show good correlation between the two sets of data and verify the accuracy of two-dimensional DIC.

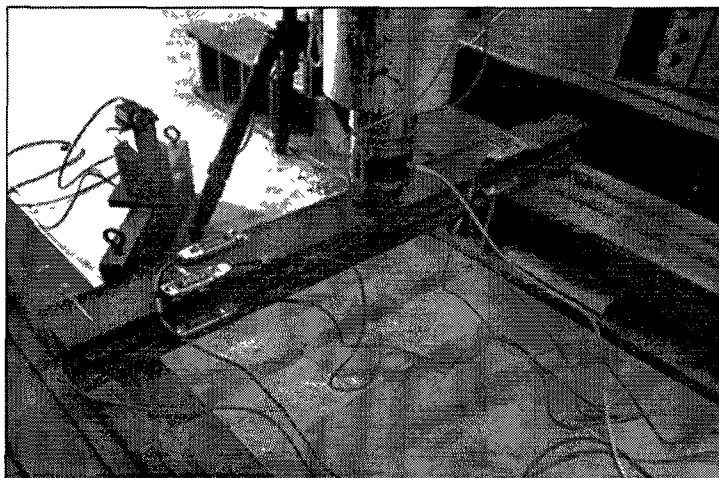


Figure 7 - A laboratory test measuring displacement of a wide flange beam.

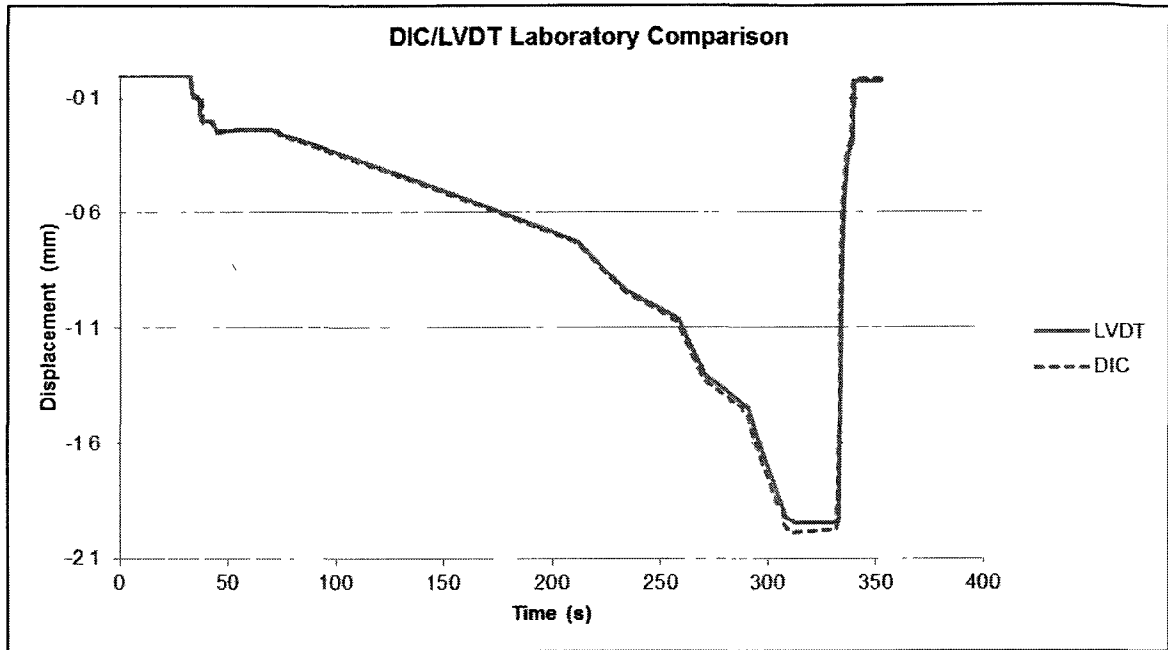


Figure 8 - Comparison of vertical deflection measurements by DIC and LVDT.

In addition to static testing, two dimensional dynamic testing was conducted using high speed cameras that were capable of capturing images at a rate of 250 frames per second. A shake table and single degree of freedom structure (Figure 9) was utilized for this testing. The 5-foot square shake table is capable of simulating maximum ground accelerations of 3g through a hydraulic actuator with a stroke of 6 inches. Two cameras were used during this test; one camera captured base movement while the other captured the single DOF movement. Numerous combinations of amplitude and frequency were tested and the DIC system was able to accurately report displacements through all of the tests. Frequencies tested ranged from .5 Hz to 6 Hz with amplitudes ranging from .1 to 1 inch. Figure 10 shows results from one of the tests.

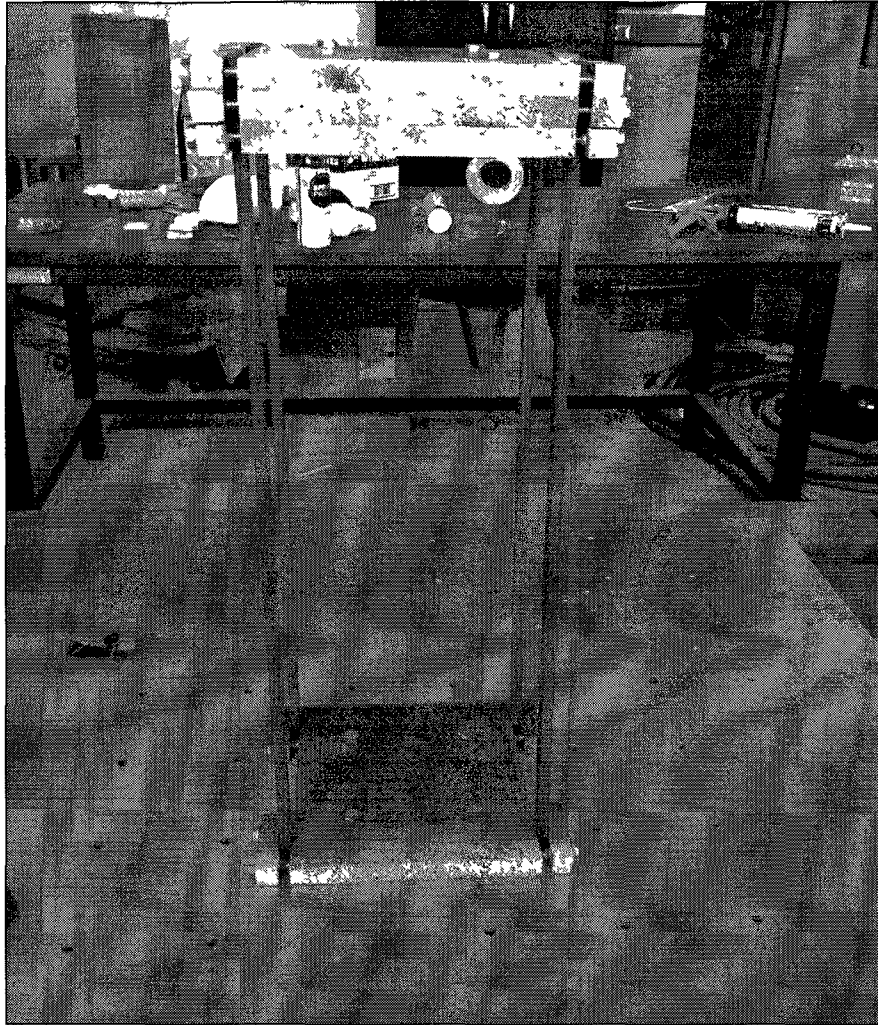


Figure 9 - A SDOF system on a shake table.

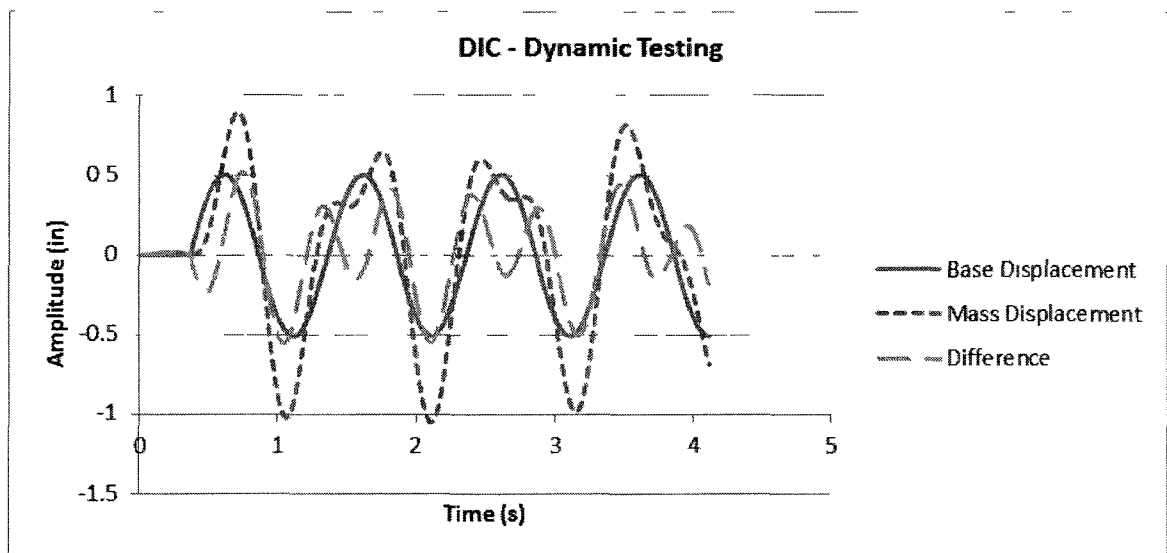


Figure 10 - Dynamic test results with a base amplitude of 1-inch at a frequency of 1 Hz.

3.2 Field Verification

Two separate field experiments were conducted to confirm that DIC could actually collect reliable results at an in-service bridge. Results from both locations were used to refine DIC field testing protocol. Testing locations included the Vernon Avenue Bridge in Barre, Massachusetts and a small concrete slab bridge in Gilford, New Hampshire. Each experiment had a different set of goals, circumstances, and findings.

The Vernon Avenue Bridge (VAB) is located in Barre, Massachusetts and was reconstructed in 2009. The new structure is a three span, continuous girder bridge with a reinforced composite deck (Figure 11). The bridge is unique because it is part of a collaborative project between Tufts University, the University of New Hampshire, and FST funded by the NSF PFI grant “Whatever Happened to Long-Term Bridge Design” in which the VAB was instrumented with strain gauges, tilt-meters, and accelerometers during fabrication, prior to erection. The collected data from this instrumentation was used to calibrate structural models that would enable tracking of long term bridge performance in previous research (Lefebvre, 2010). Additional information related the Vernon Avenue Bridge and the instrumentation plan is presented in Chapter 4.



Figure 11 – The newly constructed Vernon Avenue Bridge.

The second site used for verification was a small concrete slab on steel girder bridge that was under renovation. The renovation consisted of removal of the beams and addition of fiber reinforced polymer (FRP) strips on the underside of the deck. The designer, Dubois & King, Inc. of Bedford, NH, approached the research team and requested a “before and after” performance test to objectively verify the strength increase provided by the FRP (Whittemore & Durfee, 2011). Instrumentation can be seen in Figure 12.



Figure 12 – Installation of LVDT equipment underneath the bridge in Gilford, NH, post-renovation.

3.2.1 Vernon Avenue Bridge Verification Experiment

Testing occurred at Vernon Avenue Bridge on three separate occasions, the first two of which were concept verification tests that were limited in the number of measurements collected but which showed potential in the system. Chalk was used to create a speckle pattern on the web of the beam and spotlights were used to create a

consistent light source. An LVDT was used to verify the accuracy (Figure 13). The bridge was excited using a 72-kip, tri-axel dump truck driving at a constant speed of 5 miles per hour over the bridge travelling in predetermined lanes and stopping at predetermined points (Table 2). Figure 14 shows the close correlation between LVDT and DIC results. The results are essentially an influence line about the point of interest. The point of interest is the exterior girder of the far span in Figure 11. The sequence of the response in the graph shown in Figure 14 shows the truck quickly backing over the bridge (1), then driving onto the span at which measurements are being taken and stopping (2), the continuing onto the mid span and stopping (3), driving over the third span (4), and again back over the bridge (5). The shape of this line is expected giving the loading pattern.

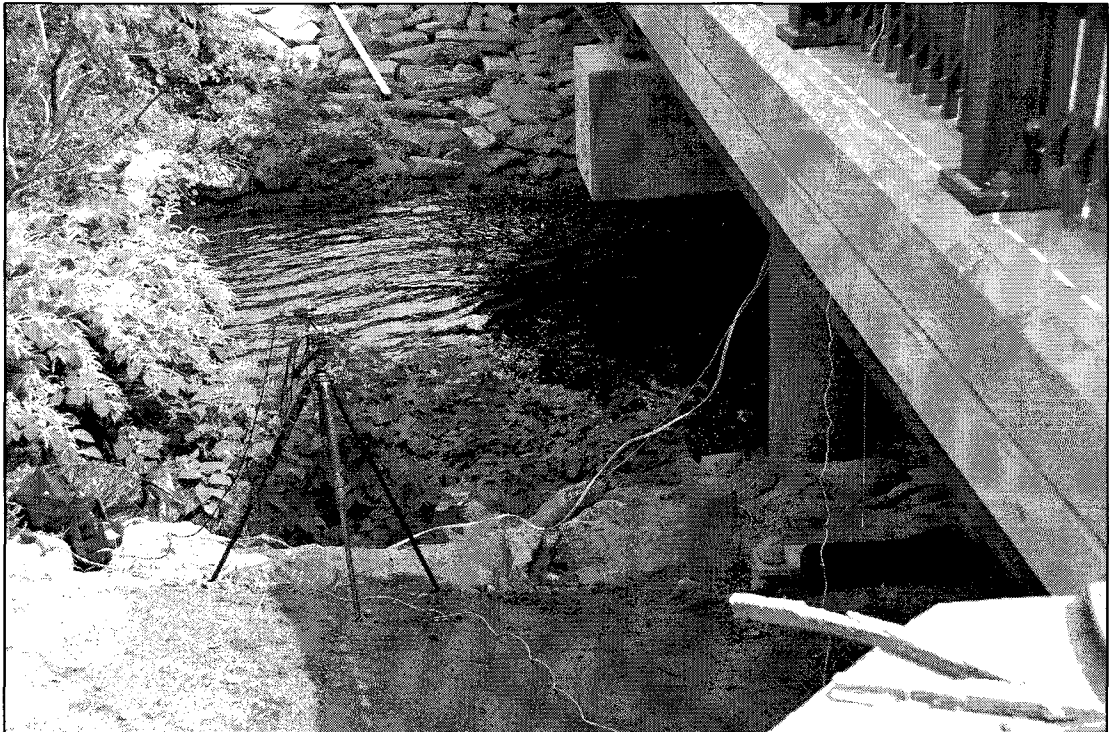
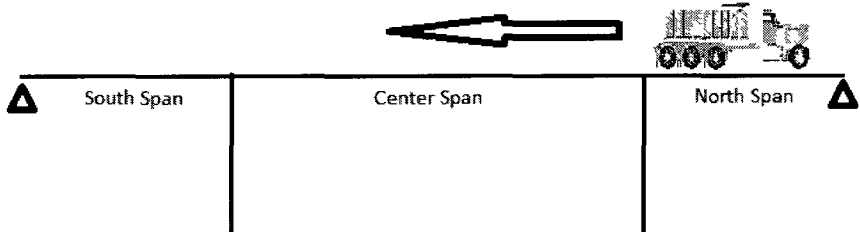
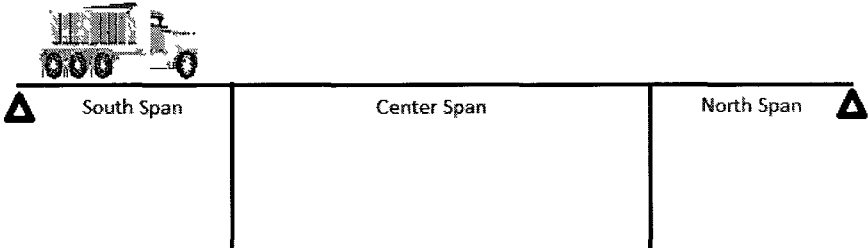
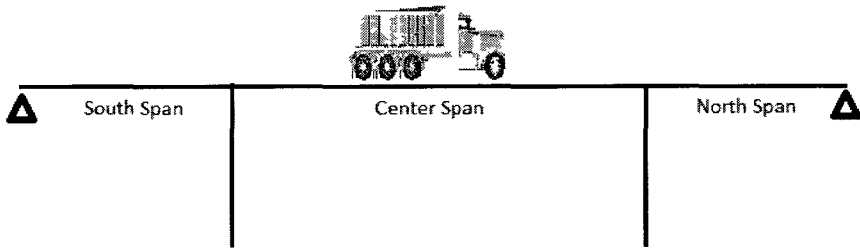
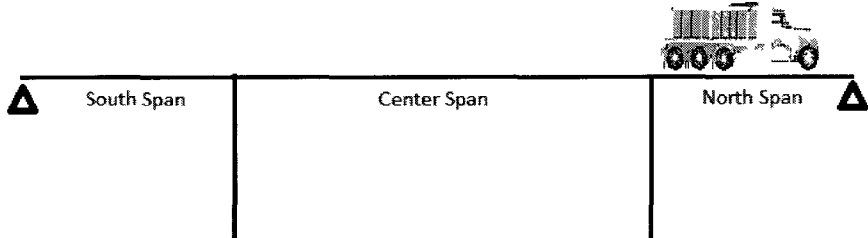
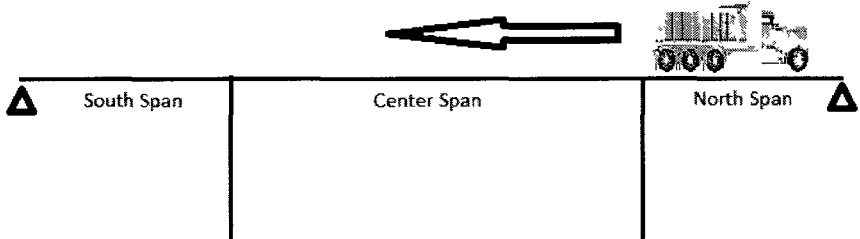


Figure 13 - The setup at the VAB in 2009. Cameras were focused on a point on the exterior beam in the south span.

Table 2 - Load locations corresponding to the locations numbered on response graph.

Location on Figure 14	Location on Bridge
1	 <p>The diagram shows a bridge divided into three spans: South Span, Center Span, and North Span. A truck is positioned on the North Span, and a knife is positioned on the Center Span. Triangles at the ends of the bridge represent supports.</p>
2	 <p>The diagram shows a bridge divided into three spans: South Span, Center Span, and North Span. A truck is positioned on the South Span. Triangles at the ends of the bridge represent supports.</p>
3	 <p>The diagram shows a bridge divided into three spans: South Span, Center Span, and North Span. A truck is positioned on the Center Span. Triangles at the ends of the bridge represent supports.</p>
4	 <p>The diagram shows a bridge divided into three spans: South Span, Center Span, and North Span. A truck is positioned on the North Span. Triangles at the ends of the bridge represent supports.</p>
5	 <p>The diagram shows a bridge divided into three spans: South Span, Center Span, and North Span. A truck is positioned on the North Span, and a knife is positioned on the Center Span. Triangles at the ends of the bridge represent supports.</p>

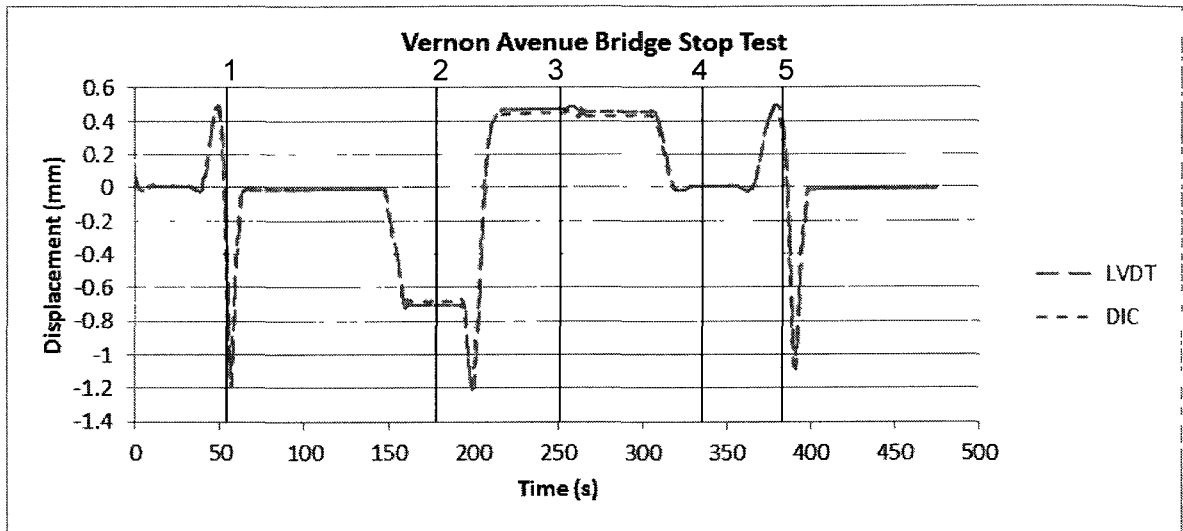


Figure 14 – Stop test results at Vernon Avenue Bridge. Measurements are taken at the south span.

3.2.2 Gilford Bridge Verification Experiment

While results from the Vernon Avenue Bridge verification experiment were encouraging, the later test in Gilford, New Hampshire helped identify limitations of DIC. A recent evaluation had deemed the bridge’s health unsatisfactory. Dubois & King, Inc. designed a rehabilitation that called for removal of the non-composite stringers and installation of FRP strips on the underside of the bridge (Whittemore & Durfee, 2011). In order to evaluate the contribution of the newly installed FRP strips researchers decided to collect displacement measurements before and after installation using LVDTs and digital image correlation. For the “before” test, it was decided to excite the bridge with a small, empty, dump truck that was owned by the town of Gilford. The truck was left empty due to concerns that the bridge was unable to support any significant weight with no supporting superstructure in place (Figure 15). The weight of the front and rear axles of the truck were 12,500 lbs. and 11,020 lbs., respectively. DIC measurements were taken at 3 points across the center of the bridge (Figure 16).



Figure 15 - View of the top of the bridge and load truck in Gilford, New Hampshire.

After the images had been post processed and the data was examined, the center of the concrete deck had only displaced vertically -0.07 mm, a value that was determined only after considering the LVDT data. To make a valid comparison, the same load had to be used in the second test, which showed slightly less deflection. The DIC system, equipped with 75 mm lenses, was not able to zoom into the points of interest to collect sufficiently clean data in either case in field conditions. Figure 17 shows the LVDT and DIC data for one of the tests and though accuracy was lacking, it was encouraging to see that the DIC data followed the expected trend of displacement. Although small displacements were not able to be measured precision in this application, mechanical engineering applications can utilize DIC to measure displacements on the order of hundredths of millimeters due to close proximity of the subject. (Yang & Wu, 2007).

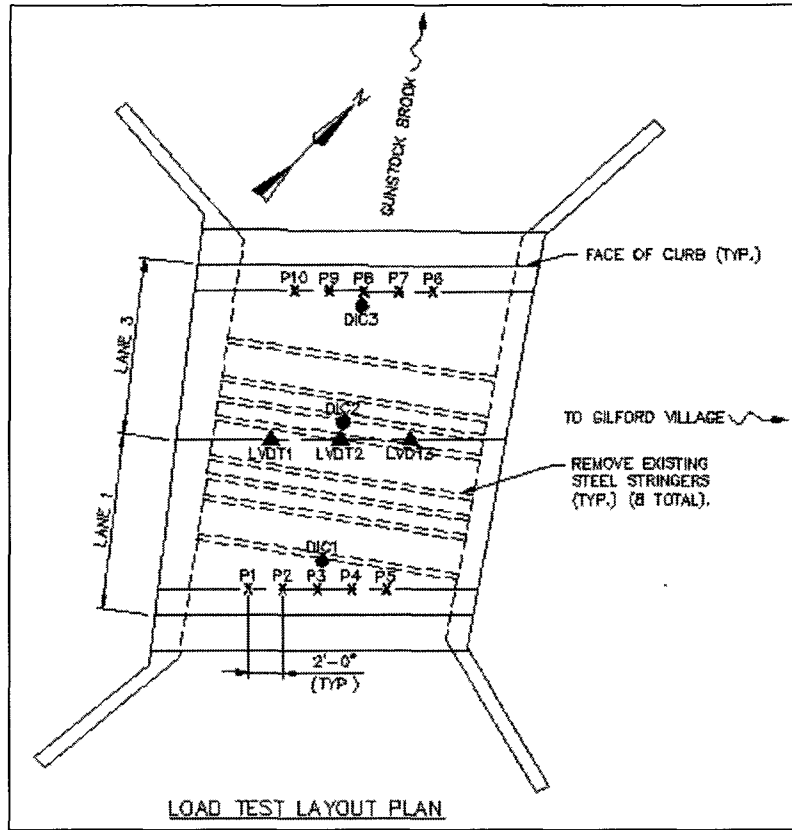


Figure 16 - Gilford Bridge load test layout plan.

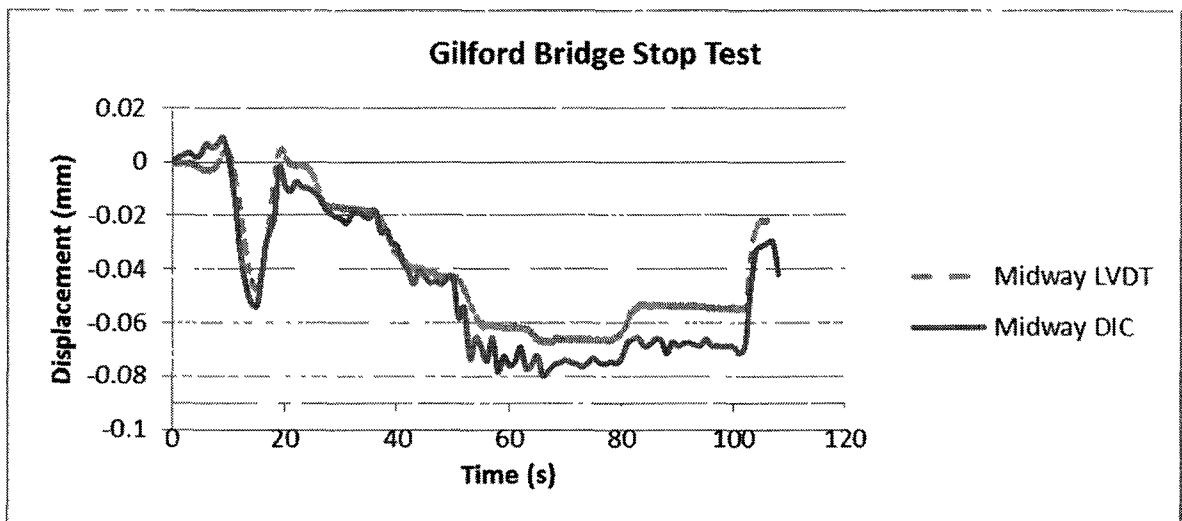


Figure 17 - Data from a test at the bridge in Gilford, NH. The DIC data is visibly noisier than the LVDT data at small scale displacements.

3.3 Experimental Techniques Used in DIC Testing

Many data collection techniques have been evaluated throughout this project. While there are only two ways that the data can be processed, two-dimensional analysis or three-dimensional analysis, the ways that the data can be collected are numerous. Variables in data collection include the speckle pattern, cameras, lenses, target location, and light source.

In preliminary testing the speckle pattern was primarily created by spray painting the point of interest (POI). The POI would first be painted entirely white then be speckled with black paint. The easiest technique to create the black speckles was to hold a nail in front of the aerosol can nozzle while spraying. While this was practical for laboratory experiments it was not likely that a bridge owner would agree to this application. Researchers also experimented with sidewalk chalk as a speckle pattern (Figure 18). Not only was it easy to apply chalk by scraping it on the web of a beam, it was also easy to clean. This technique was used during one of the VAB verification tests and worked sufficiently. The biggest challenge that both chalk and spray paint pose is the issue of applying the speckle pattern to POI's at large heights, over a river for instance.

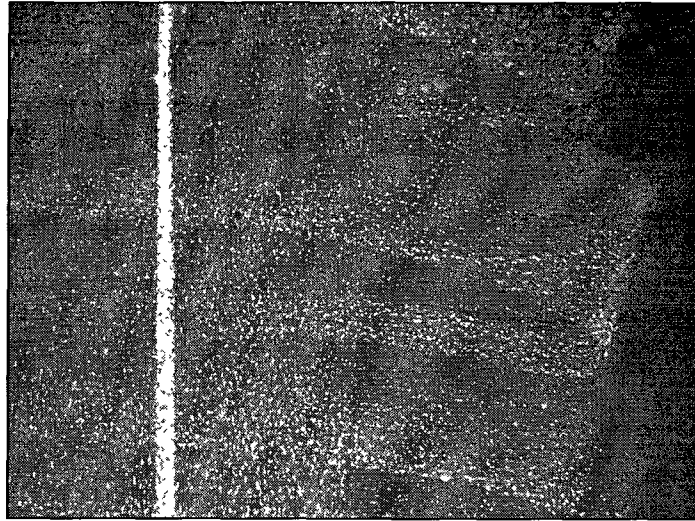


Figure 18 - A typical speckle pattern created with chalk on the web of a beam at the VAB.

Tools that allowed collection of displacements at POIs at heights up to 5 meters without permanently defacing the bridge and that could be applied and removed in seconds were developed as part of this research effort. One was created using a rigid length of PVC pipe with a neodymium magnet attached to one end and a cut of sheet metal with a speckle pattern on it attached to the other. These are relatively inexpensive and easy to assemble at a cost of approximately \$20 each. The sheet metal alone can also be used in easy-to-reach situations by bending one side of it at a 90 degree angle and gluing it to a horizontal surface, referred to in this research as tabs. Figure 19 and Figure 20 show the speckle patterns applied in the field at the Vernon Avenue Bridge.

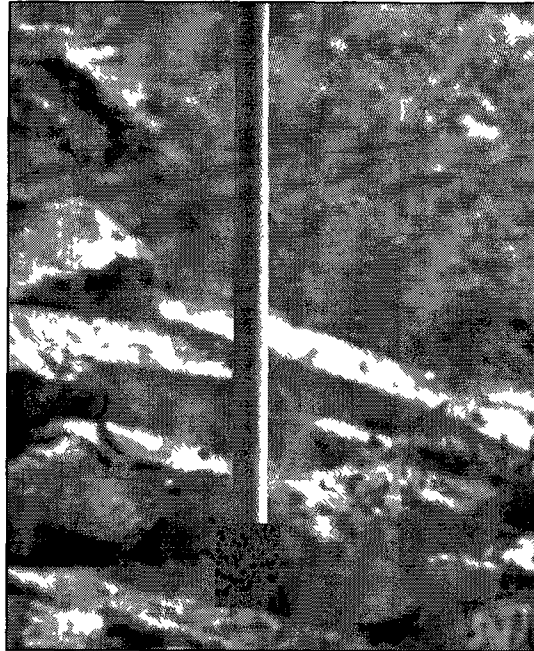


Figure 19 - A rigid PVC pipe attached to the bottom flange of a girder. The speckle pattern translates vertically with the beam.

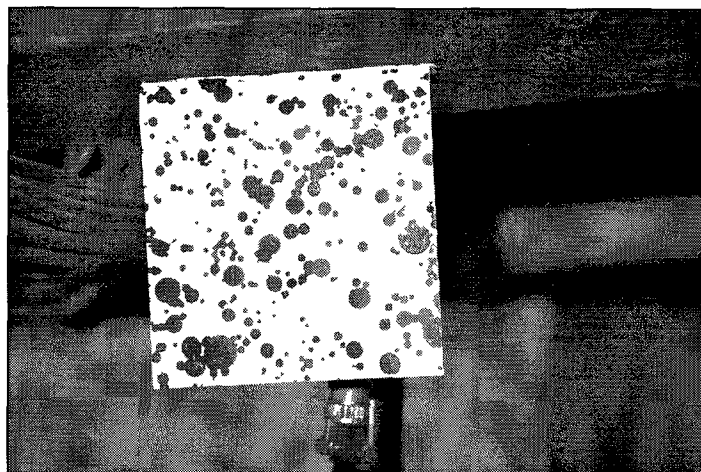


Figure 20 - A cut of sheet metal with a speckle pattern (tab) attached to the bottom flange of a beam.

Camera and lens choice also have an impact on the results. A camera with higher resolution will allow more pixels per square inch of picture. The cameras that were used in this research had a resolution of 2.0 megapixels. Only one type of camera was used in this research but lenses of different focal lengths were included in experiments. A lens with a larger focal length allows the user to zoom in on the POI, therefore allowing the cameras to be further from the target. Longer focal lengths were used as this project progressed and as the need to capture deflections at far distances

increased. By the final test, displacements were being measured at a distance of 35 meters using a lens capable of a focal length of 300 mm. The experiment results showed that the addition of the larger lens greatly improved the accuracy of digital image correlation at far distances.

Illumination of the POI is another test variable. A combination of daylight and spotlight was used during verification tests. Daylight is easier to use during tests but is not as reliable as an auxiliary light source, as it varies with the movement of clouds and time of day. Weather also has an impact on DIC usage in the field. Wind can cause unwanted movement in the POI target and/or camera setup. Rain, snow, and other falling objects may interfere with results by appearing in test images resulting in inaccurate measurements.

The effect of these variables on data collection is best mitigated through familiarization of site conditions. Testing at night with an auxiliary light source, operating the cameras beneath a structure, and choosing the most significant POIs are all worthwhile considerations when planning an experiment.

3.4 Summary

Digital image correlation is an experimental technique for collecting displacement data on both small and large scales. Because its use is still in an experimental state, researchers conducted verification tests in the laboratory and in the field in which DIC data was compared against LVDT data. Two-dimensional DIC was found to be as effective as LVDTs in many cases, varying by no more than 0.1 mm in any experiment conducted. Field experiments at in-service bridges verified accuracy and also led to improvements in procedure including POI target application and large focal length lens

use. Knowledge gained from these tests helped identify limitations and greatly aided researchers in subsequent load tests.

CHAPTER 4

CASE STUDY: VERNON AVENUE BRIDGE

A single structure, referred to as the Vernon Avenue Bridge in this project, was the basis for much of the research presented in this thesis. MassDOT and the town of Barre, Massachusetts permitted the research team to take advantage of the reconstruction of the VAB for data collection and long-term bridge performance evaluation beginning in 2009. Located in central Massachusetts, the VAB spans the Ware River and connects Vernon Avenue with Route 122 (see Figure 21). The bridge is used by 2000 to 2500 vehicles per day (Fay, Spoffard, & Thordike, LLC, 2007). Barre is primarily a rural community, but a recycling facility and a regional landfill lie within a quarter mile of the bridge, subjecting it to moderate truck traffic. Though it is most certainly a contributing factor to the deterioration of the old bridge truck traffic created an ideal situation for research.



Figure 21 - An aerial view of the Vernon Avenue Bridge and nearby recycling and landfill facilities.

4.1 History

Also known as the Powder Mill Pond Bridge, the date of original construction of the VAB is unknown. According to Barre Historical Society, the name Powder Mill Pond is in reference to a small gun powder mill that was located at a small dam upstream of the bridge. This gun powder mill was the largest supplier of gun powder to Union forces during the Civil War. In 1938, a hurricane flooded much of the surrounding area. The dam was overrun and the wooden Powder Mill Bridge was washed out.

The original bridge was replaced with a steel stringer/reinforced concrete deck bridge and, due to more flooding, the Army Core of Engineers built the Barre Falls Dam to replace the older dam. The replacement bridge remained in service until June of 2008. The last inspection report noted full-depth section loss in the deck which had to be covered by large steel plates to prevent further failure. The replacement bridge, finished in the summer of 2009, is the bridge targeted for this research.

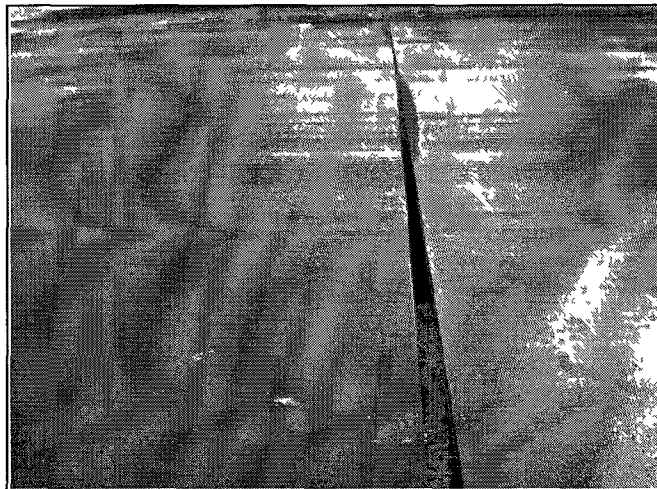


Figure 22 - Steel plates covered the old bridge deck at the time of closure.

4.2 Detailed Bridge Description

The VAB is a 3-span continuous steel girder bridge topped with a composite reinforced concrete deck. The end spans and center span are 11.75 meters and 23.50

meters, respectively, for a total bridge length of 47.0 meters. Though not skewed, the bridge does have a grade of 3.47% with the north side being the high side (Figure 24).

The concrete deck is 200 mm thick and is reinforced with epoxy coated reinforcing bars (Figure 23). The 4 interior girders are W920x238 and the exterior girders are W920x345 (Figure 26). There is a variation in the number of girders on the north span in which two outriggers, W920x201, flare out, for a total of 8 girders. The main 6 beams are spaced at 2.25 meters on center throughout the length of the bridge. The beams sit on elastomeric 61mm thick bearing pads (Figure 27) on the piers and abutments. The beams are welded to sole plates, which sit on the bearing pads, that are free to move at the abutments, but are bolted to the piers. The piers are made up of a reinforced concrete pier cap that sits on 3 columns. The abutments are also cast-in-place reinforced concrete. The piers and abutments sit on foundations of drilled shafts.

There is a wearing surface of hot mix asphalt on the deck that is 40.0 mm thick (Figure 25). Other components of the bridge include a 1.8 meter-wide sidewalk, steel railings on both sides of the bridge, and a utility bay that carries a water pipe over the river that is located in between girders 4 and 5. While two traffic lanes actually exist on the bridge, for the purposes of this research three lanes will be used for live load effects due to the width of the bridge per provision 3.6.1.1.1 of the LRFD bridge design specifications (AASHTO, 2011).

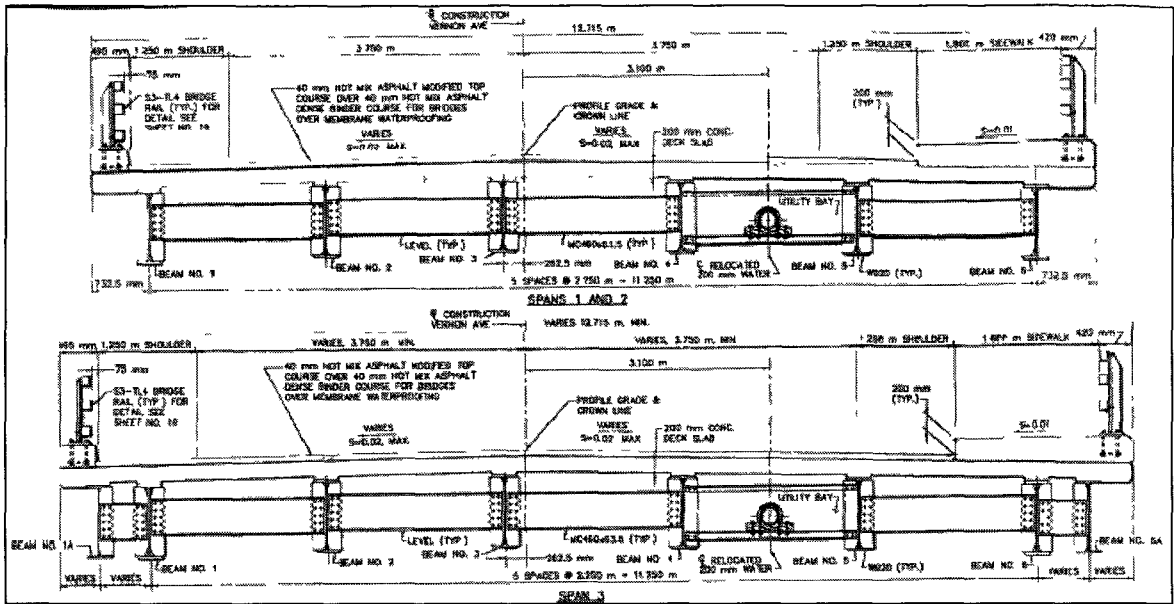


Figure 25 - Typical deck sections on the VAB.

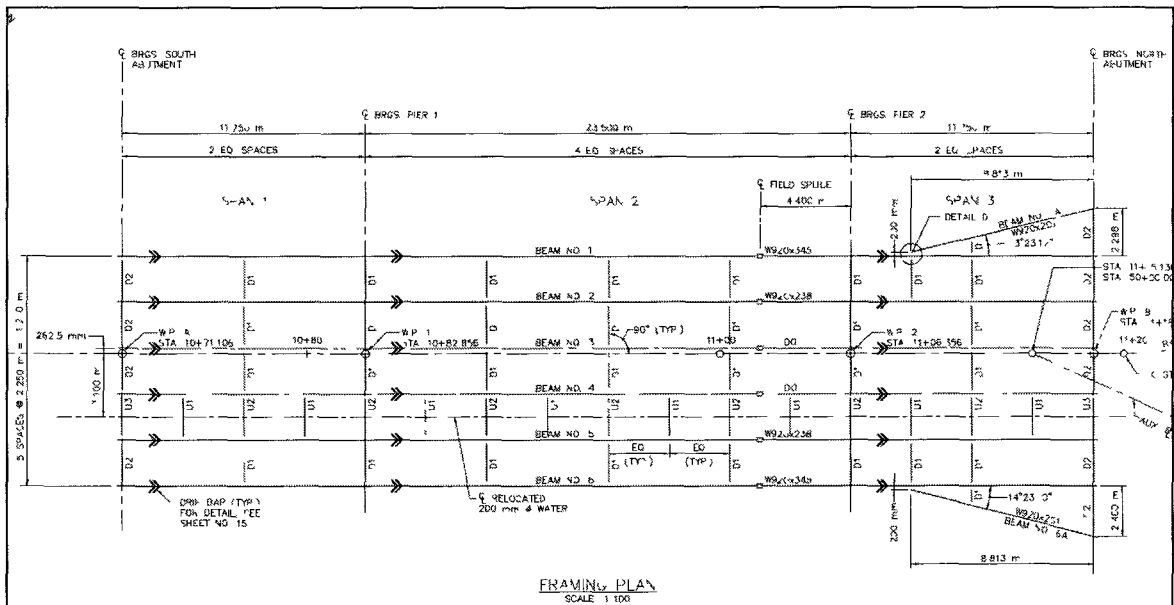


Figure 26 - Framing plan of the Vernon Avenue Bridge.

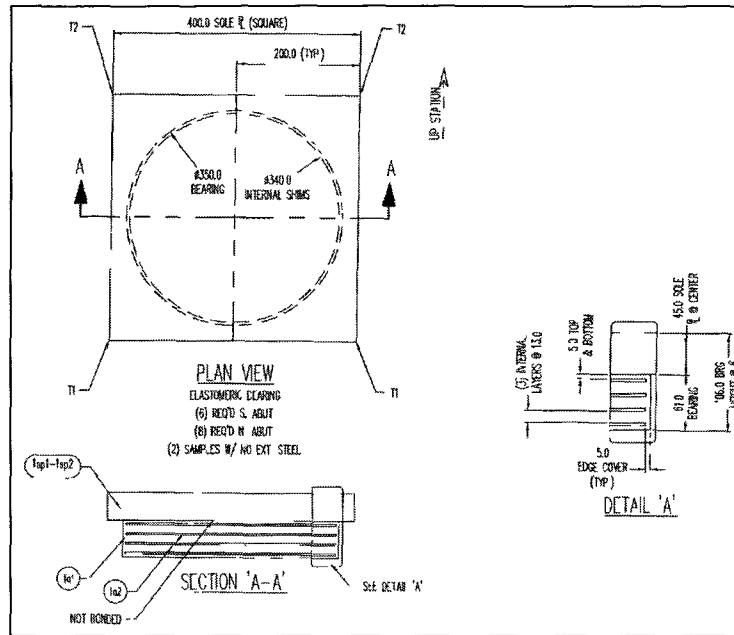
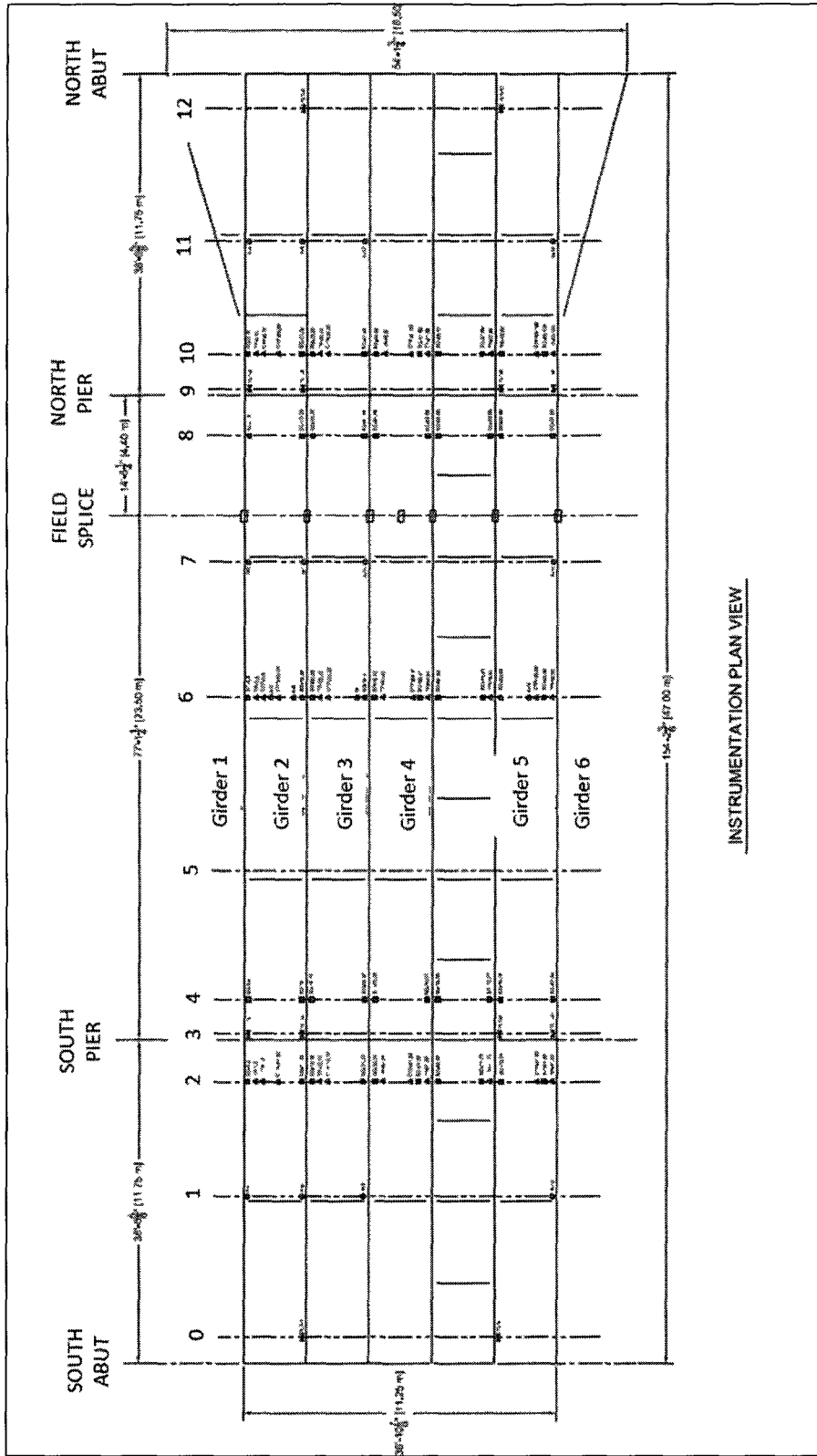


Figure 27 - Bearing pad detail (D.S. Brown).

4.3 Instrumentation

As part of a collaborative project funded by the National Science Foundation under a Partnership for Innovation grant (0644683) in 2009, the Vernon Avenue Bridge was instrumented with a multitude of sensors. Strain gauges, tilt-meters, accelerometers, and thermocouples were installed in an effort to track long term bridge behavior. Collaborators on this project are Tufts University, the University of New Hampshire, Fay, Spoffard, & Thorndike, GeoComp Corporation, and the MassDOT.

Strain gauges, temperature gauges, and all cables were installed at High Steel, located in Pennsylvania, by graduate students. 100 strain gauges, 66 thermocouples, 16 tilt-meters, 16 accelerometers, and 2 pressure cells were installed for a total of 200 sensors. Figure 28 is a plan view of the VAB that indicates the stations at which sensors are located. All sensors are wired into data collection boxes provided by GeoComp. The data collection boxes, also known as iSite boxes, are connected to an onsite computer which makes the data available online and able to be post processed by graduate students.



INSTRUMENTATION PLAN VIEW

Figure 28 – VAB instrumentation plan.

4.4 September 2011 Load Test

The third annual load test at the Vernon Avenue Bridge occurred on September 25, 2011. The load test plan was created by the research team, with a majority of the effort orchestrated by Jesse Sipple, a Ph.D. candidate at Tufts University, and included 39 sequences of data collection. There were several teams of researchers that were collecting different types of data simultaneously. Accelerations due to a portable shaker were measured by the Tufts team on the bridge deck, strain and temperature data were collected by the University of New Hampshire, displacements due to truck passes were collected using DIC (University of New Hampshire) and interferometric radar (Olson Engineering). The result of this test was a wealth of data that will help the research team study long term bridge health. This thesis focuses on the data collection of displacements by DIC.

The load truck used to excite the bridge for displacement purposes was rented from D & P Trucking. Figure 29 shows the load test truck with axle dimensions. It was loaded with aggregate and weighed at the plant and again on site by team members. Axle weights, as measured on site, from front to back were 84.8 kN, 134.8 kN, and 134.1kN, for a total weight of 353.7 kN or 79.5 kips. The test plan prescribed 5 lanes that the truck would drive over. These lanes were determined by Merve Iplikcioglu of Tufts University to induce the maximum response from the girders. Figure 30 shows the lane locations in relation to the bridge cross section.

In previous VAB tests, only 2 points of displacement on the south span of the bridge were able to be collected. It was the goal of researchers in 2011 to collect 18 points of displacement, one at each girder in each span. To do this in an efficient manner, targets were placed at each location prior to the test and two cameras were set up in a location at which all targets could be seen. Because there were only 2 cameras

used, the load truck drove along lane X2, nine times to allow for displacement collections at all 18 locations. It was important to collect data at all points for a single load case. Each run took approximately 4 minutes to complete for a total time of 36 minutes for displacement collection at 18 points due to a single load case. It is worthy to note that this time could have been reduced had there been more cameras used. Figure 31 shows the location of the cameras and the points of measurement.

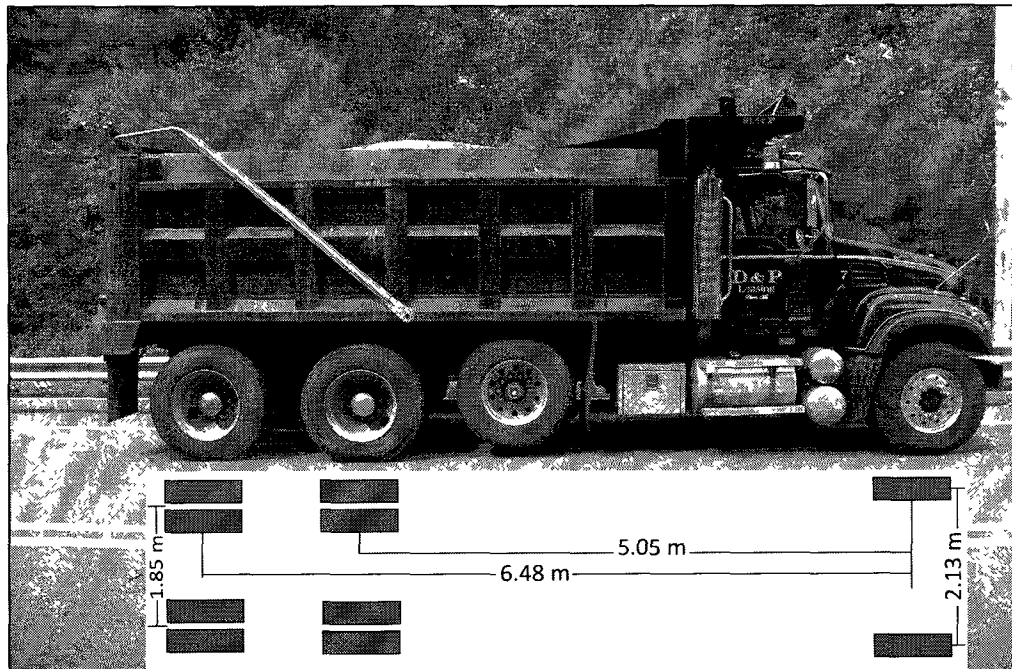


Figure 29 - The load truck used at the 2011 VAB bridge test.

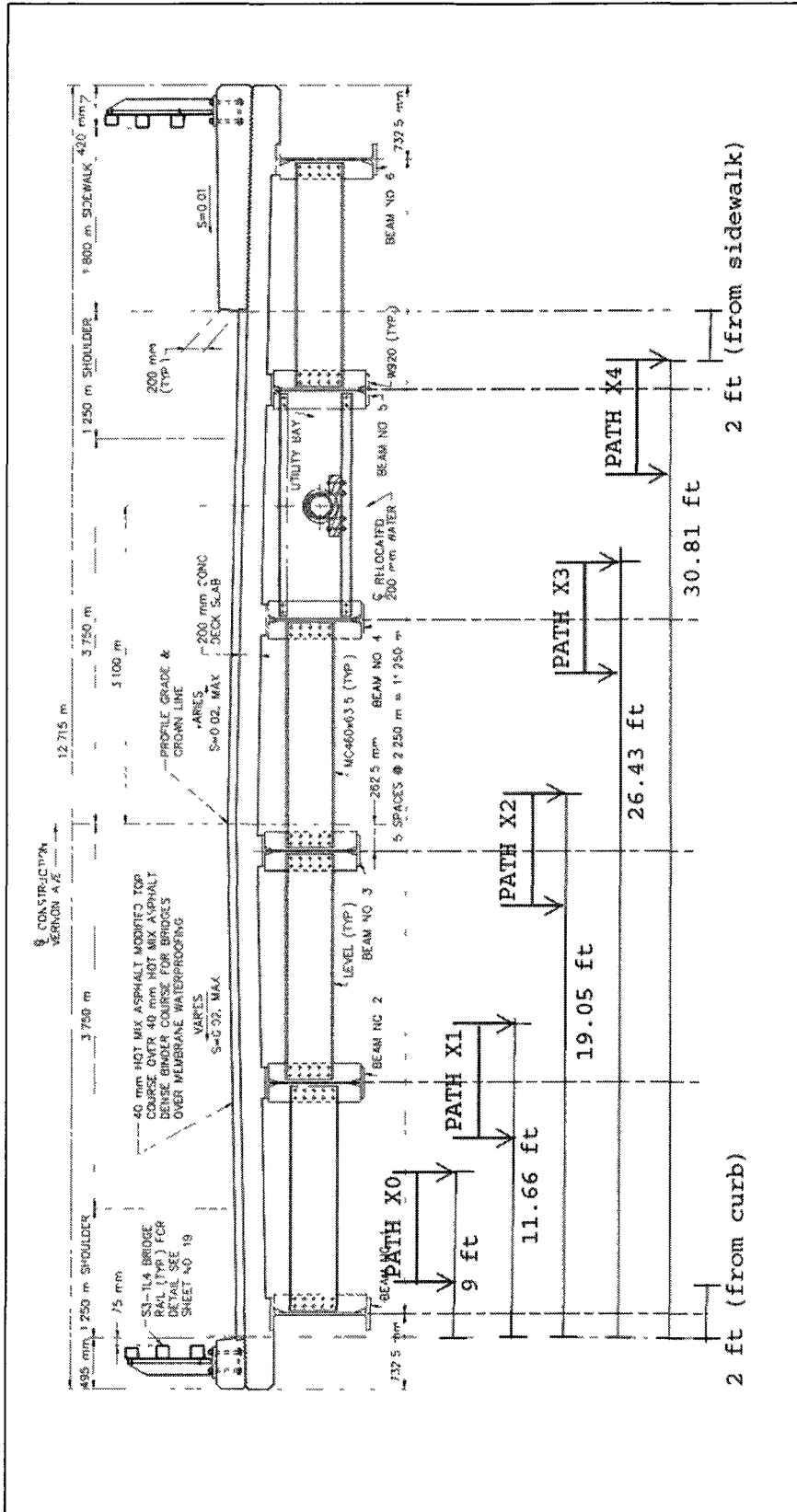


Figure 30 - Diagram of the truck paths during the 2011 VAB load test.

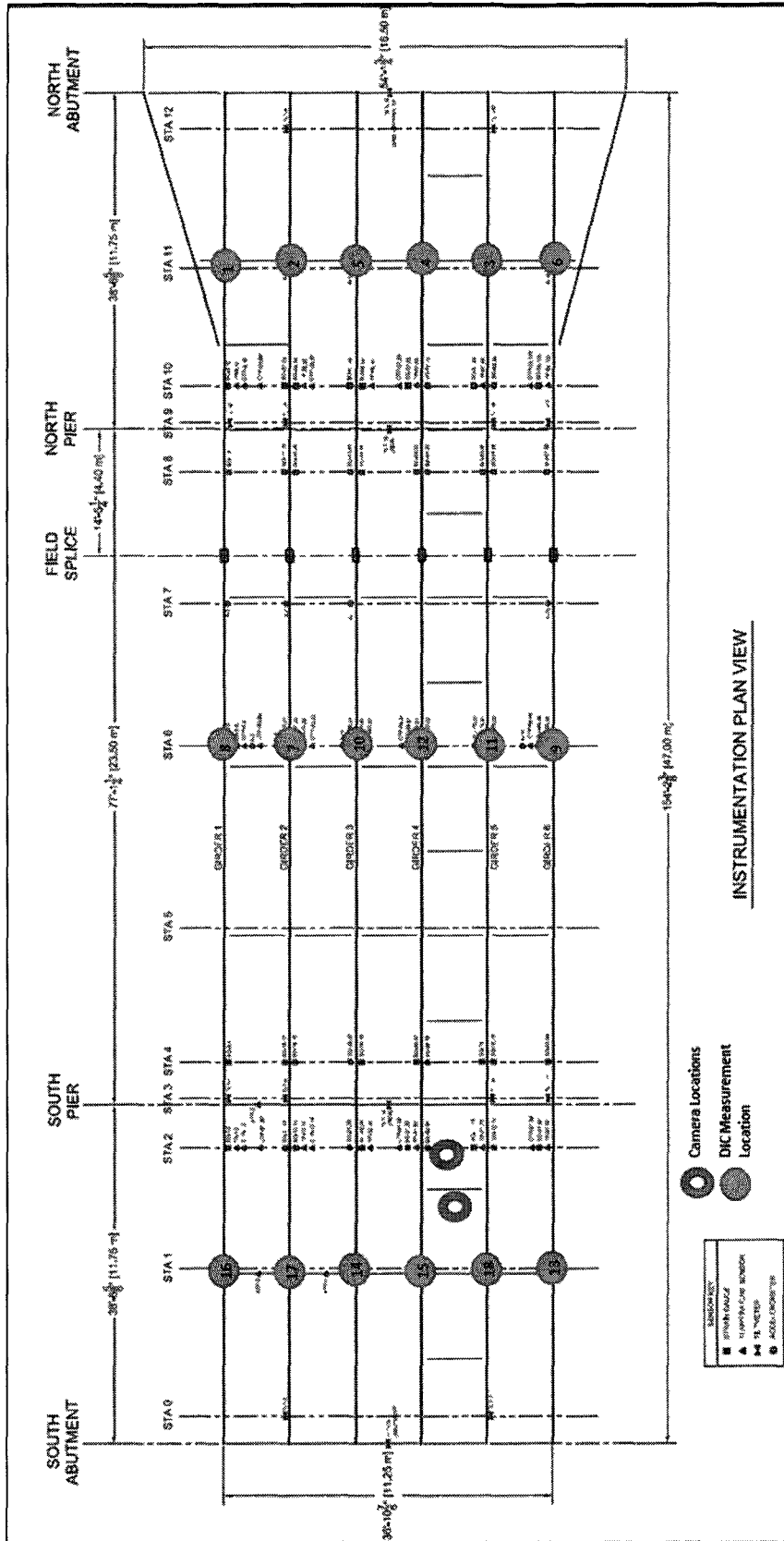


Figure 31 - Locations of DIC measurements during the 2011 VAB load test.

Figure 32 is a picture taken from the south pier, by which the two cameras were located. This picture shows the PVC pipe data collection tool at POIs with targets attached to them. Without the use of the PVC pipes at the VAB, a ladder, scaffolding, or snooper truck would have had to be used to collect measurements at the midspan. Collection of displacement measurements using LVDTs at those points would have posed major challenges due to the height of the beams. Figure 33 and Figure 34 show the two cameras that were used.



Figure 32 - A view of the targets located at each POI at the 2011 VAB load test.

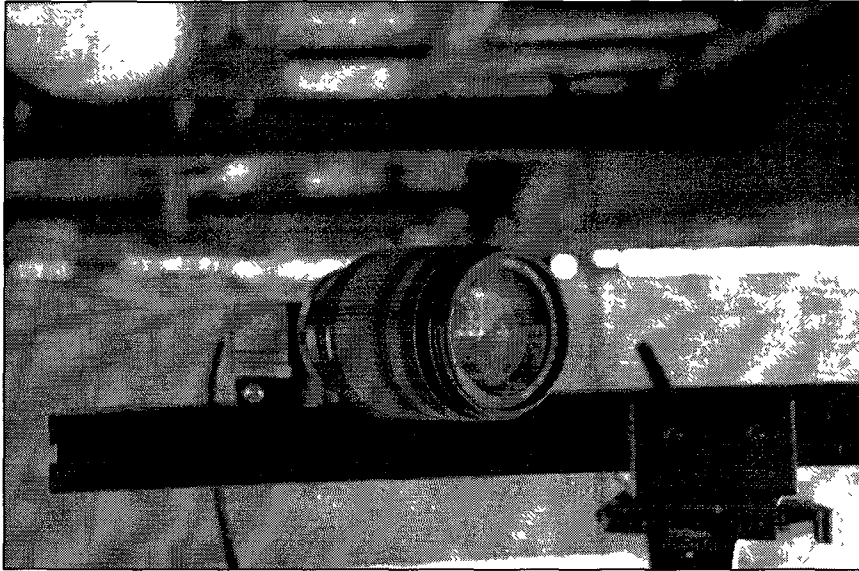


Figure 33 - One of the DIC cameras at the 2011 VAB load test, capturing displacements at station 1.

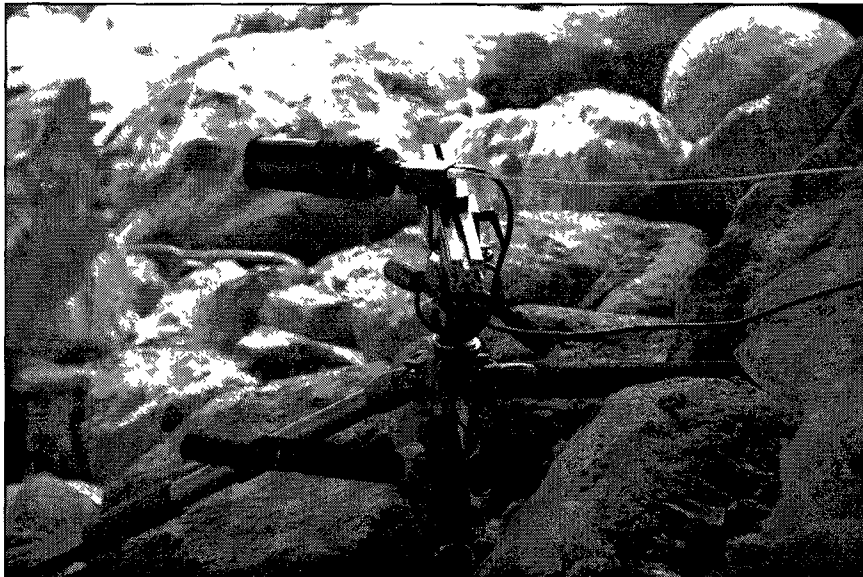


Figure 34 - One of the DIC cameras at the 2011 VAB load test, capturing displacements at stations 8 & 11.

This test demonstrated the capabilities of this particular DIC setup. POIs were located as close as one meter from the cameras and as far as 37 meters. While the results were satisfactory for the most part, post processing and examination of the data revealed some truths that should be taken into account in the next test. Most importantly, the speckle pattern on the targets should be fairly fine, dot diameter less

than or equal to 1 cm, and uniformly cover the entire area of the target. Poor speckle patterns were easily singled out by unacceptable data. Additionally, and somewhat obvious, the closer the POI was to the camera, the cleaner the data was.

Environmental observations at this test were also noted and should be taken into account in future tests. The weather on the day of the test was partly cloudy and because of this the light varied during the tests as clouds blocked the sun. Because the post processing is highly dependent on the grey value of the image varying light can hinder results. The points of interest closer to the center of the bridge had a more constant light source, but the points on the exterior girders experienced major swings of light during the test. Consequently the POIs on the exterior girders returned noisier results.

The data collected during this test was used in conjunction with a FEM that was created in CSiBridge 15.

4.5 The Vernon Avenue Bridge Model

The creation of structural models is a relatively new aspect to bridge design and analysis. Most structural analysis programs use the finite element method (FEM) to perform internal calculations. The analysis package used to model the VAB for purposes of this research was CSiBridge v15.1.1, created by Computers & Structures, Inc. CSiBridge is a well-known software package among state department of transportations (DOT). The model created is considered an enhanced designers model (EDM) (Lefebvre, 2010). A reasonable amount of time was spent to create a model that accurately reflects the bridge's response. Major components including beams, deck, wearing surface, diaphragms, and sidewalk were included but minor elements such as railings and utility pipes were excluded due to an assumed minimal impact on bridge

performance. Although this is an EDM, available data, such as concrete strength and bearing pad data, was implemented to make the model as precise as possible. The goal in creating this structural model is to simulate dead and live load effects on members and use analysis results to assess structural health and derive a load rating that can be compared to traditional techniques.

4.5.1 Model Creation

The CSiBridge software package includes a tool called the Bridge Wizard, formerly known as Bridge Modeler (BRiM) in SAP2000®, which was used to create the model of the VAB. The Bridge Wizard steps the user through a number of value inputs in which information is entered about the bridge, and then creates the model. This section will summarize the information that was inputted into the program at each step and detail how the model was used to formulate a load rating. Screenshots of each step are located in Appendix B.

The layout line is the reference line by which all components of the bridge are laid out. Information included in the layout line is the initial station, end station, and the grade of the bridge, all of which were known from the highway drawings, see Figure 24. The Bridge Wizard does not allow the user to continue until at least one layout line is defined.

4.5.2 Material Properties and Frame Sections

Relevant materials for the bridge are added in the material properties definition window. Grade 345W Weathering steel, grade 60 rebar steel, 4000 psi concrete, and deck concrete were added to the list of materials. The deck concrete properties for the deck in this case were not the design values, but are from core sample test data from the actual deck to more accurately reflect its strength. Table 3 summarizes the

properties of the deck concrete. Using field material measurements makes the model predication of response more accurate.

Table 3 - Material properties entered for deck concrete.

Property	Value
Weight per Unit Volume	21.917 kN/m ³
Modulus of Elasticity	26780000 kN/m
Poisson's Ratio	0.2
Coefficient of Thermal Expansion	9.900E-06
Compressive Strength	34725 kN/m ²

All structural sections are imported in the frame sections dialog. Three rolled steel sections were imported for the steel stringers: W36X232 (English), W920X238 (Metric), W920X201 (Metric) which are the exterior beams, interior beams, and outriggers, respectively. Due to an internal dimension error in CSiBridge, the English section W36X232 was imported instead of the metric section W920X345 for the exterior beams. Five additional sections were also imported to be used as diaphragms: MC460X63.5, C310X45, W100X19.3, L76X76X9.5, and W690X140. Concrete sections were created to be used as the pier cap and bent columns. The user defines the shape and rebar configuration when creating custom concrete sections.

4.5.3 Deck Sections

The assemblage that makes up the cross section of the bridge (beams, haunch, and deck) is created in the deck sections component of the Bridge Wizard. Two sections needed to be created for the VAB because of the addition of the outriggers in the north span. Properties entered in this section are generally geometric and include number of beams, beam spacing, slab thickness, overhang length, as well as other

details (Fay, Spoffard, & Thordike, LLC, 2007). If the user inputs values that create an overlap in geometry the CSiBridge will indicate that the section is not legal and forces the user to correct the error before moving on.

4.5.4 Boundary Conditions

Bridge bearings can be defined in the Bridge Wizard by prescribing fixity for each of the six degrees of freedom, see Figure 35. Elastomeric bearing pad data was available in this case (D.S. Brown Company) and stiffness values were formulated by former graduate students Paul J. Lefebvre and John Phelps (Lefebvre, 2010). In the case that this information is not available, bearing stiffness is a parameter that could be manually updated to match experimental data.

$560 \frac{\text{kN}}{\text{mm}}$	•	•	•	•	•
•	Fixed	•	•	•	•
•	•	Fixed	•	•	•
•	•	•	0	•	•
•	•	•	•	$1765000 \frac{\text{kN}\cdot\text{mm}}{\text{rad}}$	•
•	•	•	•	•	0

Figure 35 - Stiffness values used for specification of the bearing pads.

For the purposes of this research it was decided that any movement of the foundation should be negligible in comparison with the rest of the bridge and therefore all degrees of freedom were fixed. A more in depth study of the bridge and substructure may permit realistic stiffness calculations, especially if a seismic analysis was being conducted. This parameter would be a focus for future work where the model could be updated using modal data.

Bridge abutments were modeled as springs that are attached to the girder (see Figure 36). The girders at the VAB were not cast integrally with the abutments.

Therefore the option was chosen to connect the rigidly stiff foundation springs to the bottom of the girders.

For the two piers, cap beam and column geometry was taken from the structural drawings and both were modeled as the frame sections created earlier. Like the abutments, the pier caps connect to the bottom of the girder only. Also, the VAB is made up of continuous girders, and therefore, has one bearing line on each pier cap.

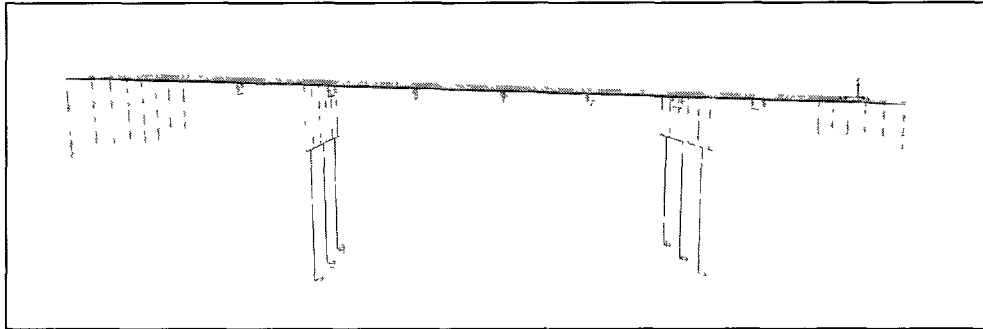


Figure 36 - An elevation view of the structural model.

4.5.5 Bridge Object Definitions

For purposes of this model, the bridge objects definition option is used for defining the span and bent locations. The spans are created by defining the station at which there should be a bent, or the station at which that particular deck section ends and another begins. In this case there are 3 spans and one location where the deck section changes from 6 girders to 8 girders. By default the Bridge Wizard will model a bent at the end of every new section. For example, where there was a change in deck section at station 1109.24, the Bridge Wizard placed a bent. The user must choose the Bents assignment and indicate that there is no bent at the end of that particular section.

4.5.6 Parametric Variations

The Bridge Wizard also allows the user to vary portions of a deck section. The VAB has outriggers where the deck widens on each side of the bridge in the north span

(Figure 37), which is why two deck sections were created in an earlier step. The Bridge Wizard allows you to define the linear change in width over the length of the section. For example, over the 8.813-meter length of one of the outriggers, the spacing increases by 2.38 meters. Since the deck widens and exterior girder spacing increases in the north span, a variation had to be created for each of those elements. The variation is created in this step, but is applied in the next step, deck sections assignment.

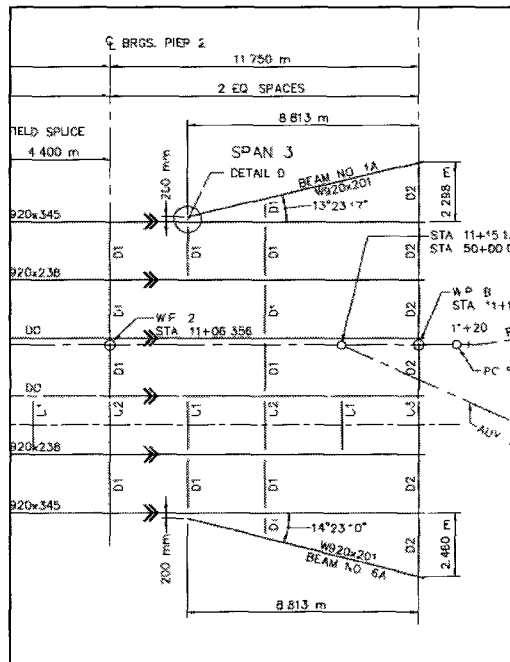


Figure 37 - Outriggers cause a deck variation in span 3.

4.5.7 Diaphragms

Diaphragms were added to the model and provide a significant increase in system stiffness. Eamon and Nowak (2002), it was shown that the addition of diaphragms lowered the AASHTO girder distribution factor of the modeled bridge (Eamon & Nowak, 2002). Information from the structural plans was entered into the diaphragm assignment window and CSiBridge automatically placed the diaphragms into the model.

4.5.8 Update Linked Model

After all structure information is entered into the Bridge Wizard, the user inputs the preferred mesh size and the model is created, this is called updating the linked model. The bridge model can also be unlinked which allows the user to make additions to the bridge that the Bridge Wizard does not recognize. This is the last step in the model creating process. See Figure 38 for the complete bridge model. Figure 39 is the updated linked model in an extruded view, which can help the user verify correctness of geometry. The difference between the two models is purely graphical and represents no difference structural elements.

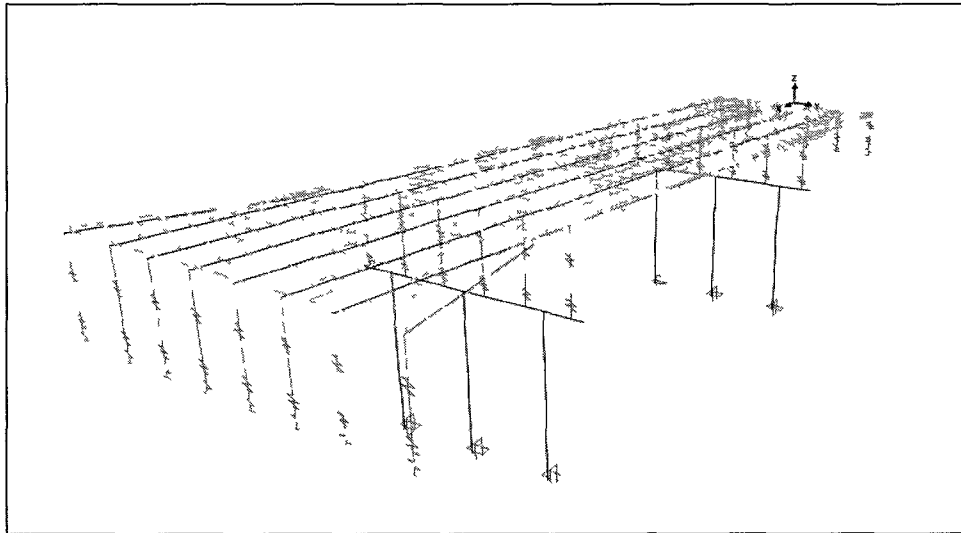


Figure 38 - The updated linked model.

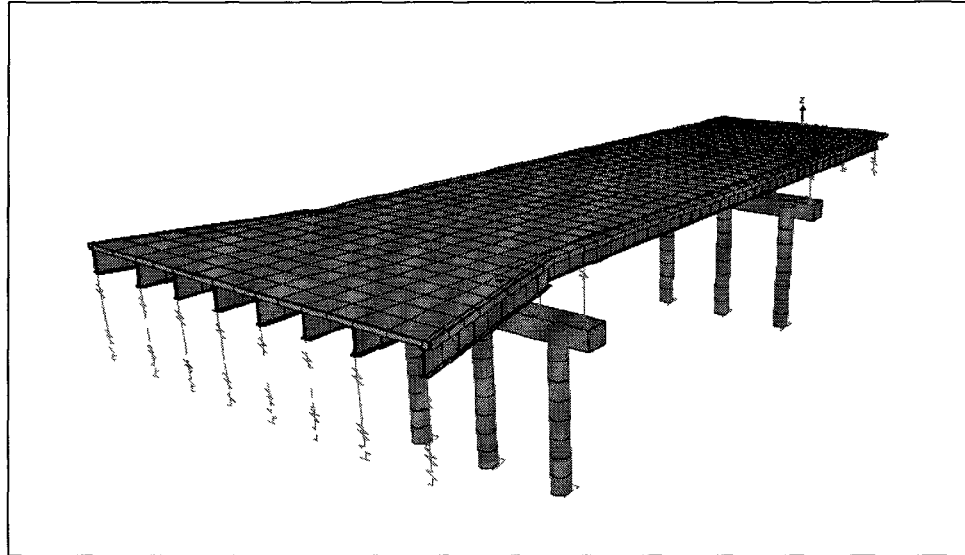


Figure 39 - The updated linked model in an extruded view.

4.5.9 Remarks

The structural model of the Vernon Avenue Bridge took an experienced CSiBridge user approximately 3 hours to create. Factors that influence time are familiarity with the FEM software package, familiarity with the bridge that is being modeled, and how complicated the structure is. Also, not every element on the actual bridge was modeled, as minor elements were left out due to presumed insignificance of influence on bridge response.

The predicted responses from this model are compared to measured responses from DIC in Chapter 5.

CHAPTER 5

INTEGRATION OF LOAD TEST DATA WITH MODEL

A structural model is a modern convenience that is available to today's engineers to use with appropriate judgment. The accuracy of a model can be verified by using field test data which can be considered the truth. Digital image correlation was used to collect displacement data at 18 points on the Vernon Avenue Bridge during the September 2011 load test. This displacement data was used to assess the structural model of the VAB. A load case matching that of the September 2011 load test was created in CSiBridge and model displacements were compared with actual displacements.

5.1 Digital Image Correlation Displacement Results

During the September 2011, a total of 48 single-point, displacement, history-over-time graphs were created. Of the 48 sets of data that were collected, 12 sets correspond to a single load pattern and were used for the research discussed in this thesis. These sets of data represent the vertical response of the bridge, due to the load truck traveling over girder 3, at 2 longitudinal locations: the mid-point of span 2 and the mid-point of the span 1 (Figure 40). Data was collected at points in the north span but not all the data was deemed precise enough for use. All data sets are presented in Appendix A.

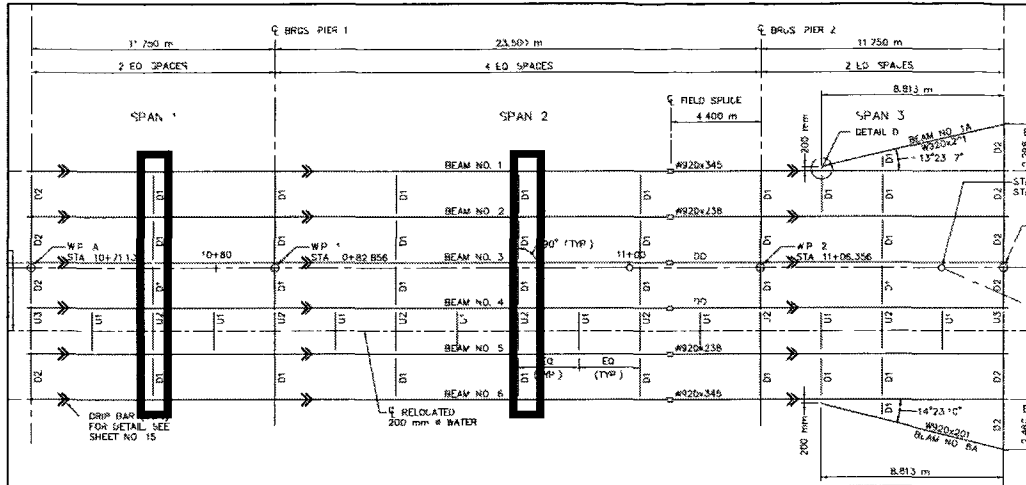


Figure 40 - Transverse displacement measurements were taken at 2 locations along the bridge, indicated by boxes.

Data presented in Figure 41 and Figure 42 show the transverse distribution of displacement on the center of span 2 and the span 1, respectively, due to the load truck travelling across the bridge. Displacements measured on span 1 appear less noisy because they were closer in proximity to the cameras than the center span POIs and had better speckle patterns. Table 4 provides truck locations corresponding to the numbers on the displacements curves.

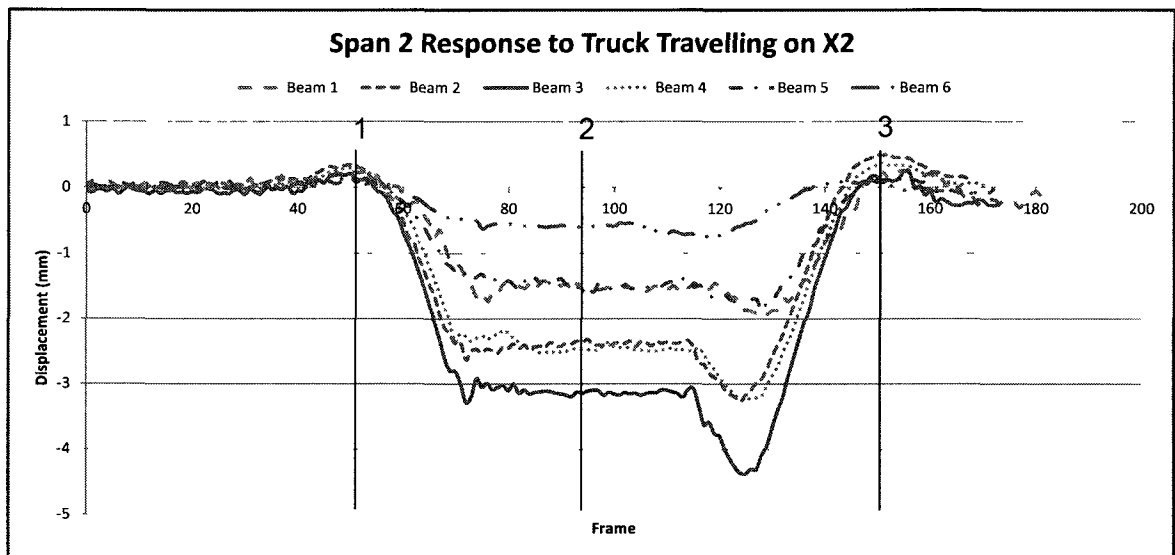


Figure 41 - Displacements on all 6 girders at the midpoint of span 2.

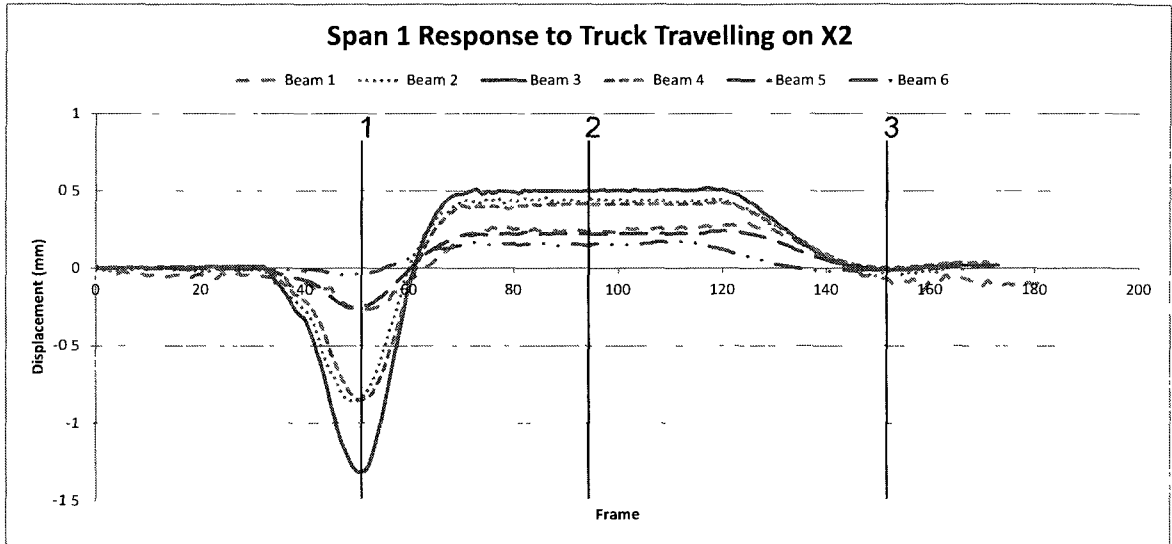





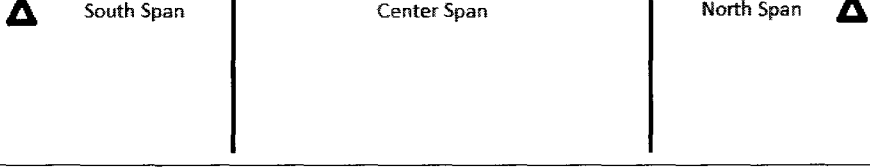


Figure 42 - Displacements on all 6 girders at the midpoint of span 1.

Table 4 - Truck locations corresponding to indicators on graphs.

1	 
2	 
3	 

The transverse distribution of displacements presented in Figure 41 and Figure 42 indicate that the bridge dished in toward girder 3. This response was also seen in graphical model output results.

5.2 Model Assessment

The data collected at the September 2011 VAB load test was used to assess the accuracy of a finite element model. In order to assess the structural model created in CSiBridge, the September 2011 VAB load case had to be created in the program. Creating a vehicle live load in CSiBridge requires the user to 1) define a live load lane 2) define the load truck as a load pattern and 3) assign the load pattern to a load case.

The X2 lane, which straddles girder 3, was defined in the lane editor (see Figure 43). CSiBridge will not allow a vehicle load case to be run without lanes defined. Next, the load truck was created. The front axle weighed 84.78 kN. 5.08 meters behind the front axle, the middle axle weighed 134.7 kN. The rear axle, located 1.41 meters from the middle axle weighed 134.1 kN. The width of each axle was input as 2.13 meters. A load pattern was then created that moved the truck from the south to the north at a speed of 1 m/s. Lastly, the load pattern was assigned to a live load case.

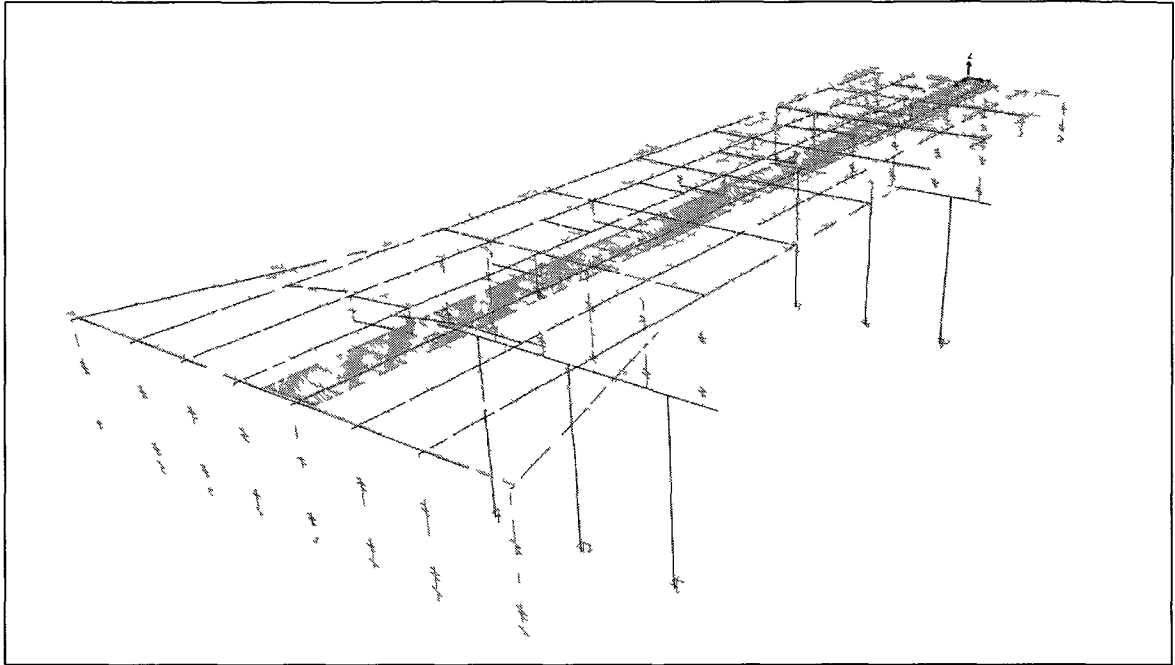


Figure 43 - Lane X2 was defined in CSiBridge

Tables below compare displacement data from the structural model and the load test for span 2 and span 1, respectively. The displacement from DIC and CSiBridge are listed, with the percent difference reported. Figure 44 and Figure 45 provide a visual representation of the correlations between measured and predicted displacement values.

Table 5 – Comparison of maximum negative displacements on span 2

Beam	DIC (mm)	CSiBridge (mm)	Difference (mm)	Percent Difference
1	-1 970	-2 66	0 690	35 0%
2	-3 25	-3 86	0 610	18 8%
3	-4 37	-4 43	0 060	1 4%
4	-3 24	-3 58	0 340	10 5%
5	-1 880	-2 14	0 260	13 8%
6	-0 781	-0 943	0 162	20 7%

Table 6 - Comparison of maximum positive displacements on span 2.

Beam	DIC (mm)	CSiBridge (mm)	Difference (mm)	Percent Difference
1	0.251	0.234	0.017	6.8%
2	0.507	0.252	0.255	50.3%
3	0.244	0.251	0.007	2.9%
4	0.378	0.227	0.151	39.9%
5	0.1439	0.181	0.037	25.8%
6	0.1644	0.130	0.034	20.9%

Table 7 – Comparison of maximum negative displacements on span 1.

Beam	DIC (mm)	CSiBridge (mm)	Difference (mm)	Percent Difference
1	-0.260	-0.418	0.158	60.8%
2	-0.860	-0.810	0.050	5.8%
3	-1.31	-1.040	0.270	20.6%
4	-0.850	-0.800	0.050	5.9%
5	-0.260	-0.440	0.180	69.2%
6	-0.040	-0.180	0.140	350.0%

Table 8 - Comparison of maximum positive displacements on span 1.

Beam	DIC (mm)	CSiBridge (mm)	Difference (mm)	Percent Difference
1	0.291	0.318	0.027	9.3%
2	0.457	0.337	0.120	26.3%
3	0.521	0.337	0.184	35.3%
4	0.428	0.301	0.127	29.7%
5	0.242	0.239	0.003	1.2%
6	0.1739	0.164	0.010	5.7%

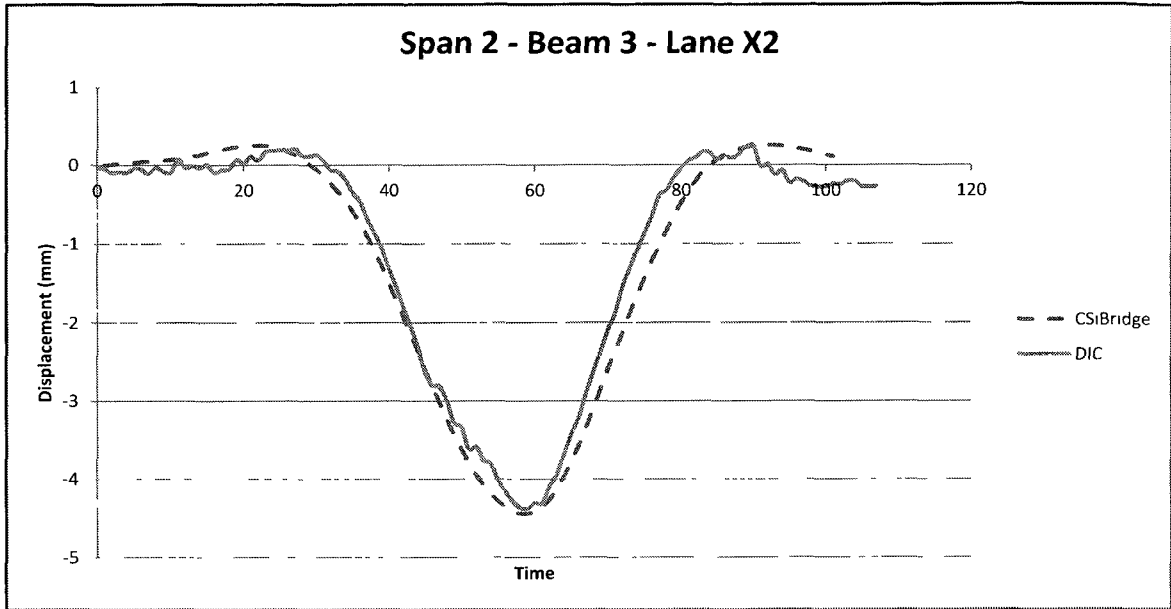


Figure 44 - Displacement results from DIC and CSiBridge at the midspan of beam 3.

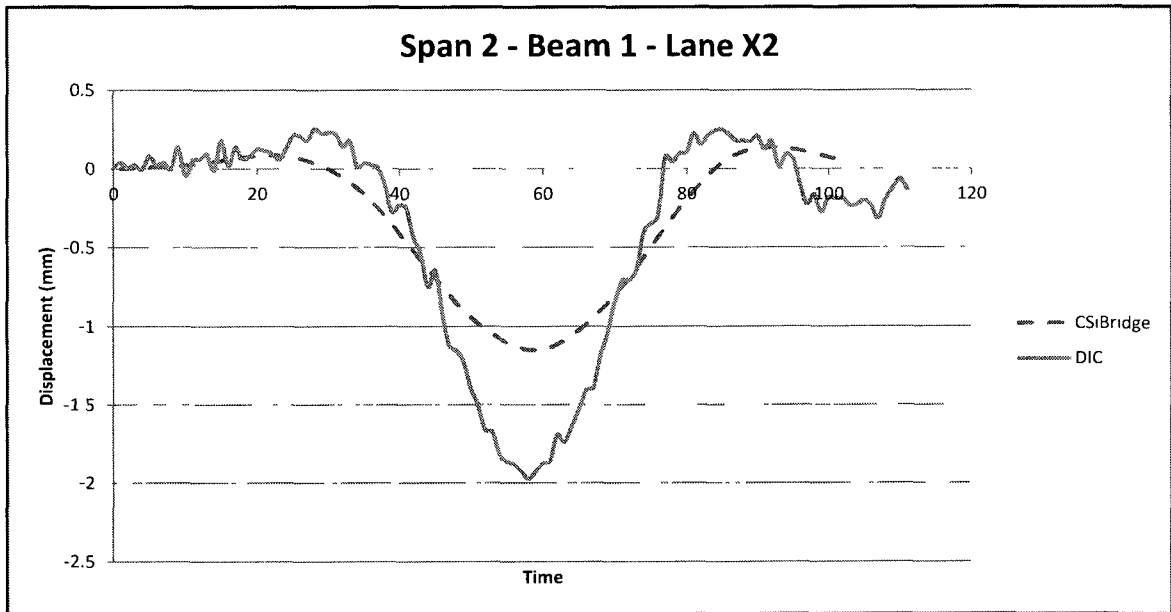


Figure 45 - Displacement results from DIC and CSiBridge at the midspan of beam 1.

A statistical analysis was conducted on the difference between measured values and predicted values for displacements measured (Figure 46). The sample population is made up of the difference between 23 measured and predicted displacements. The previously mentioned data point that exhibited an error of 350% was considered an

outlier and removed from the data set. Omitting this value, there was an average delta of 0.127 mm, or 22%, and a standard deviation of 0.207 mm, or 19%. The 95% confidence interval for percent error is 16% to 30%. Tables below offer more detailed statistics and were created using JMP statistical analysis software. Values being compared are only the maximum and minimum displacements from each test.

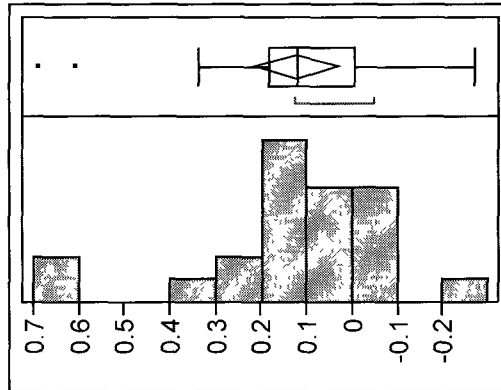


Figure 46 - Histogram and outlier box plot of error. Units are in mm.

Table 9 - Error quintiles.

100.0%	maximum	0.69
99.5%		0.69
97.5%		0.69
90.0%		0.502
75.0%	quartile	0.184
50.0%	median	0.12
25.0%	quartile	-0.007
10.0%		-0.05
2.5%		-0.27
0.5%		-0.27
0.0%	minimum	-0.27

Table 10 - Error moments.

Mean	0.126
Std Dev	0.211
Std Err Mean	0.044
Upper 95% Mean	0.218
Lower 95% Mean	0.035
N	23

Table 11 – 95% confidence interval associated with model error.

Parameter	Estimate	Lower CI	Upper CI	1-Alpha
Mean	0.126	0.035	0.218	0.950
Std Dev	0.211	0.163	0.298	0.950

5.3 Discussion of Model Accuracy

The goal of assessing any structural model is determining the degree of accuracy to which the model provides and to be able to accept that model as accurate (Thacker, et al., 2004). Defining the state of acceptably accuracy is difficult. Different systems may have different acceptance criteria. A simple system, such as a simply supported beam, may have an acceptability threshold of 1% error, but an intricate system, such as a bridge, should have a higher error threshold as a function of its complicated nature. Classifying a model as “accurate enough” is the responsibility of the user as there is no standard currently in place for acceptability criteria of a structural model. As a goal of future research, a protocol for acceptability of structural models should be developed.

Comparisons of the results indicate that there are some measurements that match the model well and others that do not. The maximum negative displacement at girder 6 on the south span shows the largest discrepancy of 350 percent. Upon further investigation of this particular value, the speckle pattern that was used at this location was not an effective one, the lighting was too dark and the field of view only captured half of the target (Figure 47). Figure 48 shows a speckle pattern that provided better result. Beam 6 was also the farthest beam from the applied load.



Figure 47 - An ineffective speckle pattern (south span of girder 6).

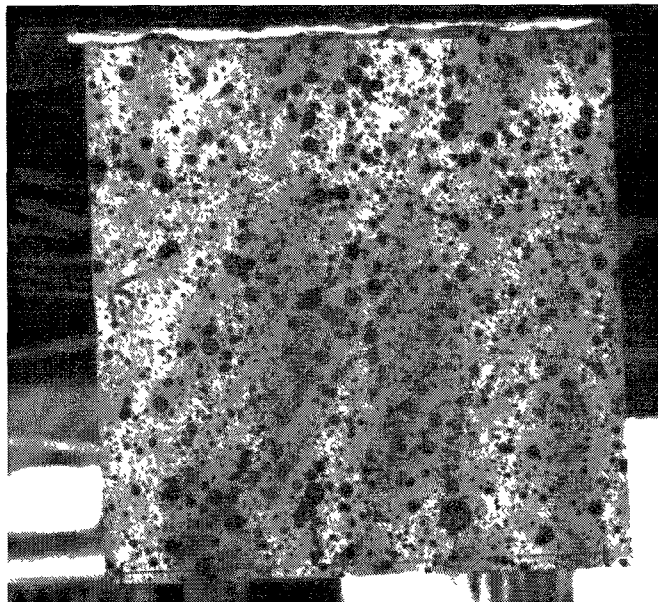


Figure 48 - An effective speckle pattern (south span of girder 4).

The confidence in the accuracy and precision of DIC measurements was found to be high for targets with reliable speckle patterns and illumination. Repeatability, an important testing characteristic, of DIC results at the VAB load test was confirmed (Table 12).

Table 12 - Repeatability of the DIC measurements was confirmed.

Test #	Girder 4, South Span	Girder 4, Center Span
Run 33	-1.265 mm	-3.850 mm
Run 34	-1.247 mm	-3.769 mm
Run 35	-1.252 mm	-3.853 mm

The 95% confidence interval associated with the difference between measured and predicted data is such that there will be an error between .03mm and .21mm for the majority of measurements. A larger sample size may provide more conclusive results, and could be achieved with additional testing with many more points of displacement data.

CHAPTER 6

LOAD RATING OF THE VERNON AVENUE BRIDGE

Load rating of bridges has been a mandated aspect of bridge management since the 1960s (Mn/DOT, 2008). In an ideal world all bridges would be load rated in a similar fashion and results would be stored in a national database for comparison between similar structures. Despite efforts for standardization, all bridges are not load rated equally. There is a tendency to load rate using the methodology of which the bridge was designed; LRFD, LFD, or ASD. This seems like a logical choice but each methodology results in different rating factors. Additionally, rating factors, as they are calculated today, do not take into account the behavior of a bridge as a system which could result in a more favorable rating factor. The general equation for a rating factor is Equation 7-1 (AASHTO, 2011).

$$RF = \frac{\text{Capacity} - \text{Dead Load}}{\text{Live Load}} \quad 7-1$$

If the rating factor (RF) is less than 1 the bridge is not capable of safely carrying the prescribed live load and the bridge must have a posted weight limit enforced. If the rating factor is greater than 1, the bridge is fully capable of carrying the live load that it was designed for and is considered adequate. Live load and dead load values are calculated using unit weights for materials and vehicles. The capacity of the bridge is calculated by taking the strength of the bridge as designed and then subtracting strength to account for section loss or damage to concrete such as spalling. Load factors are added to each of the components as applicable (AASHTO, 2011).

To explore the differences in load rating techniques, 10 rating factors were developed using 5 different methods; LRFR, LFR, ASR, structural modeling and experimental field testing. The calculations for each method can be found in Appendix C, and were completed in MathCAD. Table 13 summarizes equations used for LRFR, LFR, and ASR. An inventory and operating rating factor was developed for each method. An inventory level rating is defined as “the capacity rating for which the vehicle type used in the rating that will result in a load level which can safely utilize an existing structure for an indefinite period of time.” An operating level rating is defined as “the absolute maximum permissible load level to which the structure may be subjected for the vehicle type used in the rating. This rating determines the capacity of the bridge for occasional use (DeIDOT, 2009).” Figure 49 describes the load rating process.

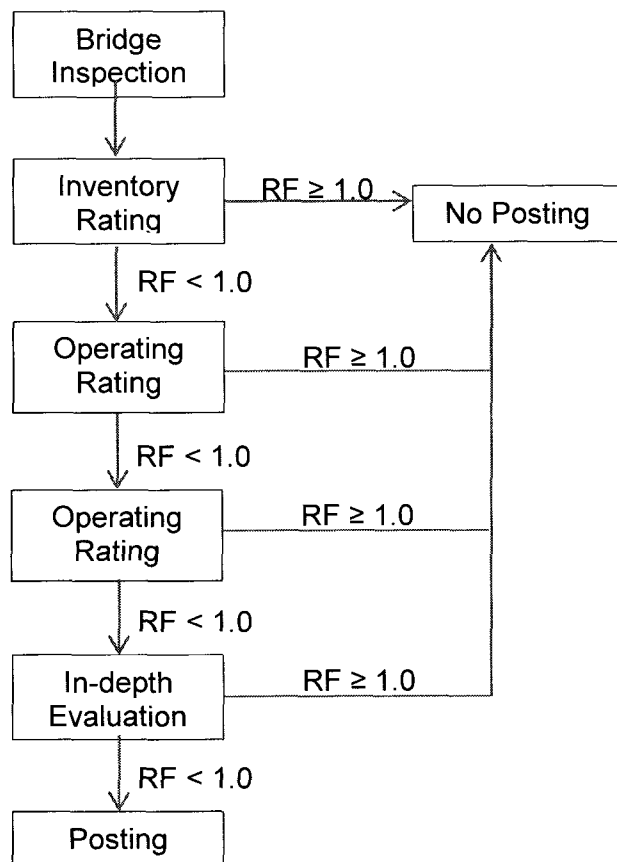


Figure 49 – Flow chart of load rating decisions.

Table 13 - Equations and factors of the three different load rating methodologies.

	ASR	LFR	LRFR
Equation	$\frac{C - (A_1)(D)}{(A_2)L(1 + I)}$	$\frac{C - (A_1)(D)}{(A_2)L(1 + I)}$	$\frac{C - (Y_{DC})(DC) - (Y_{DW})(DW) \pm (Y_p)(P)}{(Y_{LL}) * (LL + IM)}$
Dead Load Factor	$A_1 = 1.0$	$A_1 = 1.3$	$Y_{DC} = 1.00 - 1.25$ $Y_{DW} = 1.50$ $Y_p = 1.00$
Live Load Factor	$A_2 = 1.0$	$A_2 = 1.3$ or 2.17	$Y_{LL} = 0.80 - 1.75$
Impact Factor	Varies	Varies	$IM = 0.33$

Table 14 - Factor definitions

Factor	Definition
C	Capacity of the member
A_1	Factor for dead loads
A_2	Factor for live loads
D	The dead load effect on the member
L	The live load effect on the member
I	The impact factor
DC	Dead load effect due to structural components
DW	Dead load effect due to wearing surface and utilities
P	Permanent loads other than dead loads
LL	Live load effect
IM	Dynamic load allowance
Y_{DC}	LRFD load factor for structural components and attachments
Y_{DW}	LRFD load factor for wearing surfaces and utilities
Y_{LL}	LRFD load factor for live loads

Some general assumptions were applied to the LRFR, LFR, and ASR methods in this research. First, positive moment capacity included the beam and the deck, acting in composite, but negative moment capacity only included the capacity of the beam as a conservative measure. Secondly, dead load was distributed evenly to all girders, though one exception to this assumption was the self-weight of the beams. Distribution of dead loads evenly across all beams is a common assumption and is used when designing multi-girder bridges as well. The outriggers were not included in any of the hand calculations. Lefebvre (2010) found that the dead load distributed to the 6 main girders did not differ when the north span width increased. Lastly, some dead loads were not taken into consideration because they were not included in the structural model, including the ductile iron water pipe and steel railing.

A considerable difference between the three load rating methods is the live load that is applied to the member. In LRFR, the HL-93 design live load is applied whereas in LFR and ASR only the HS-20 design truck is applied (AASHTO, 2011). The HL-93 is a combination of the HS-20 design truck (Figure 50) and a distributed live load of 9.34 kN/m to each lane. The smaller live load in LFR and ASR is compensated for in the distribution factor which is more conservative than that of the LRFR distribution factor.

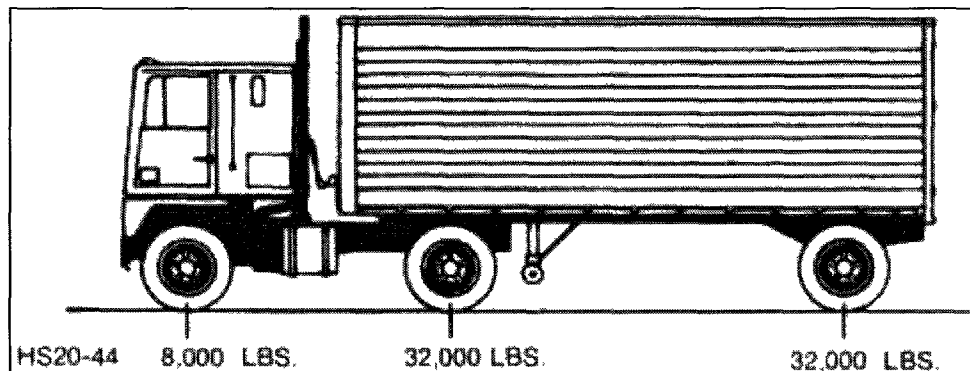


Figure 50 - The HS-20 design truck.

The general procedure for developing a load rating is the same for all methods: the capacity of the section is found, dead loads are calculated, and then live loads are calculated taking into account the distribution factor. The capacity and loads are then input into an equation with appropriate safety factors applied.

6.1 Distribution Factor

The distribution factor (DF) is used in bridge design to prescribe a probabilistic percentage of live load in a lane to a girder for analysis (AASHTO, 2011). For example, if a DF is calculated to be .650, this means that 65% of the live load would be applied to the girder during analysis. As design methodologies have evolved over the years, so has the distribution factor.

For steel girder bridges, ASR and LFR distribution factors are calculated by dividing the on-center beam spacing by 5.5, a relatively simple calculation compared to LRFR. LRFR divides distribution factor calculations into 4 categories; interior girder, exterior girder, one lane loaded, and two or more lanes loaded. Equations 7-2 and 7-3 represent the equations for an interior girder with one lane loaded an interior girder with two lanes loaded, respectively. The greater of the two values controls.

$$mg = 0.06 + \frac{S^{0.4}}{14} + \frac{S^{0.3}}{L} + \left(\frac{K_g}{12.0Lt_s^3} \right)^{0.1} \quad 7-2$$

$$mg = 0.075 + \frac{S^{0.6}}{9.5} + \frac{S^{0.2}}{L} + \left(\frac{K_g}{12.0Lt_s^3} \right)^{0.1} \quad 7-3$$

$$e = .77 + \frac{d_e}{9.1} \quad 7-4$$

$$g = e g_{interior} \quad 7-5$$

When calculating the DF for an exterior beam with one lane loaded, the lever rule is used (Figure 51). The lever rule is executed by summing the moments from two wheel (point) loads, and the exterior girder, about the first interior girder assuming the deck is hinged over the interior girder. For an exterior girder with two or more lanes loaded, equations 7-4 and 7-5 are used. Again, the greater of the two values controls. These equations were taken from the AASHTO LRFD Bridge Design Specifications, Fifth Edition, and are located in Table 4.6.2.2b-1 and Table 4.6.2.2d-1. It is important to note that all values entered into these equations must be English units.

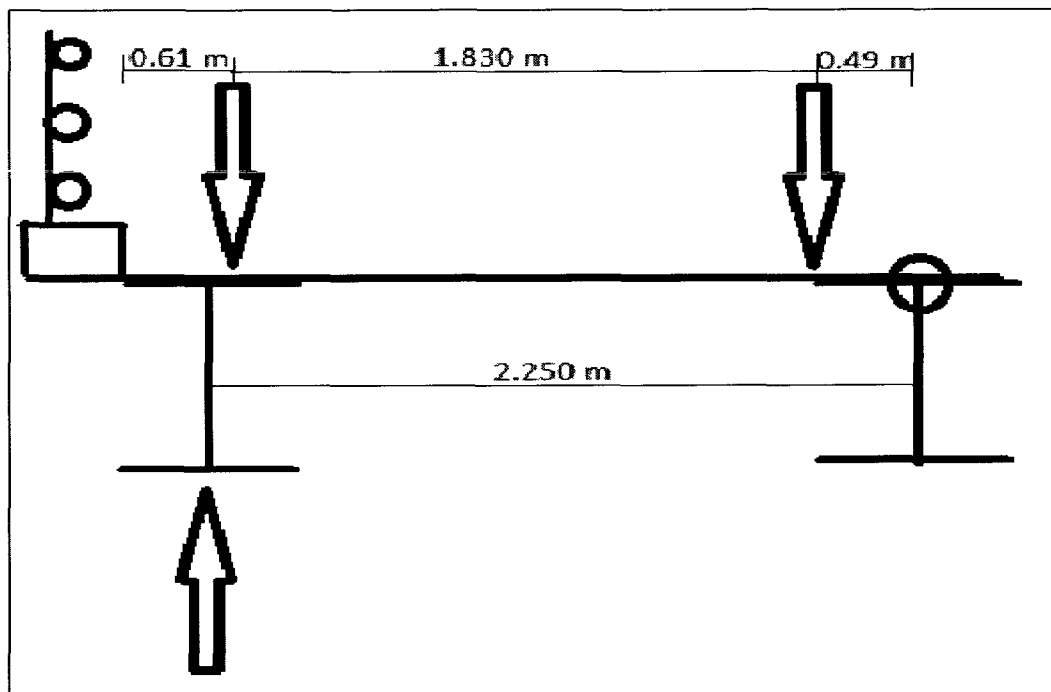


Figure 51 - The lever rule as applied to the VAB.

6.2 Load and Resistance Factor Rating

LRFR is the latest method to be adopted by AASHTO, therefore this is the method by which all other methods will be compared to. A DF of .569 was calculated for interior girders and .514 for exterior girders. Other factors that had to be chosen were dead load factor, wearing surface factor, live load factor, and impact factor. The dead load and wearing surface factors are 1.25 and 1.50, respectively. The impact factor

applied to wheel loads was 1.33. The live load factor varies depending on what type of rating is being conducted, 1.75 for inventory and 1.35 for operating.

Many rating factors may be calculated for a bridge, but the lowest value controls. Thus, the controlling LRFR factor for an interior beam was 2.08 and 2.70 for inventory and operating, respectively. The rating factors for an exterior beam were 3.79 and 4.91 for inventory and operating, respectively. The controlling rating factors on the VAB were due to maximum negative plastic moments in all instances.

6.3 Load Factor Rating

Based on the load factor design methodology LFD, load factor rating varies from LRFR in several ways including the distribution factor, live load, load factors, and equation. The distribution factor for LFD, for both interior and exterior beams, is calculated as 1.34, which seems quite conservative, but is offset by less conservative load factors and live load.

The dead load factor is 1.30 for both inventory and operating ratings and the live load factor is 2.17 for inventory and 1.30 for operating. The impact factor is calculated as 0.247 using Equation 7-6. Note that L, which is the length of the span, must be in the units of feet when using this equation.

$$\frac{50}{L + 125} \qquad 7-6$$

The load factor rating method resulted in interior girder rating factors of 1.07 and 1.79 for inventory and operating ratings, respectively. For exterior girders, values of 1.77 and 2.95 were calculated for inventory and operating ratings, respectively.

6.4 Allowable Stress Rating

Allowable stress ratings are calculated using the same formula as LFD but are based on maximum allowable stress and account for different stages of composite action of the bridge deck section. Dead load effects are split into two categories; dead load and superimposed dead load. Dead load includes all loads that are present before the bridge section acted in composite. Superimposed dead loads are those loads that were added after composite action began, including wearing surface and sidewalk. The dead load moments are multiplied by the ratio of the short term composite section modulus to the non-composite section modulus. The superimposed dead load moment is multiplied by the ratio of the short term composite section modulus to the long term composite section modulus and the dead load effect is normalized by the construction stage at which the load acts on the girder.

$$\frac{C - D_{DL} - D_{SDL}}{L(1 + I)} \quad 7-7$$

While load factors are taken as 1.0 for both inventory and operating, the allowable stress capacity for an inventory rating is reduced to $.55F_y$ and $.75F_y$ for an operating factor. Equation 7-7 produced an inventory rating factor for interior and exterior beams of 0.99 and 1.52, respectively and operating rating factors of 1.46 and 2.17.

6.5 Load and Resistance Factor Rating with Structural Model

Of the five rating factors being formulated in this research one depends heavily on the response of the structural model. Using a structural model for load rating can be advantageous because of the ability to induce damage in a particular area of the deck or on one of the girders, which is not possible when load rating by hand calculations. For example, if there was section loss on a 4-meter section of an exterior girder it would be

easy to decrease the area on that particular area and run an analysis. If the bridge were load rated by hand calculations, the section loss would have to be applied to the entire girder resulting in a lower rating factor. The model would report a moment that takes into account the redistribution of load due to the damage.

The model also has the advantage of analyzing the bridge as a system. Diaphragms, adjacent beams, and the deck all act together when a load is applied to a real bridge. Unlike approximate analysis, the EDM takes into account this extra strength.

Similar to the model assessment procedure, the HL-93 load case had to be created in CSiBridge. Three 3.65 meter lanes were defined initially (Figure 52). The HL-93 live load case is made up of an HS-20 design vehicle and a distributed lane load. The standard axle loads of the HS-20 were multiplied by 1.33 to account for impact before being entered into the Bridge Wizard. The HL-93 load pattern was multiplied by 1.75 in the live load case for an inventory rating. When the analysis is run, the program moves a design vehicle in each lane from the south span to the north span at a constant speed.

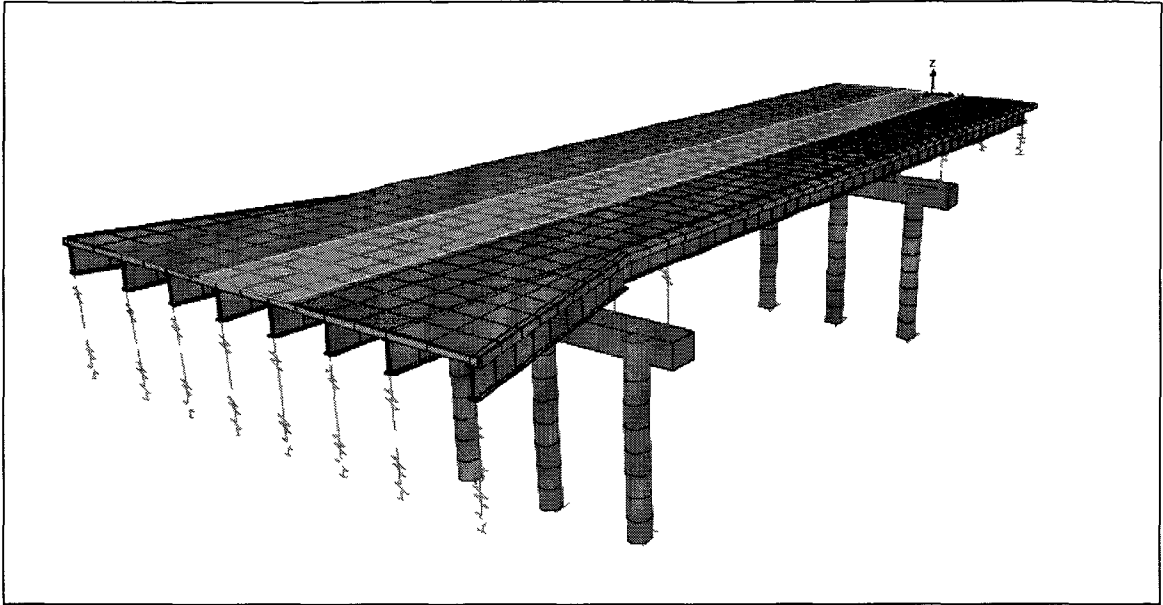


Figure 52 - The three lanes can be seen in different shades.

In addition to the dead load of the bridge components, the loads of the sidewalk and wearing surface were also included in the model. Area loads were created for the sidewalk and pavement in the units of force per area. The pavement's load was entered as 0.88 kN/m and the sidewalk's load was 10.92 kN/m. The area loads were assigned to a load pattern, which were then assigned to a load case that encompassed dead loads. Multipliers were added to each load in the load case and were 1.25 for DC loads and 1.50 for DW loads.

After creating the structural model and applying load cases, the model was ready for analysis. Correctly running the analysis and understanding the results is as important as making an accurate model. The live load and dead load cases are run separately so that the effect that each has on the bridge can be independently evaluated. It should be noted that running each load case separately is only a valid assumption while the structure is acting in the elastic range. Figure 53 shows the model's maximum/minimum deflected shape envelope due to the live load case.

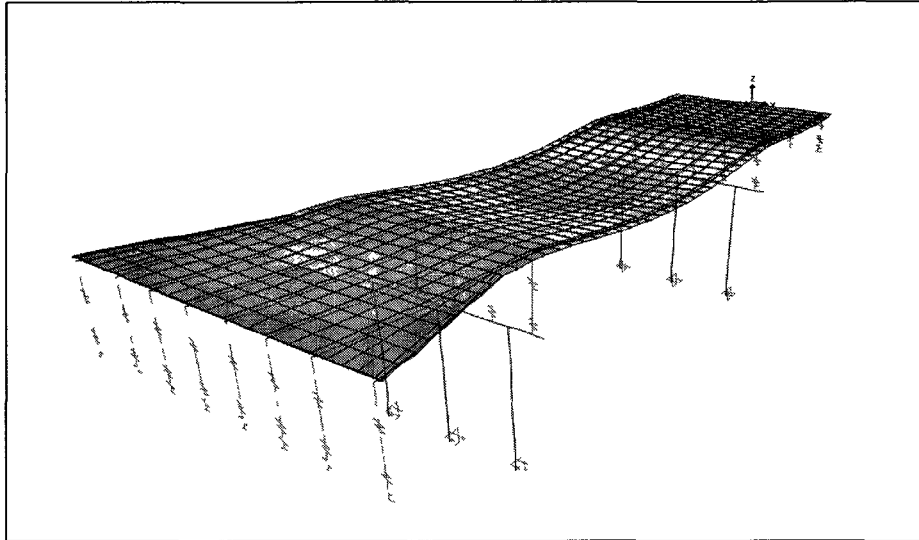


Figure 53 - A screenshot of the EDM's enveloped maximum deflected shape due to live load.

The maximum dead load and live load effects, listed in Table 15 and Table 16, were used in the LRFR formula. The capacity of the member was taken as the hand calculated capacity because the structural model does not readily provide a capacity value. This method produced inventory ratings of 2.07 and 2.68 for interior girders and exterior girders, respectively, and operating ratings of 2.96 and 3.83.

Table 15 – Maximum positive moments due to live load and dead load from the enhanced designer's model.

Girder	LL Moment (kN-m)	DL Moment (kN-m)
1	1445	568
2	1238	517
3	1289	599
4	1306	682
5	1211	771
6	1452	1108

Table 16 – Maximum negative moments due to live load and dead load from the enhanced designer’s model.

Girder	LL Moment (kN-m)	DL Moment (kN-m)
1	1319	709
2	1196	650
3	1245	715
4	1245	803
5	1154	952
6	1312	1379

The time it took an experienced user to create this model and run an analysis was approximately 6 hours and it would take much less to update it with inspection data every 24 months. A baseline model that has been verified with field test data such as displacements from digital image correlation has the potential to be a valuable tool in bridge management by producing accurate results at a low cost.

6.6 Load and Resistance Factor Rating with Experimental Distribution Factor

By definition a distribution factor describes what percentage of the live load vehicle(s) falls into the load path of a particular girder. Traditional load rating equations use a calculated DF that is elemental by nature of design. As an alternative and more realistic method of formulating a DF, researchers investigated the distribution of displacement during a load test in which one tri-axle drove over the bridge. Previous research has successfully used strain to estimate load distribution, displacement is a similar idea (Chajes, et al., 1997). Figure 54 shows the transverse distribution of both displacement and strain during a pass in which the test truck travelled directly above girder 3. The responses were normalized by moment of inertia to account for varying girder sizes (Figure 54).

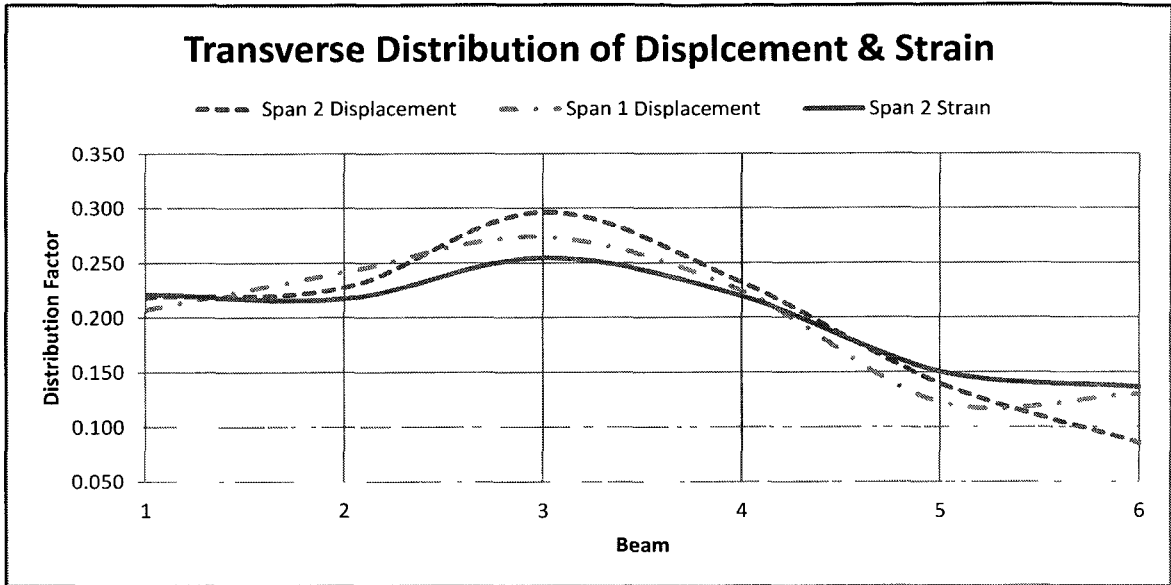


Figure 54 – The transverse distribution of displacement and strain during due to the truck travelling over beam 3.

Center Span Displacement						
Girder	Displacement	I (mm ⁴)	DF	Normalized DF	Corrected	with m
1	-1.50	6.24E+09	0.130	0.200	0.182	0.219
2	-2.40	4.06E+09	0.208	0.208	0.190	0.228
3	-3.13	4.06E+09	0.271	0.271	0.247	0.296
4	-2.45	4.06E+09	0.212	0.212	0.193	0.232
5	-1.47	4.06E+09	0.128	0.128	0.116	0.140
6	-0.59	6.24E+09	0.051	0.078	0.071	0.086
Sum	-11.54	2.87E+10	1.00	1.10	1.00	
Center Span Strain						
Girder	Strain	I (mm ⁴)	DF	Normalized DF	Corrected	with m
1	22.00	6.24E+09	0.134	0.206	0.185	0.221
2	33.20	4.06E+09	0.202	0.202	0.181	0.217
3	38.90	4.06E+09	0.237	0.237	0.212	0.255
4	33.50	4.06E+09	0.204	0.204	0.183	0.219
5	23.00	4.06E+09	0.140	0.140	0.126	0.151
6	13.55	6.24E+09	0.083	0.127	0.114	0.136
Sum	164.15	2.87E+10	1.00	1.12	1.00	

Figure 55 - A spreadsheet was created that normalized displacement and strain values.

Substituting the experimental greatest DF, .296, into the LRFR equation yielded inventory rating factors of 6.93 and 9.47 for interior and exterior, respectively, and operating rating factors of 8.98 and 12.28. As expected, these factors are considerably higher than factors from other methods because there is no factor of safety built into the

DF. Also, due to the nature of the load test, a DF for a scenario in which two trucks pass over the bridge side by side was not possible.

6.7 Summary of Rating Factors

Five methods were utilized to develop rating factors for the Vernon Avenue Bridge. Three of the methods, LRFR, LRF, ASR, were traditional methods and the remaining two were experimental methods that took advantage of structural modeling software and field testing. Table 17 and Table 18 summarize the results. The ratings that take into account the structural model and experimental distribution factor were calculated using the LRFR equation and should therefore be compared to the LRFR rating. The LFR and ASR ratings were calculated for comparison with the LRFR hand calculated rating.

Table 17 - A summary of all interior beam rating factors.

Method	Interior Inventory		Interior Operating	
	Positive	Negative	Positive	Negative
LRFR	3.59	2.08	4.65	2.70
Model / LRFR	3.90	2.07	5.05	2.68
DF from Δ / LRFR	6.89	4.00	8.93	5.19
LFR	1.68	1.07	2.80	1.79
ASR	1.24	0.99	1.88	1.52

Table 18 - A summary of all exterior beam rating factors.

Method	Exterior Inventory		Exterior Operating	
	Positive	Negative	Positive	Negative
LRFR	5.46	3.79	7.07	4.91
Model / LRFR	4.64	2.96	6.00	3.83
DF from Δ / LRFR	9.48	6.57	12.28	8.52
LFR	2.31	1.77	3.85	2.95
ASR	1.61	1.46	2.38	2.17

6.8 Remarks

Five methods were used to load rate the VAB to demonstrate the wide array of values that can be used to describe a single bridge's condition. The experimental methods were based on the LRFR method because it is the newest of the three methods, and should only be compared with the hand calculated LRFR factor. Factors based on the model for interior girders were either the same or slightly higher than hand calculations, but the factors for exterior girders were lower than hand calculations in all cases. A distribution factor of .514 was used for exterior beams in hand calculations, a value that was heavily influenced by the short horizontal distance between the curb and web of exterior beam. The model most likely distributed more load to the exterior girder because of the presence of diaphragms. This was expected because structural models act as a system, rather than only a beam and concrete block section that is used in analysis.

The factors derived using a distribution factor based on transverse displacements was much higher than any of the other factors because it was based on actual measurements, not approximate analysis. Although this method seems to provide a

more “real” bridge response, further research into the use of experimental distribution factors, based on displacements, is necessary. Additionally, the distribution factor used in this case was found by applying a truck load in one lane only. A different factor may have been found if two lanes had been loaded or if a lane load was applied to the bridge.

Observations were also made about the three traditional methods. Comparison between the three methods is not simple which highlights the lack of standardization over the years in bridge evaluation. This also further complicates the decision making process for bridge owners. If all the bridges in the inventory are rated using different methods, funding may not be allocated to the bridge in the worst condition. Combined with the subjective nature of current inspection practices, the ranking system of bridges in need of replacement is in need of revision.

CHAPTER 7

CONCLUSIONS & FUTURE WORK

Contributions of this research have taken steps towards creating a more objective protocol for assessing bridge performance. Displacements collected using LVDTs are reference dependent and typically difficult to measure due to access. Digital image correlation, a non-contact, easily deployable system for displacement measurements, has shown potential to be used in conjunction with visual inspections for a more holistic understanding of bridge health. Innovative displacement collection aids have been fabricated to be used with DIC. Lastly, a new technique for finding an in-situ distribution of live load on bridges has been explored.

Previous research has shown that DIC is able to collect reliable deformation data, with a high degree of accuracy, in controlled environments. Through laboratory and field testing, this research project verified DIC as an efficient means for collecting bridge performance data, capable of being deployed in non-controlled environments, such as a field test at a bridge. Data collection techniques were developed to make DIC a cost and time effective tool that produces results comparable to that of LVDTs. Although the initial investment of a DIC system is substantial, the return can be realized quickly in ease of use, accessibility, and versatility.

A third load test was conducted at the Vernon Avenue Bridge in September of 2011, at which DIC was able to successfully collect 48 sets of displacement data from underneath the bridge, out of the way of traffic. This method of data collection could be implemented into routine inspections, using inspection vehicles to excite a bridge response, as an objective metric for bridge health.

An enhanced designer's model of the VAB was created in a time-efficient manner, incorporating known material properties, using CSiBridge® 15. Model accuracy was assessed using DIC displacement data from the VAB load test. The model response was representative of the measured response in shape and magnitude. A sample size of 23 measured and predicted displacement values were compared, the average difference was .127 mm, or 22%. In general, larger displacements matched better than smaller displacements. It was determined that error may be attributed to non-uniformity of speckle patterns and illumination during testing, as well as model error. Efforts should be made in future load tests to eliminate varying speckle patterns and illumination.

An experimental distribution factor was formulated using the transverse distribution of displacements. It was observed that the experimental DF was less than half of that calculated by AASHTO LRFD equations. Although these results seem to provide a more "real" distribution of load, it should not be implemented into analysis due to the small sample size and limited applications at this time, and is a key area for future research.

The VAB was load rated using 5 methods which included LRFR, LFR, ASR, model-based LRFR, and an LRFR using a distribution factor based on the transverse distribution of displacements. The model-based LRFR resulted in a factor that was lower for exterior beams but higher for interior beams. The rating factor based on an experimental distribution factor was at least 50% higher than the traditional value in all cases. These five methods resulted in a wide range of rating factors for a single bridge, which highlights the need for a more uniform bridge rating system.

This research has several impacts on the bridge health monitoring community including the addition of a cost-effective bridge response measurement tool (DIC), innovative collection techniques using DIC, and the potential for a new metric for measuring load distribution.

7.1 Recommendations for Future Work

Though this research project was a successful one, lessons were learned throughout the duration of the project that should be taken into account in future applications. Application of the lessons learned will increase the accuracy, reliability, and precision of the DIC system.

Special care should be taken when creating speckle patterns for future bridge tests. A uniform template should be created so that each pattern is the same and error due to a poor pattern is minimized. One way to do this might be to drill many different sized holes in a piece of sheet metal, and apply the spray paint through it, or by printing an optimum speckle pattern on page-sized sticker labels. By regulating the speckle pattern, the user can focus their efforts on mitigating the effects of other variables.

It was found that capturing data during the hours of daylight can lead to compromised data, due to inconsistent illumination. An attempt to use DIC during a nighttime load test might result in more reliable data. Several spot lights would need to be implemented to provide artificial light. In addition to the beneficial effects on DIC, there will likely be less traffic to work around during the night, creating a safer work environment. Another measure that might be used is to attach a small LED flash light to each PVC pipe with a bracket. This would provide uniform illumination throughout the duration of the test, independent of ambient light.

An investigation into the effects of collecting image data at an angle should be conducted. All testing in this research was conducted while positioning the cameras on the same horizontal plane as the speckle pattern. If the position of the camera setup is able to drift below or above this plane, opportunities for successful testing will increase. Further investigation should determine the maximum angle at which measurements can be reliably collected.

Lastly, a protocol should be created for assessing the accuracy of structural bridge models through comparison of displacements. Factors that might be taken into account include the ratio of degrees of freedom in the model to the degrees of freedom that were measured, error threshold, and loading conditions.

This research project has demonstrated that DIC can be a valuable enhancement to current bridge inspection practices. Further investigation into the capabilities and benefits of digital image correlation will act as a stepping stone in the advancement of the bridge management paradigm.

REFERENCES

- AASHTO, 2011. *Manual for Bridge Evaluation*. s.l.:American Association of State and Highway Transportation Officials .
- American Society of Civil Engineers New Hampshire Section, 2011. *Report Card for New Hampshire's Infrastructure*, Manchester: ASCE NH.
- American Society of Civil Engineers, 2011. *2009 Report Card for America's Infrastructure*, Washington, D.C.: ASCE.
- Anon., 1908. For Bridge Testing. *Uxbridge Compendium*, 28 August.
- ASNT, 2011. *Introduction to Nondestructive Testing*. [Online]
Available at: <http://www.asnt.org/ndt/primer1.htm>
[Accessed 6 October 2011].
- Brogan, P. A., 2010. *Digital Image Correlation Application to Structural Health Monitoring*. s.l.:University of New Hampshire.
- Celesco, n.d. *What's a String Pot?*. [Online]
Available at: <http://celesco.com/faq/cet.htm>
[Accessed 11 January 2011].
- Chajes, M. J., Mertz, D. R. & Commander, B., 1997. Experimental Load Rating of a Posted Bridge. *Journal of Bridge Engineering*.
- Chiara, P. & Morelli, A., 2010. *Bridge Testing With Ground-Based Interferometric Radar: Experimental Results*. s.l., American Institute of Physics, pp. 202-208.
- Chu, T. C., Ranson, W. F., Sutton, M. A. & Peters, W. H., 1985. Applications of Digital-Image-Correlation Techniques to Experimental Mechanics. *Experimental Mechanics*, pp. 232-244.
- DeIDOT, 2009. *DeIDOT BRidge Design Manual*. [Online]
Available at:
http://www.deldot.gov/information/pubs_forms/manuals/bridge_design/pdf/bdm-04-bridge-rating.pdf
[Accessed 25 October 2011].
- Eamon, C. D. & Nowak, S. A., 2002. Effects of Edge-Stiffening Elements and Diaphragms on Bridge Resistance and Load Distribution. *Journal of Bridge Engineering*, pp. 258-266.
- Fay, Spoffard, & Thordike, LLC, 2007. *Plan and Profile of Bridge Replacement No. B-02-012*. s.l.:s.n.

- Federal Highway Administration, 2011. *LTBP: Long-Term Bridge Performance*. [Online] Available at: <http://www.fhwa.dot.gov/research/tfhrc/programs/infrastructure/structures/ltpb/index.cfm> [Accessed 5 November 2011].
- FHWA, 2011. *Status of the Nation's Highways, Bridges, and Transit: 2004 Conditions and Performance*. [Online] Available at: <http://www.fhwa.dot.gov/policy/2004cpr/chap15a.htm> [Accessed 28 October 2011].
- Graybeal, B. A. et al., 2002. Visual Inspection of Highway Bridges. *Journal of Nondestructive Evaluation*, pp. 68-83.
- Grubb, M. A., 1997. LFD vs. LRFD - What's Up With the Letter 'R' Anyway?. *Modern Steel Construction*, March.
- Ha, D., 2009. *Cost of NDT systems* [Interview] 2009.
- Hamm, S., 2009. *The Bridge to Smart Technology*. [Online] Available at: http://www.businessweek.com/magazine/content/09_09/b4121042656141.htm [Accessed 25 October 2010].
- Jin, G., Chen, J. & Meng, L., 2005. *Applications of Digital Correlation Method to Structure Inspection*. Beijing, China, SMIRT18, pp. 4005-4011.
- Lefebvre, P., 2010. *The instrumentation, testing, and structural modeling of a steel girder bridge for long-term structural health monitoring*. Durham: University of New Hampshire.
- Macro Sensors, n.d. *What Is An LVDT?*. [Online] Available at: http://www.macrosensors.com/lvdt_tutorial.html [Accessed 11 January 2011].
- Mahajan, A., Pilch, A. & Chu, T., 2000. *Intelligent Image Correlation using Genetic Algorithms for Measuring Surface Deformations in the Autonomous Inspection of Structures*. Chicago, s.n., pp. 460-461.
- Malesa, M. et al., 2010. *Monitoring of civil engineering structures using Digital Image Correlation technique*. s.l., EDP Sciences.
- Mayer, L., Yanev, B. S., Olson, L. D. & Smyth, A. W., 2010. *Monitoring of Manhattan Bridge for Vertical and Torsional Performance with GPS and Interferometric Radar Systems*. Washington, DC, Transportation Research Board.
- Mn/DOT, 2008. *Bridge Rating 101*. [Online] Available at: <http://www.dot.state.mn.us/stateaid/LoadRatingClass101/BridgeRatingClass101allsections.pdf> [Accessed 4 April 2011].

National Cooperative Highway Research Program, 1998. *Manual for Bridge Rating Through Load Testing*, Washington, D.C.: Transportation Research Board.

Pan, B., Qian, K., Xie, H. & Asundi, A., 2009. Two-dimensional digital image correlation for in-plane displacement and strain measurement: a review. *Measurement Science and Technology*, p. 2.

Roberts, G., Cosser, E., Xiaolin, M. & Dodson, A., 2004. High Frequency Deflection Monitoring of Bridges by GPS. *Journal of Global Positioning Systems*, pp. 226-231.

Santini Bell, E., Sanayei, M., Javdekar, C. N. & Slavsky, E., 2007. Multiresponse Parameter Estimation for Finite-Element Model Updating Using Nondestructive Test Data. *Journal of Structural Engineering*, pp. 1069-1079.

Santini-Bell, E. et al., 2011. *Digital Imaging for Bridge Deflection Measurement of a Steel Girder Composite Bridge*. Washington, D.C., Transportation Research Board.

Sensorland, n.d. *How sensors work - strain gauge*. [Online]
Available at: <http://www.sensorland.com/HowPage002.html>
[Accessed 11 January 2011].

Thacker, B. H. et al., 2004. *Concepts of Model Verification and Validation*, s.l.: Los Alamos National Laboratory.

Transportation for America, 2011. *The Fix We're In For: The State of Our Nation's Bridges*, Washington, D.C.: Transportation for America.

U.S. Department of Transportation, 2011. *About-LTBP: Long-Term Bridge Performance Program*. [Online]
Available at:
<http://www.fhwa.dot.gov/research/tfhrc/programs/infrastructure/structures/ltbp/about.cfm>
[Accessed 20 April 2011].

Whittemore, M. D. & Durfee, R. H., 2011. *Low-Cost Rehabilitation with FRP Strips*. Pittsburgh, s.n.

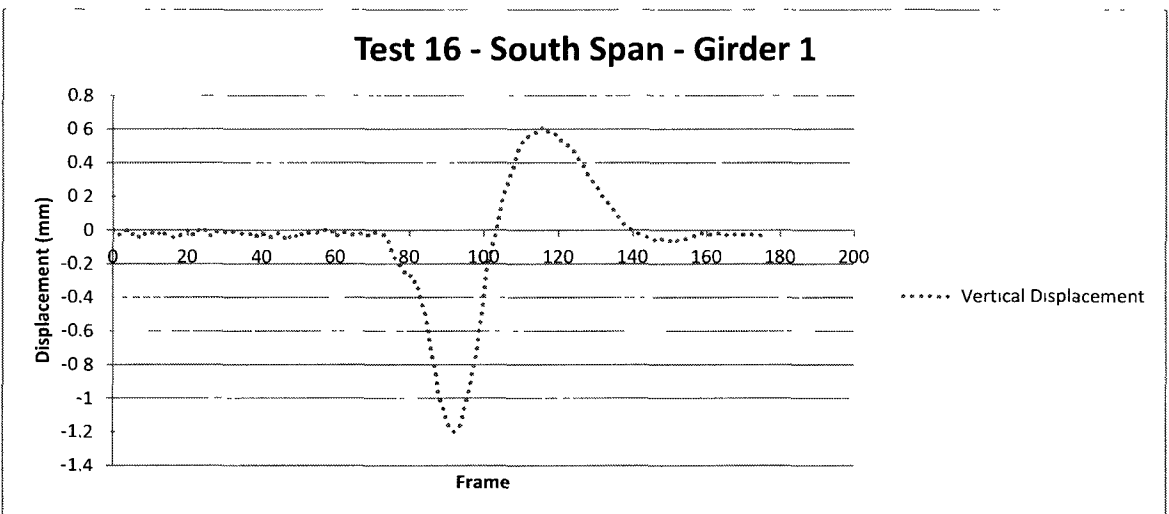
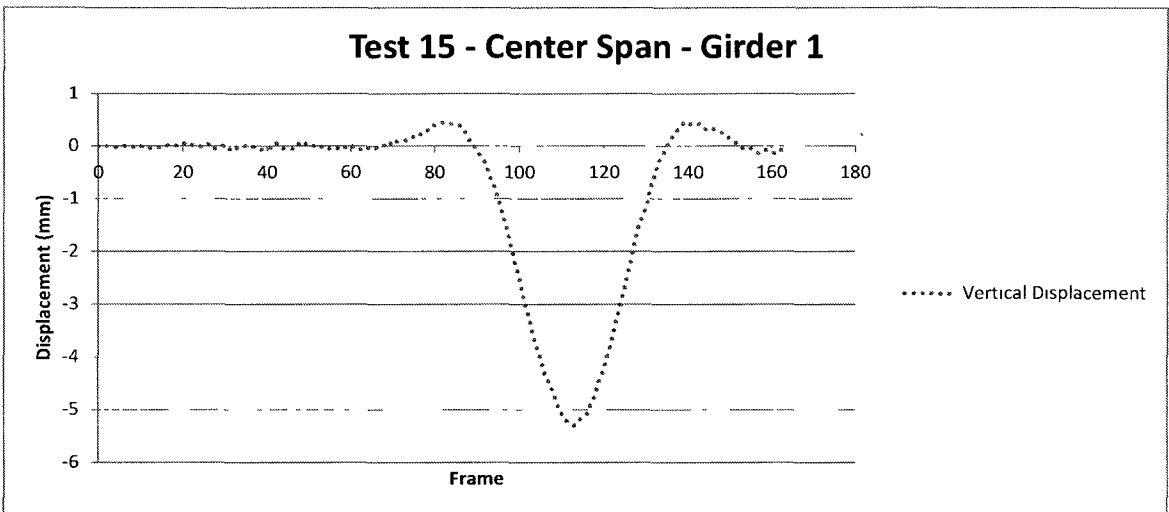
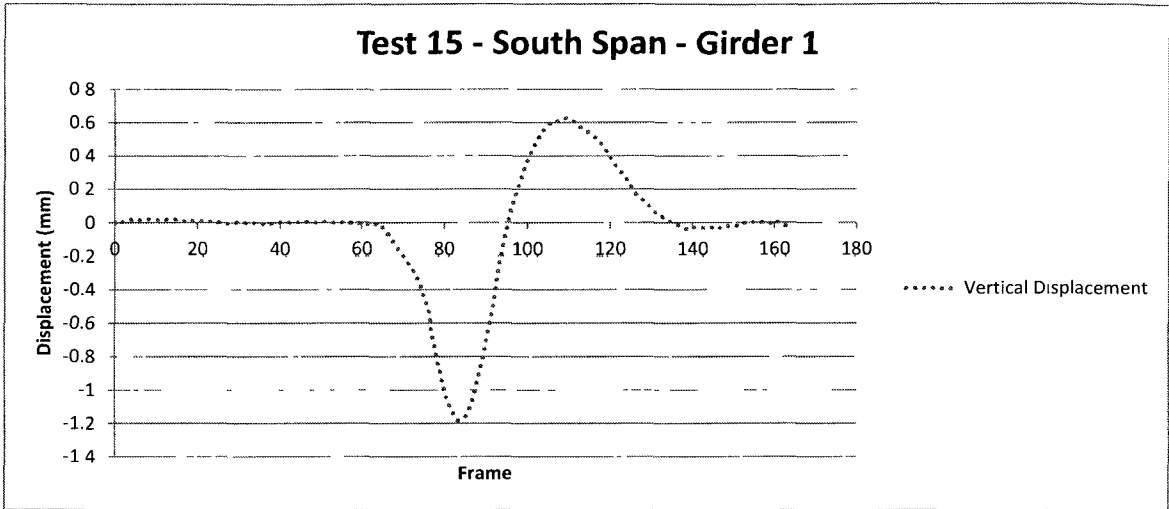
Yang, G. & Wu, K., 2007. Principles and research of a high accuracy digital image correlation measurement system. *Optical Engineering*, 21 May.

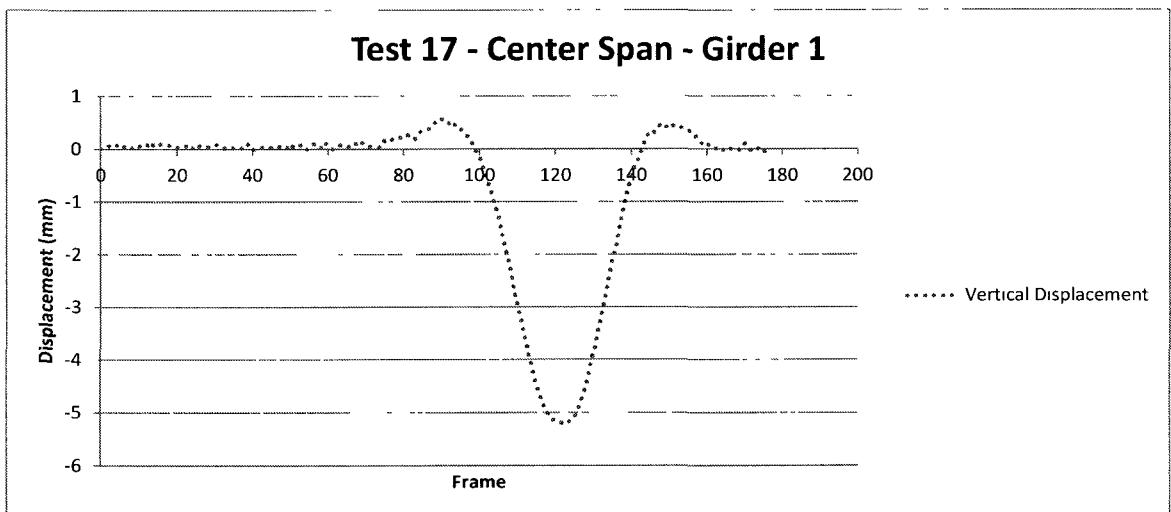
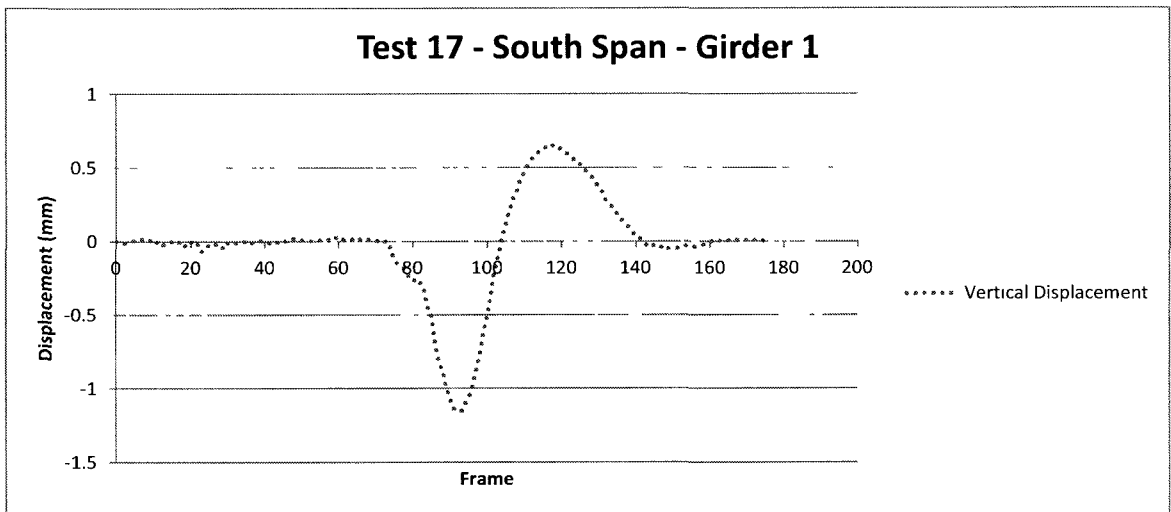
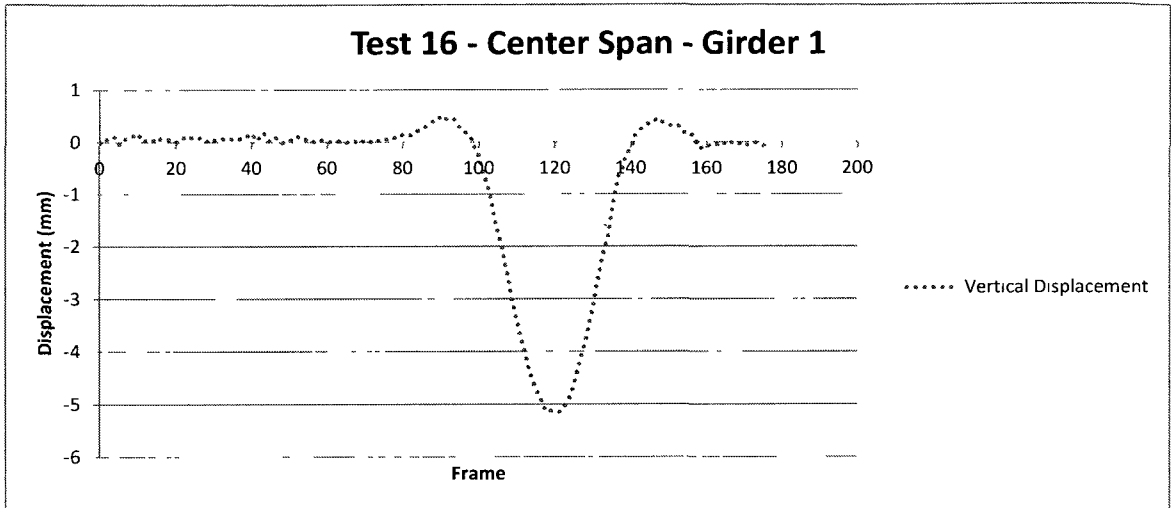
Yoneyama, S. et al., 2007. Bridge Deflection Measurement Using Digital Image Correlation. *Experimental Techniques*, pp. 34-40.

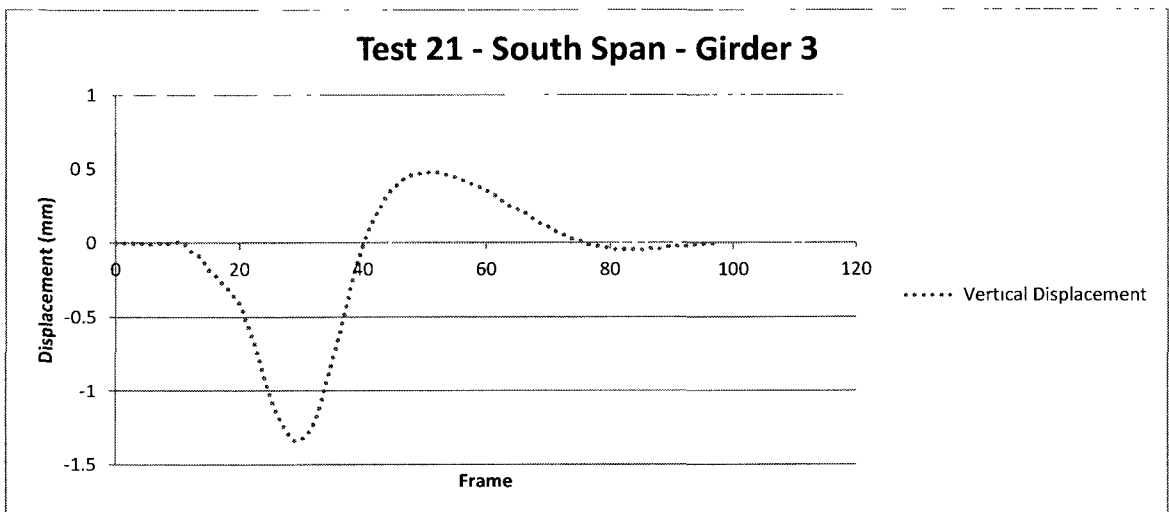
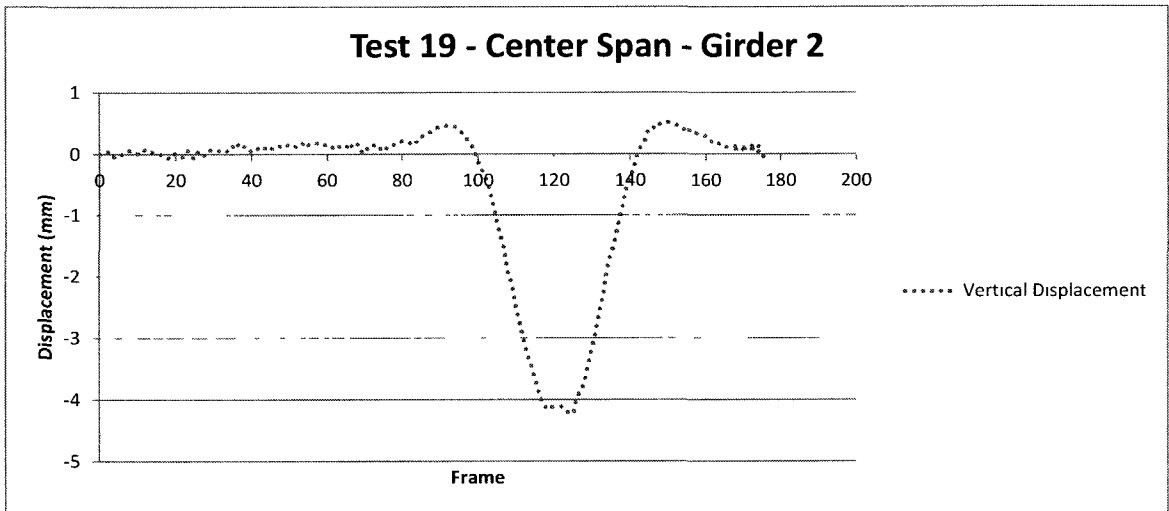
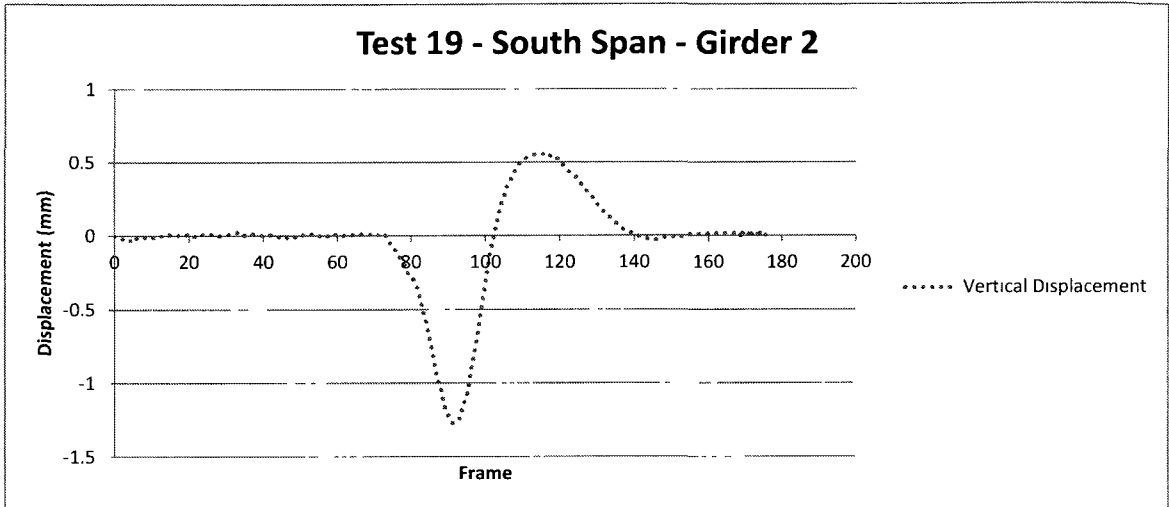
APPENDIX A: 2011 VAB LOAD TEST DATA

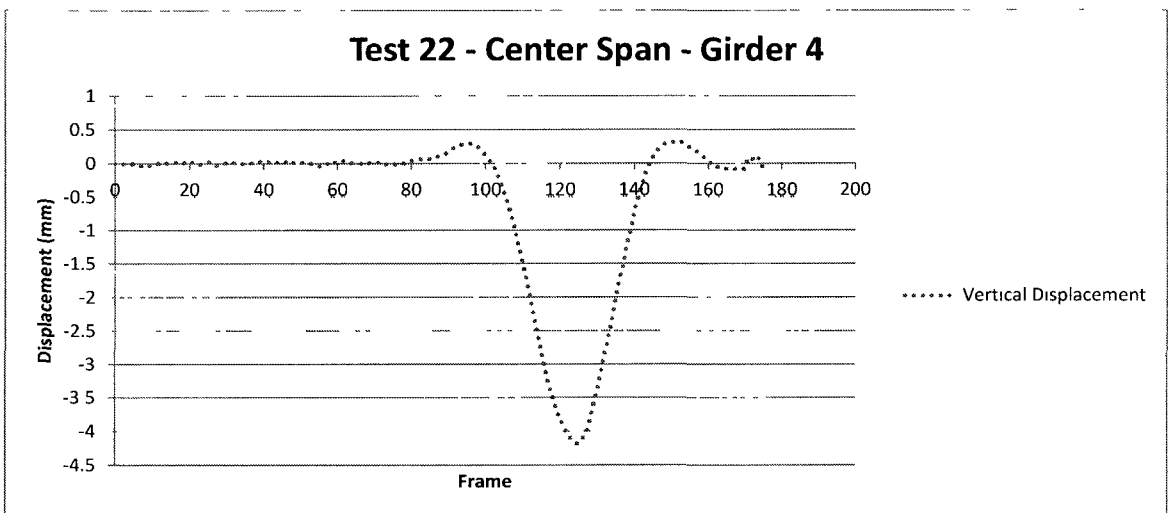
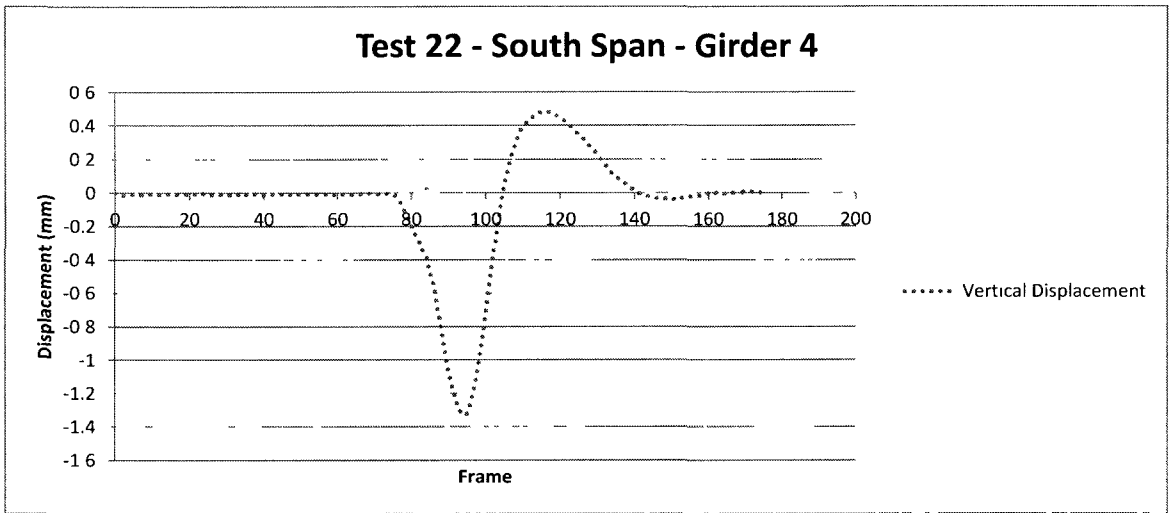
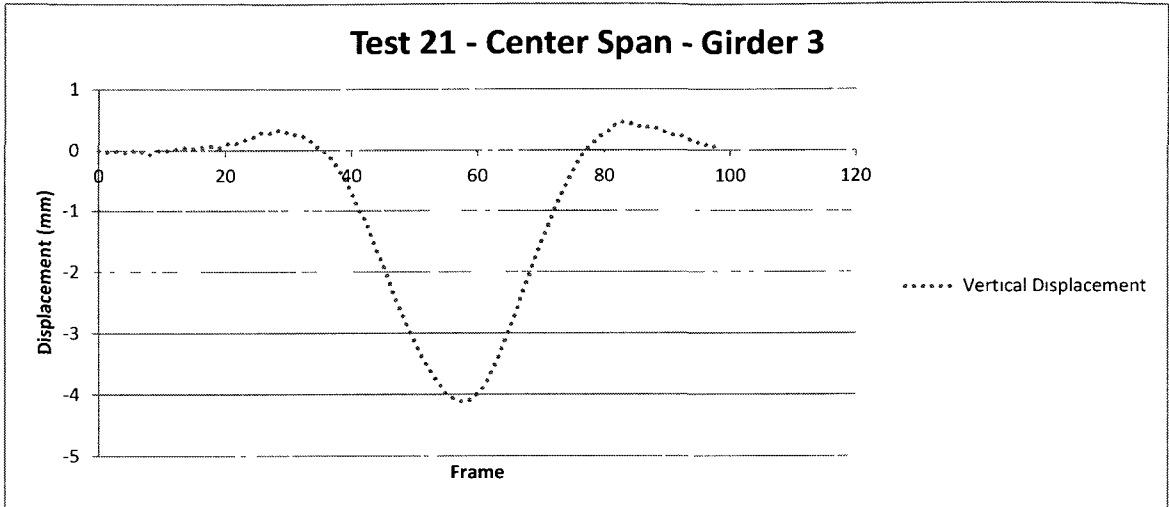
A load test was conducted on September 25, 2011 at the VAB. The load test schedule and displacement data is presented in Appendix A.

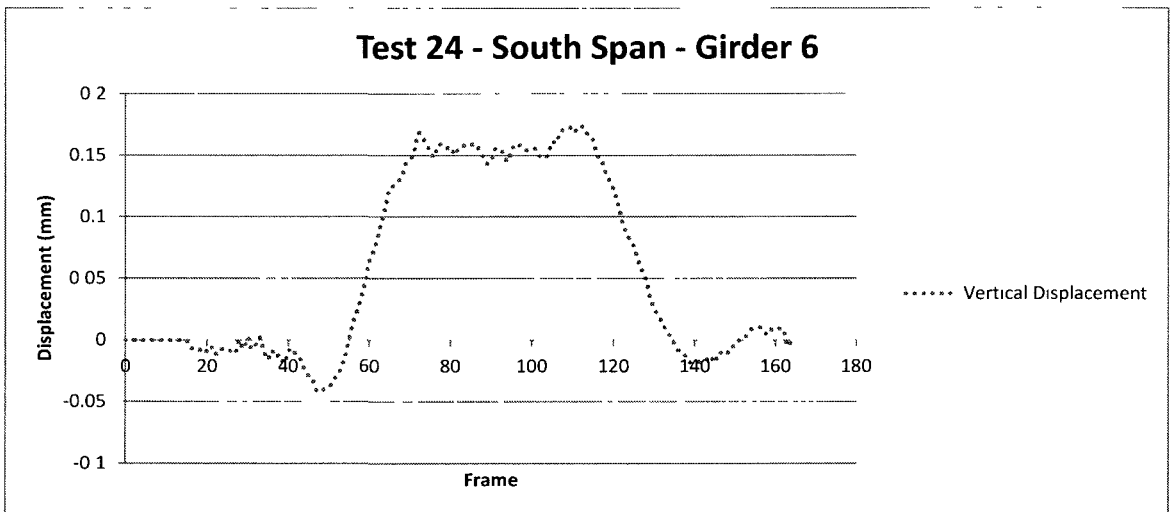
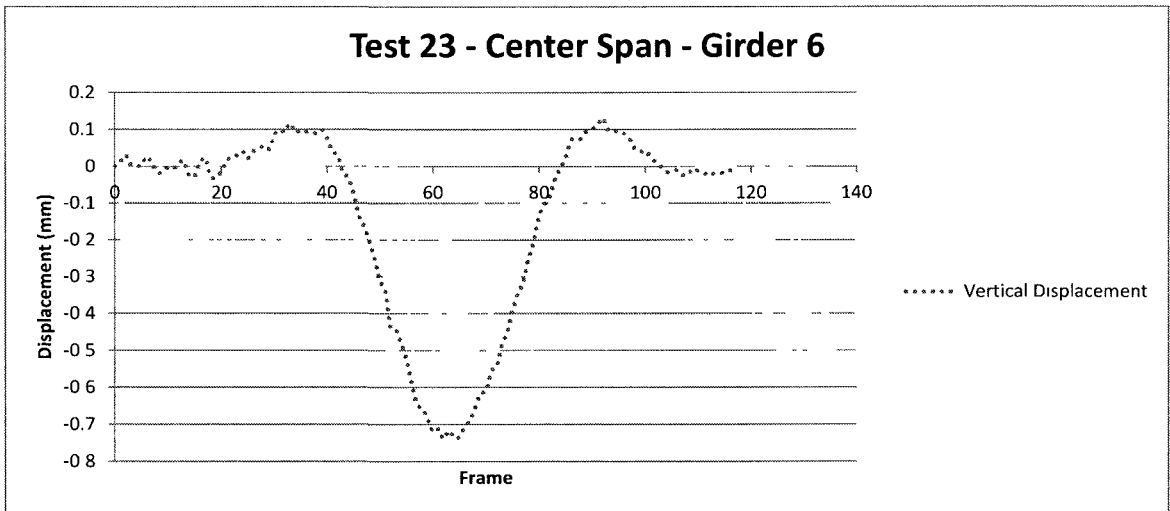
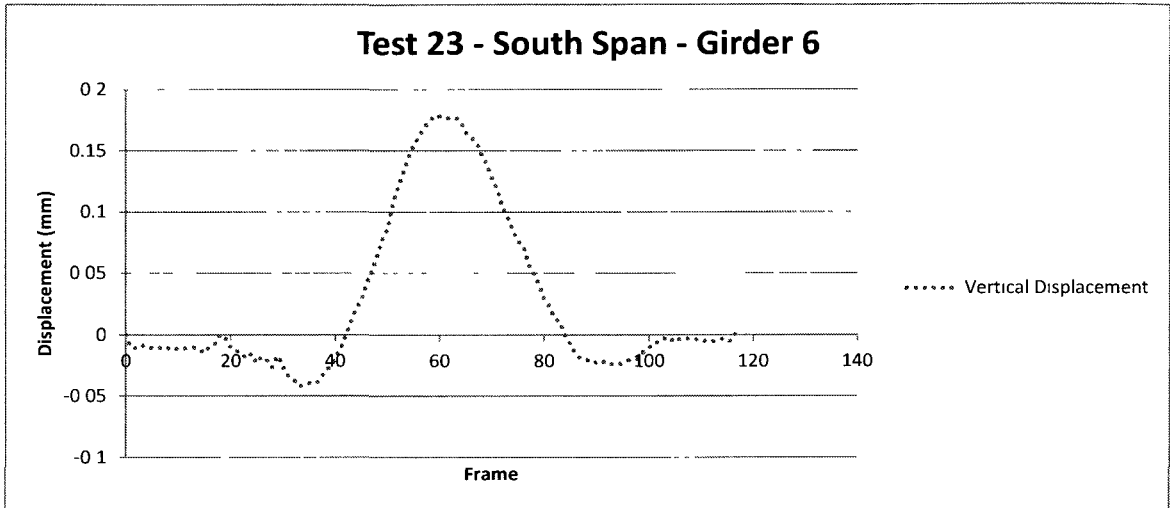
Run #	Run Description	Camera 1 Focus	Camera 2 Focus
0	iSite Ambient Conditions	No Reading	
1	Dynamic Ambient Conditions	No Reading	
2	Dynamic Ambient Conditions (w/electronics on)	No Reading	
3	AV-Dynamic Load Test	No Reading	
4	AW-Dynamic Load Test	No Reading	
5	AY-Dynamic Load Test	No Reading	
6	AZ-Dynamic Load Test	No Reading	
7	Dynamic Ambient Conditions	No Reading	
8	BX-Dynamic Load Test	No Reading	
9	CZ-Dynamic Load Test	No Reading	
10	CY-Dynamic Load Test	No Reading	
11	CW-Dynamic Load Test	No Reading	
12	CV-Dynamic Load Test	No Reading	
13	Dynamic Ambient Conditions	No Reading	
14	iSite Ambient Conditions	No Reading	
15	X0-1-Crawl Speed Load Test	16	8
16	X0-2-Crawl Speed Load Test	16	8
17	X0-3-Crawl Speed Load Test	16	8
18	X1-1-Crawl Speed Load Test	No Reading	
19	X1-2-Crawl Speed Load Test	17	7
20	X1-3-Crawl Speed Load Test	17	7
21	X2-1-Crawl Speed Load Test	14	10
22	X2-2-Crawl Speed Load Test	14	10
23	X2-3-Crawl Speed Load Test	13	9
24	X2-4-Crawl Speed Load Test w/Stop @ Center	13	9
25	X2-5-Crawl Speed Load Test w/Stop @ Center	18	11
26	X2-6-Crawl Speed Load Test w/Stop @ Center	15	12
27	X2-7-Crawl Speed Load Test w/Stop @ Center	14	10
28	X2-8-Crawl Speed Load Test w/Stop @ Center	17	7
29	X2-9-Crawl Speed Load Test w/Stop @ Center	16	8
30	X2-10-Crawl Speed Load Test w/Stop @ Center	16	2
31	X2-11-Crawl Speed Load Test w/Stop @ Center	15	4
32	X2-12-Crawl Speed Load Test w/Stop @ Center	15	4
33	X3-1-Crawl Speed Load Test	15	12
34	X3-2-Crawl Speed Load Test	15	12
35	X3-3-Crawl Speed Load Test	15	12
36	X4-1-Crawl Speed Load Test	18	11
37	X4-2-Crawl Speed Load Test	18	11
38	X4-3-Crawl Speed Load Test	18	11
39	iSite Ambient Conditions	No Reading	



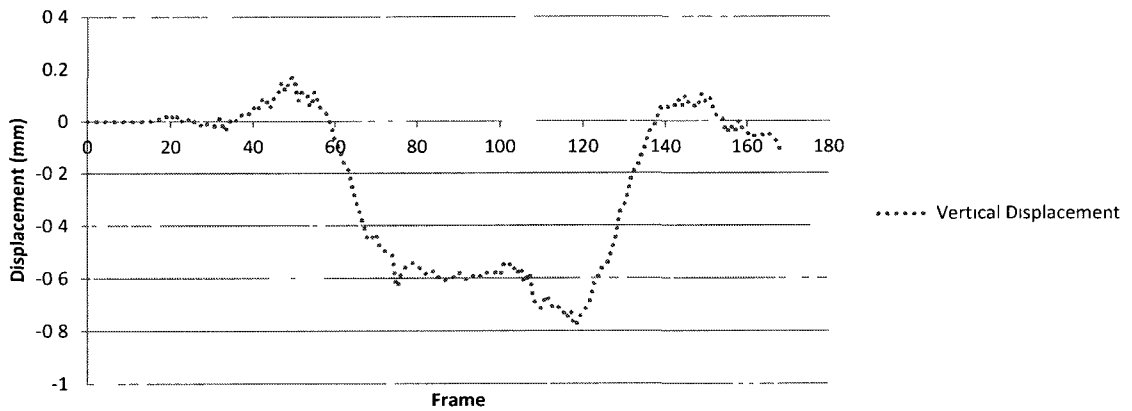




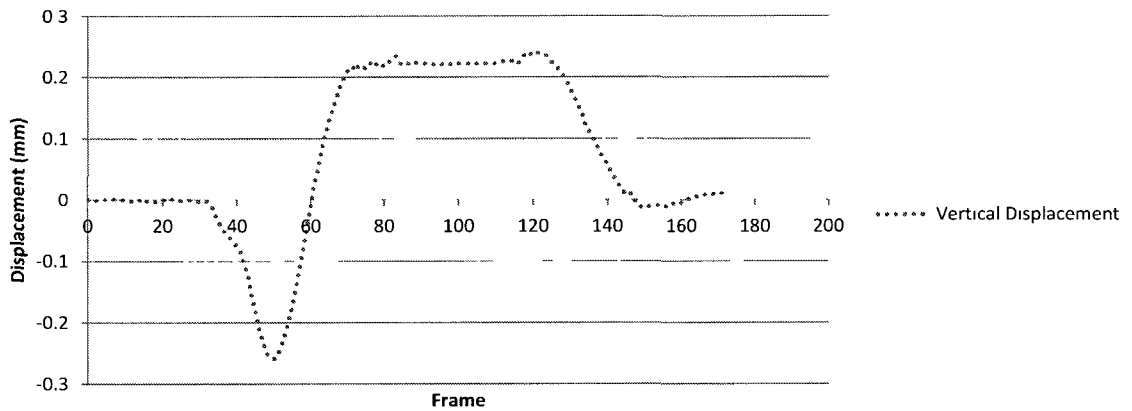




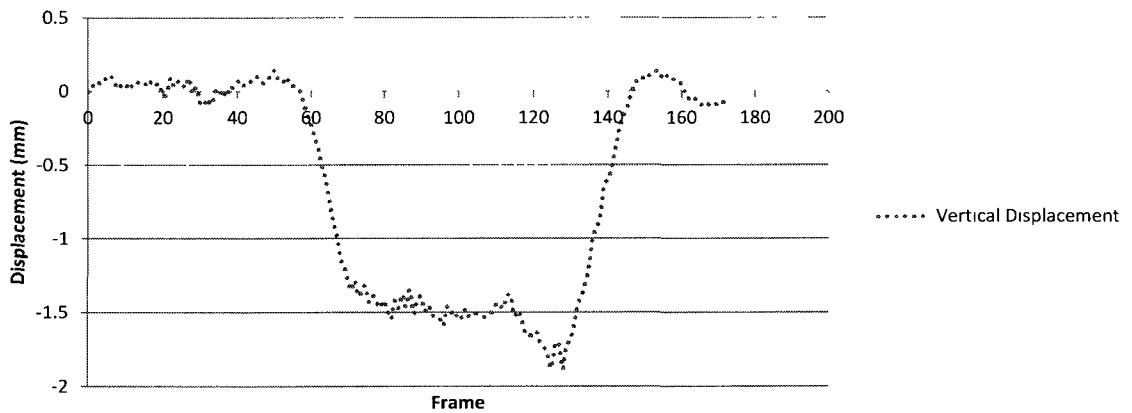
Test 24 - Center Span - Girder 6

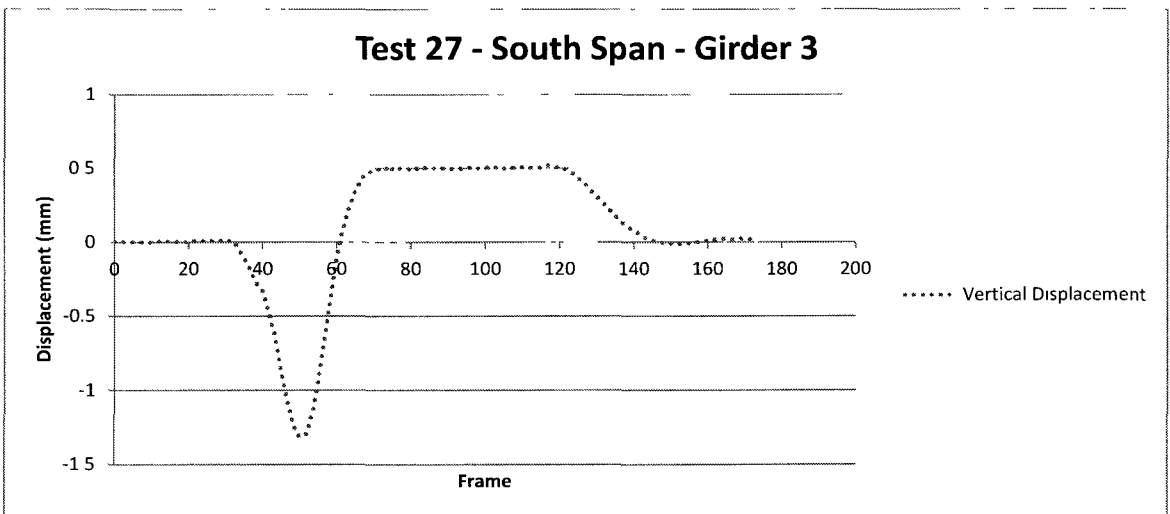
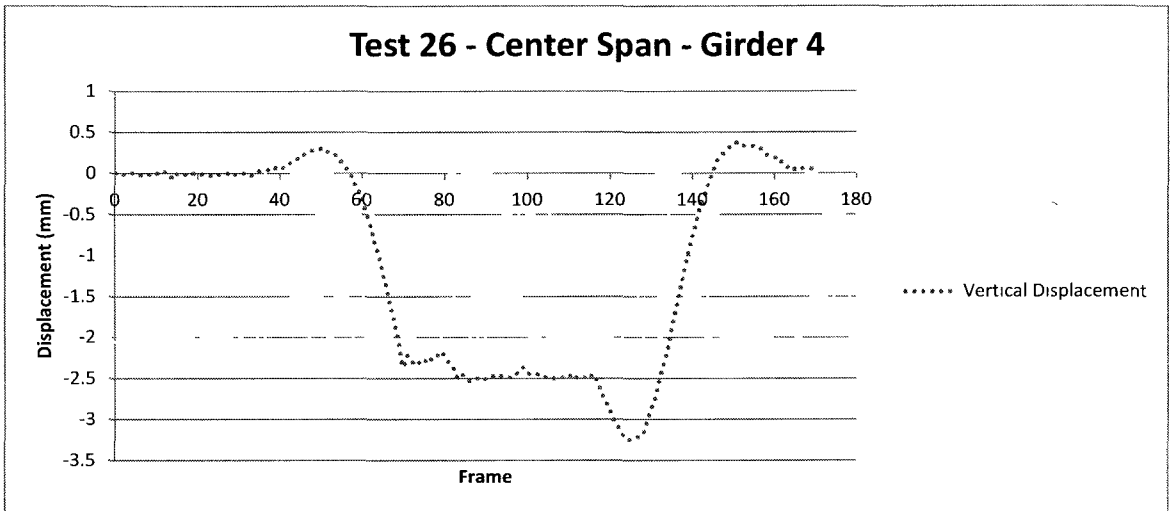
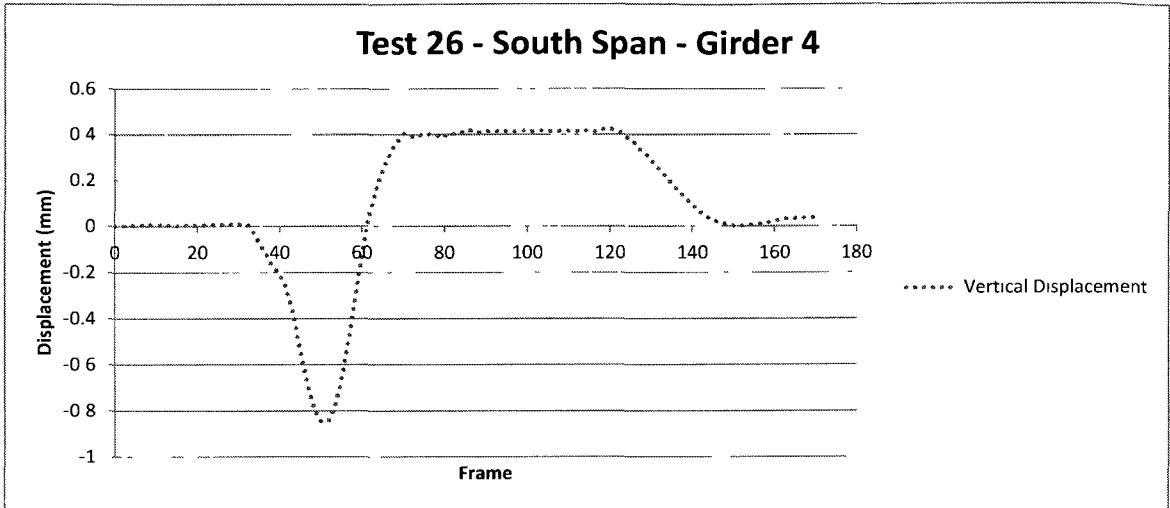


Test 25 - South Span - Girder 5

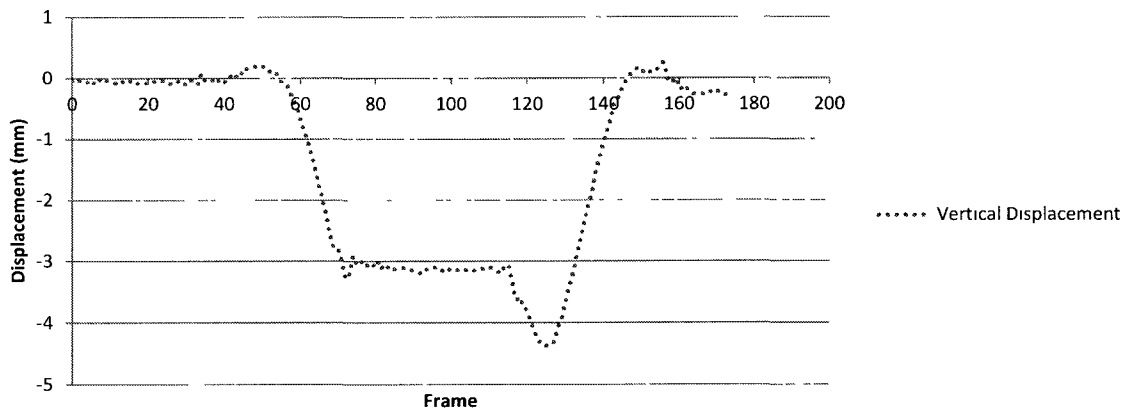


Test 25 - Center Span - Girder 5

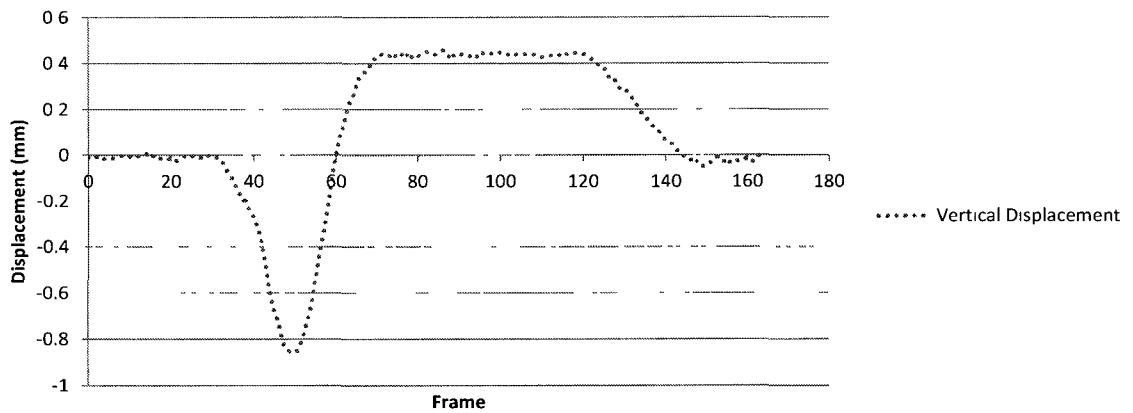




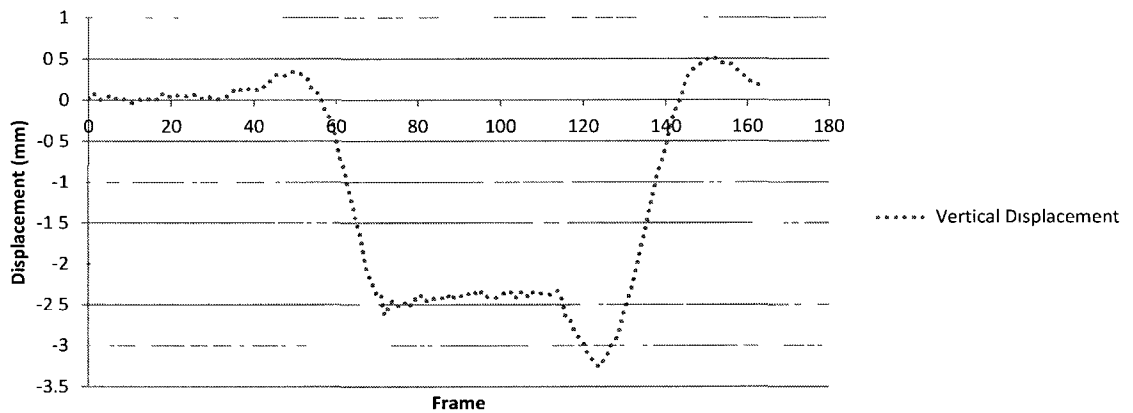
Test 27 - Center Span - Girder 3

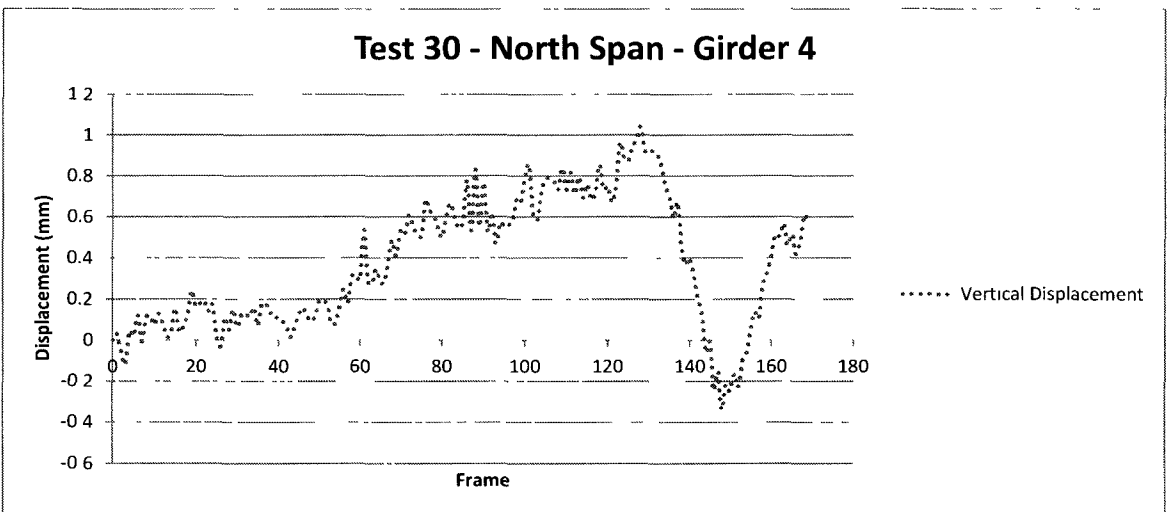
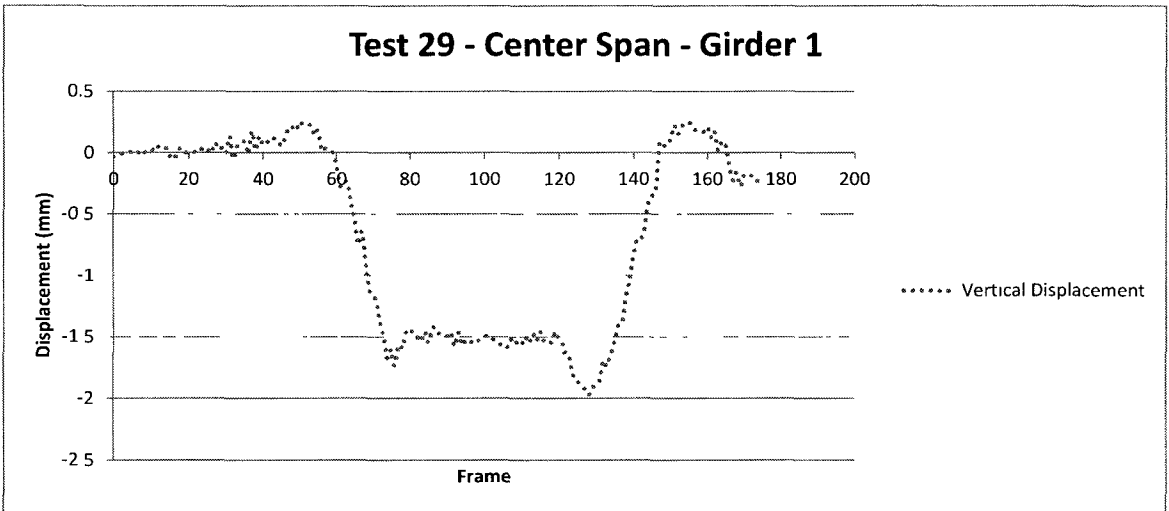
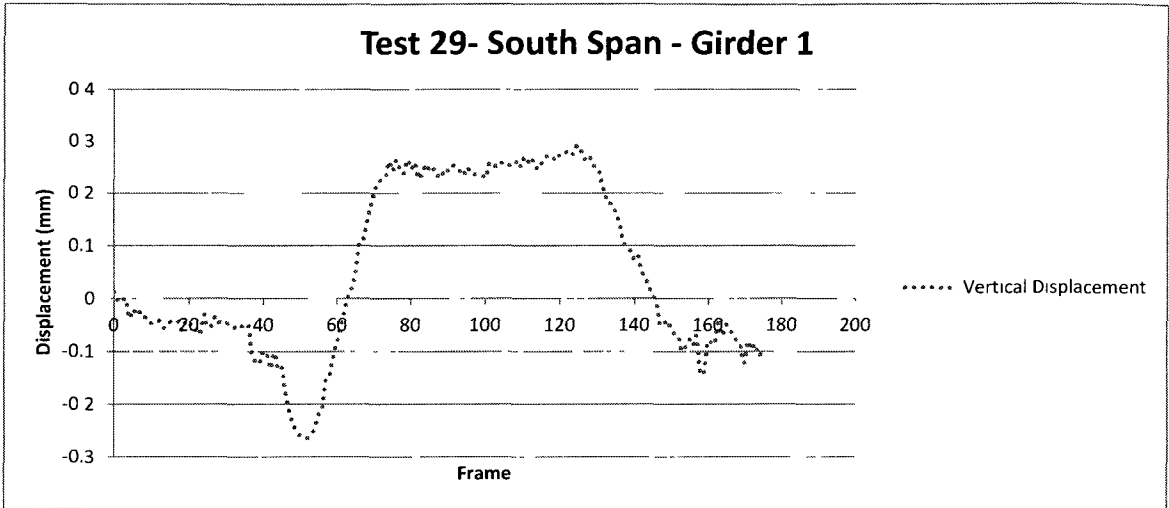


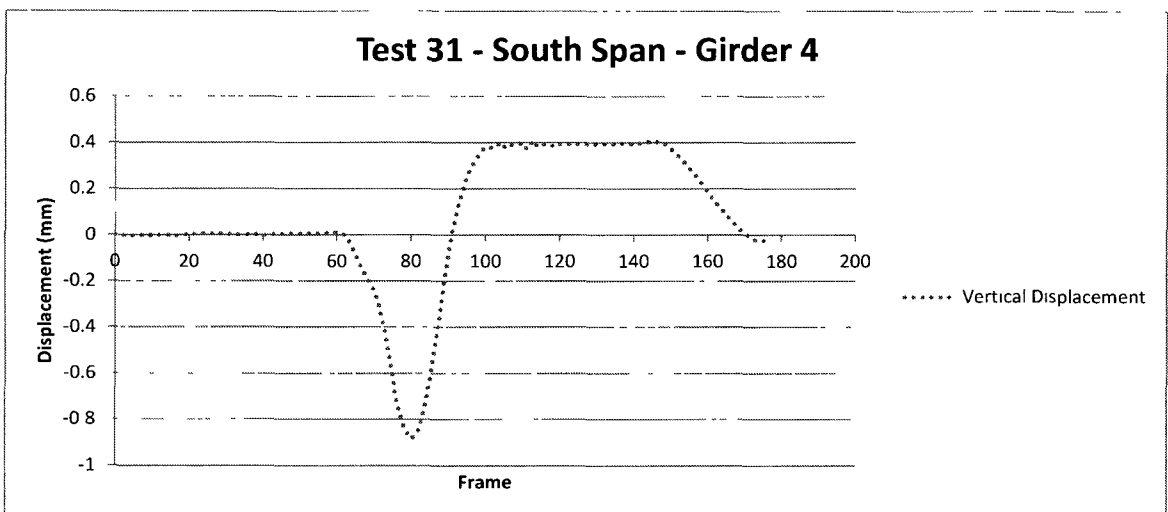
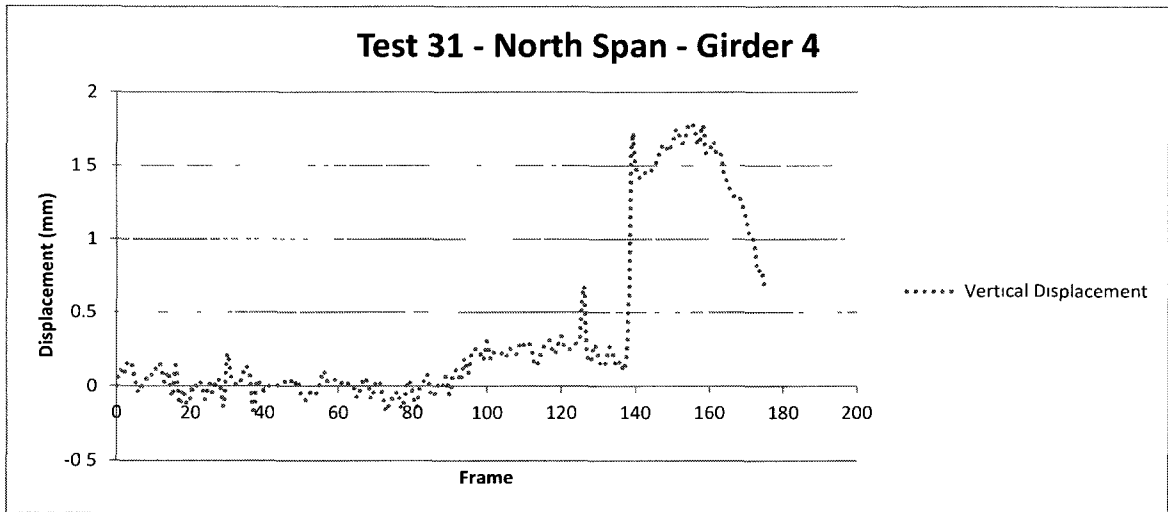
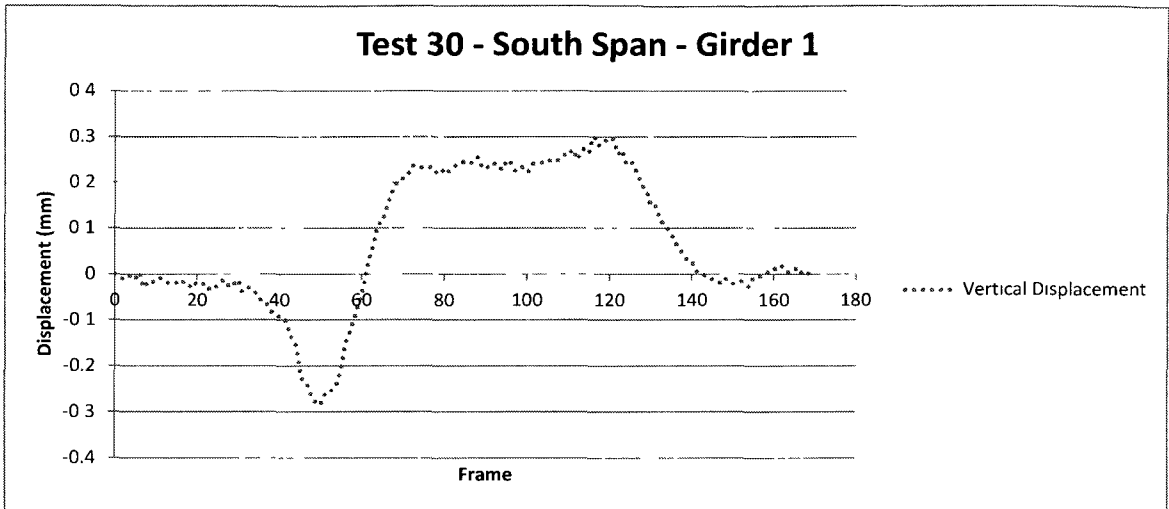
Test 28 - South Span - Girder 2

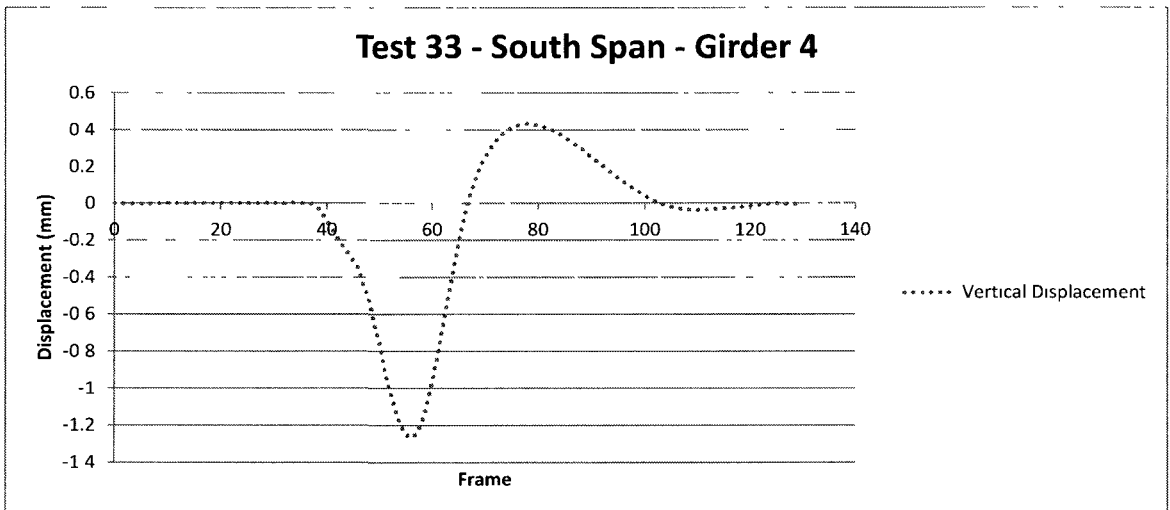
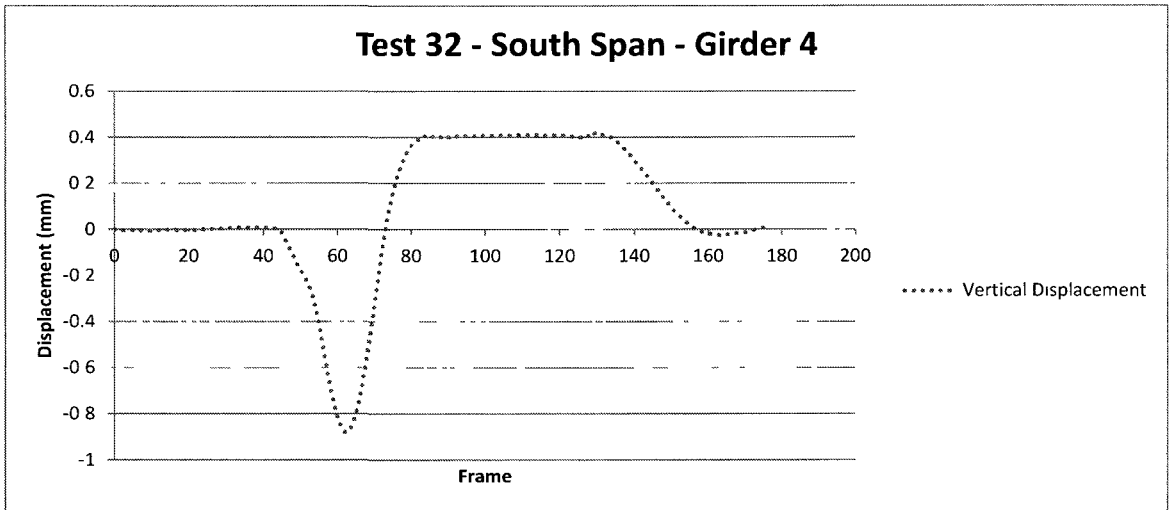
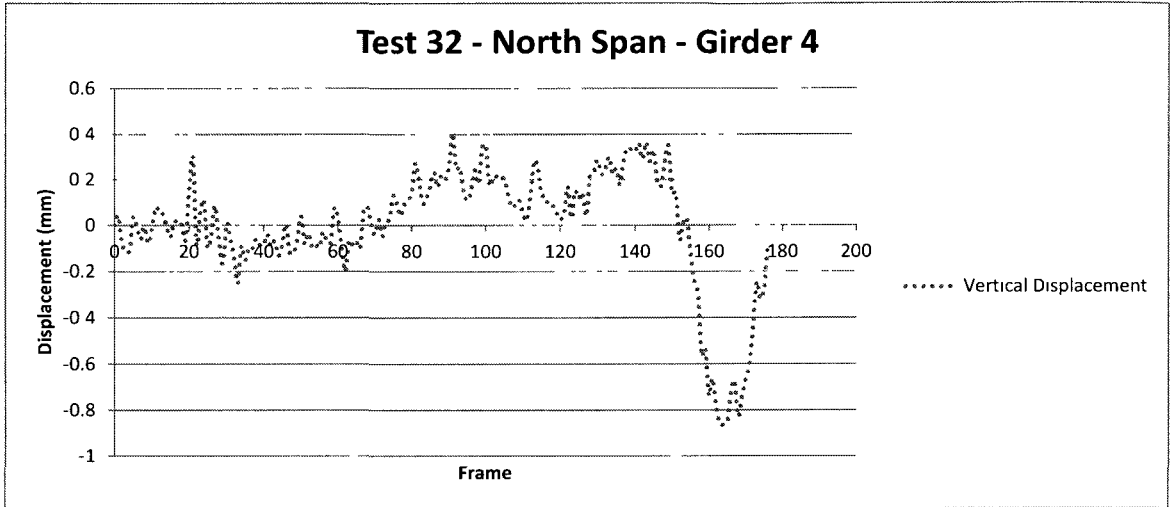


Test 28 - Center Span - Girder 2

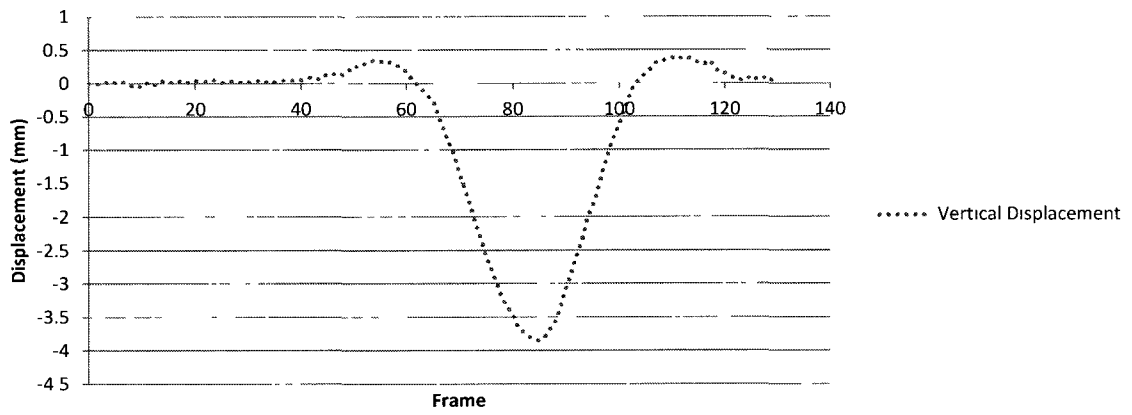




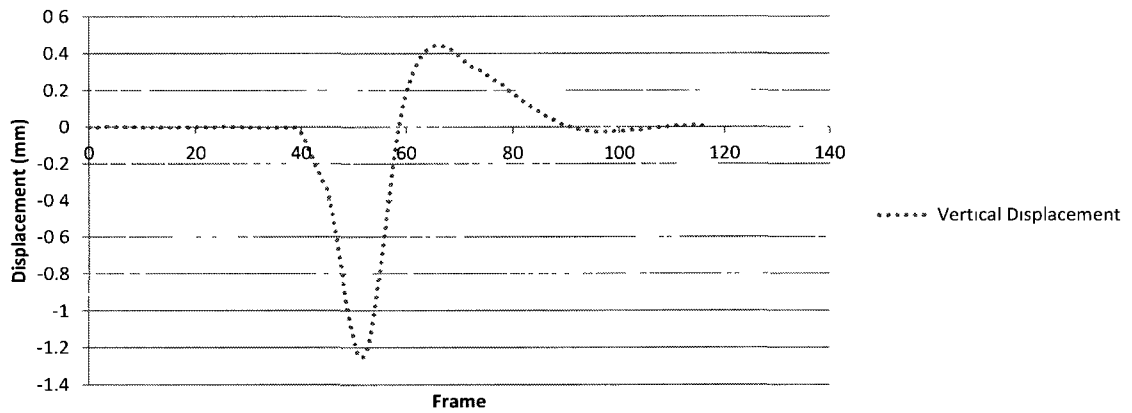




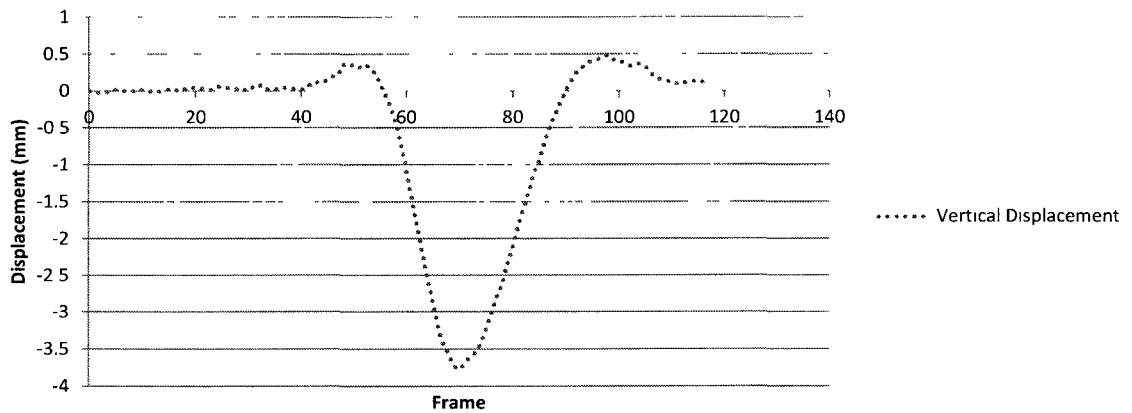
Test 33 - Center Span - Girder 4

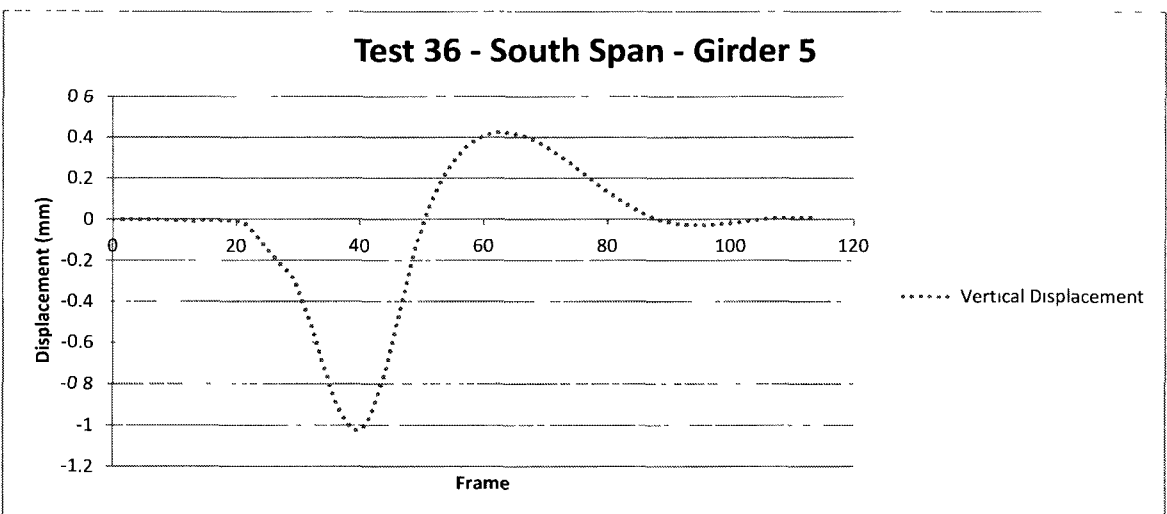
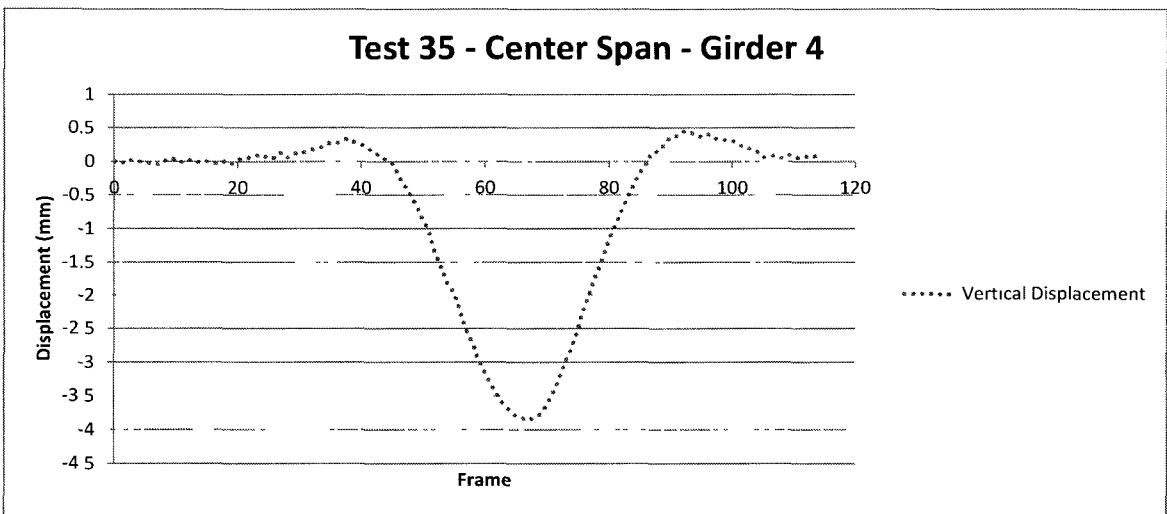
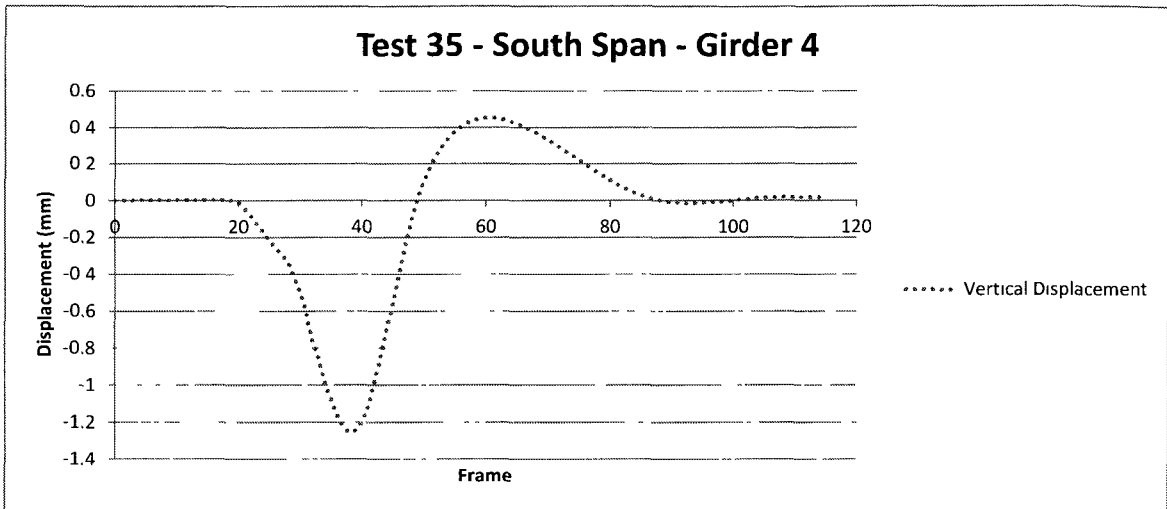


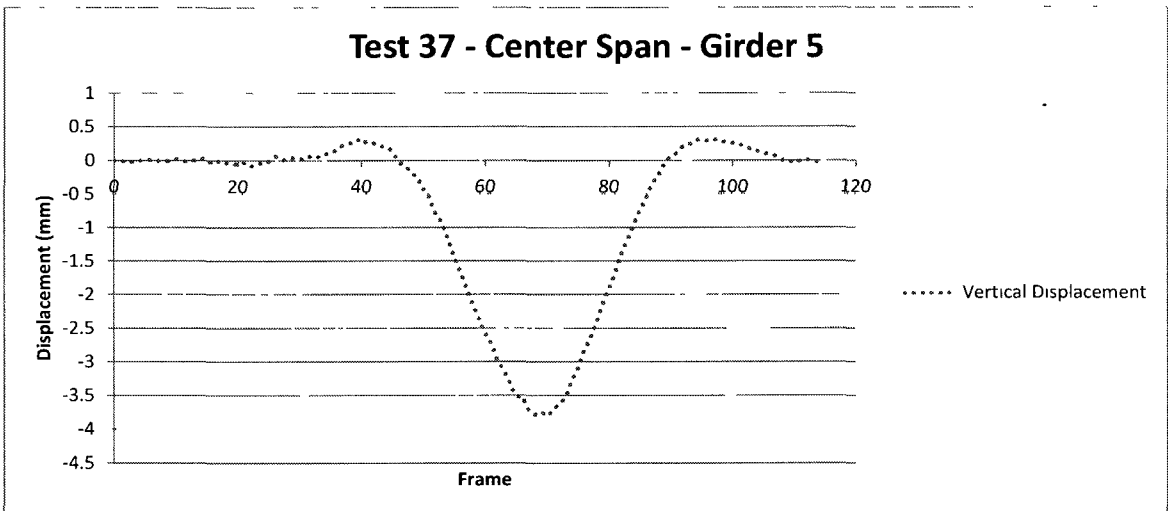
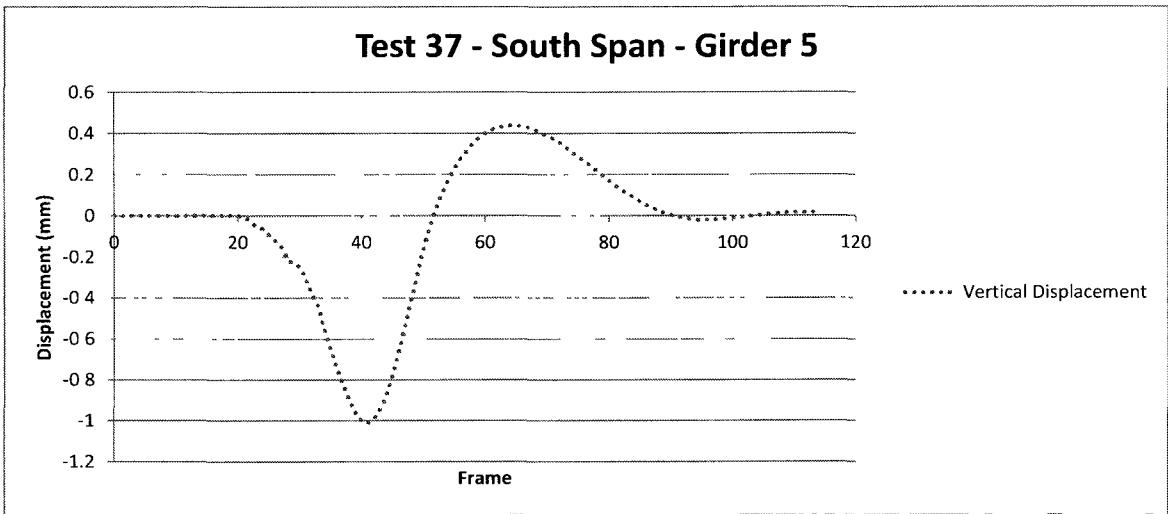
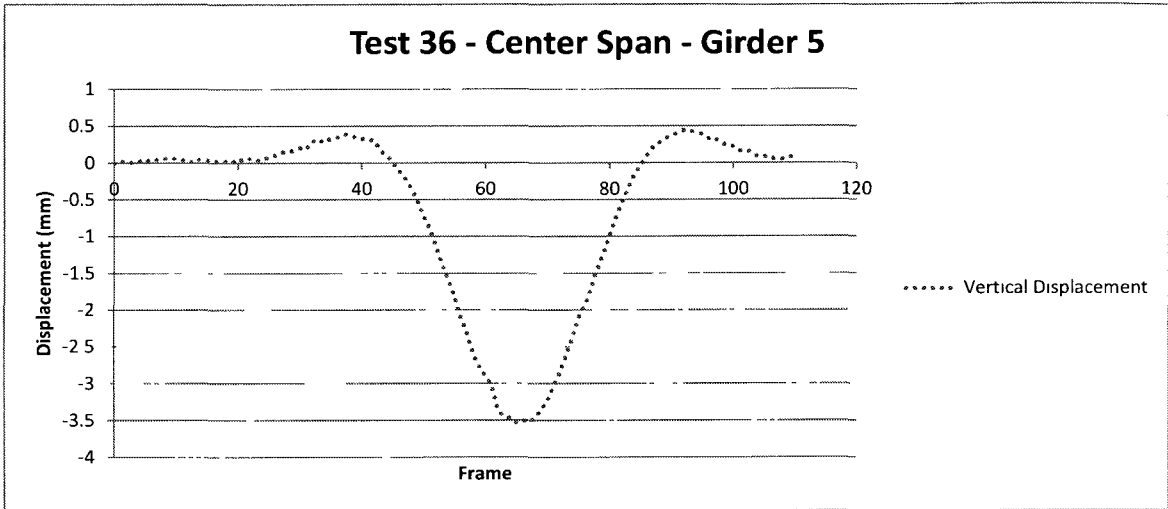
Test 34 - South Span - Girder 4

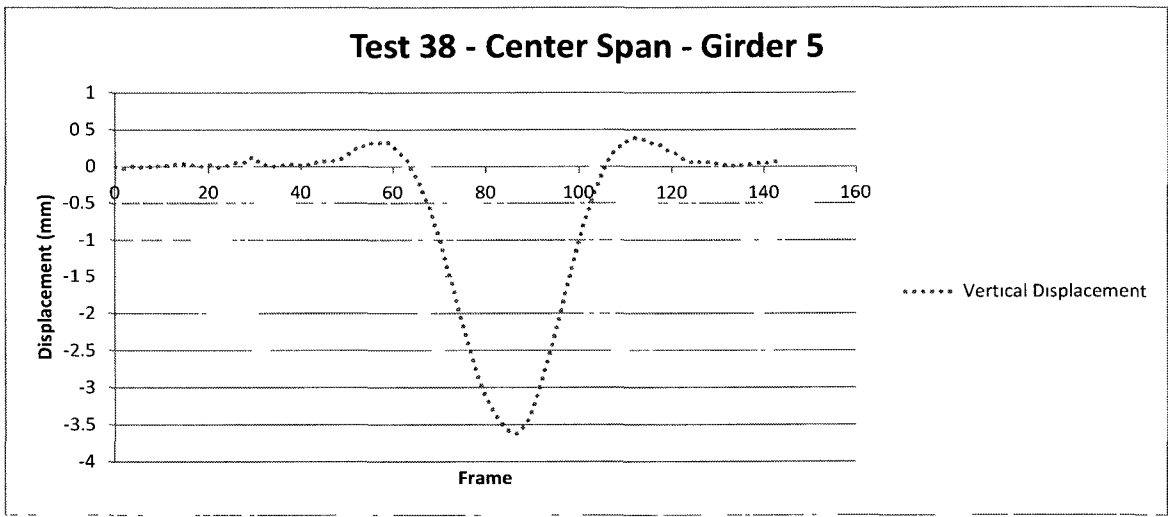
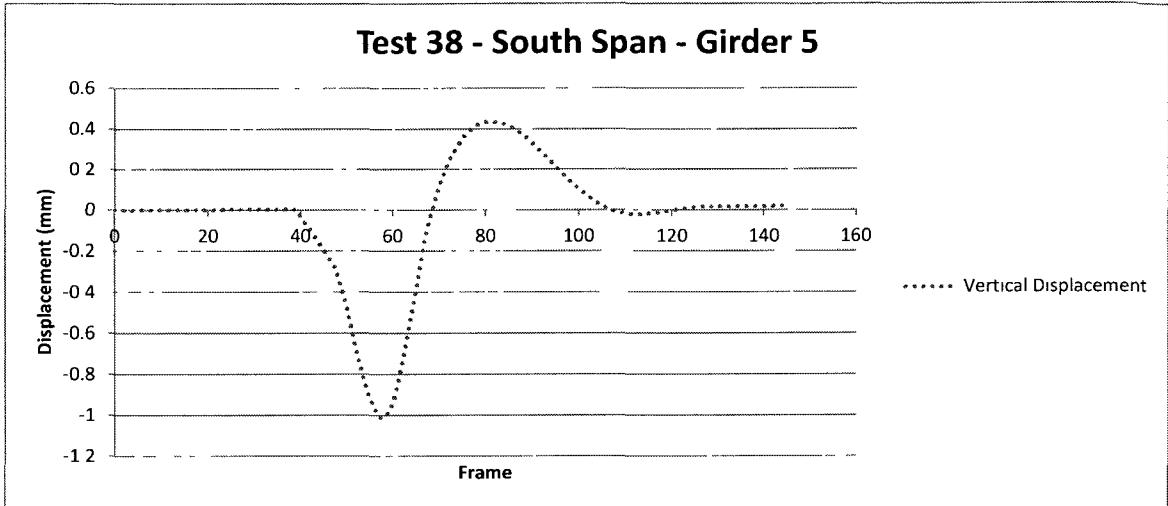


Test 34 - Center Span - Girder 4



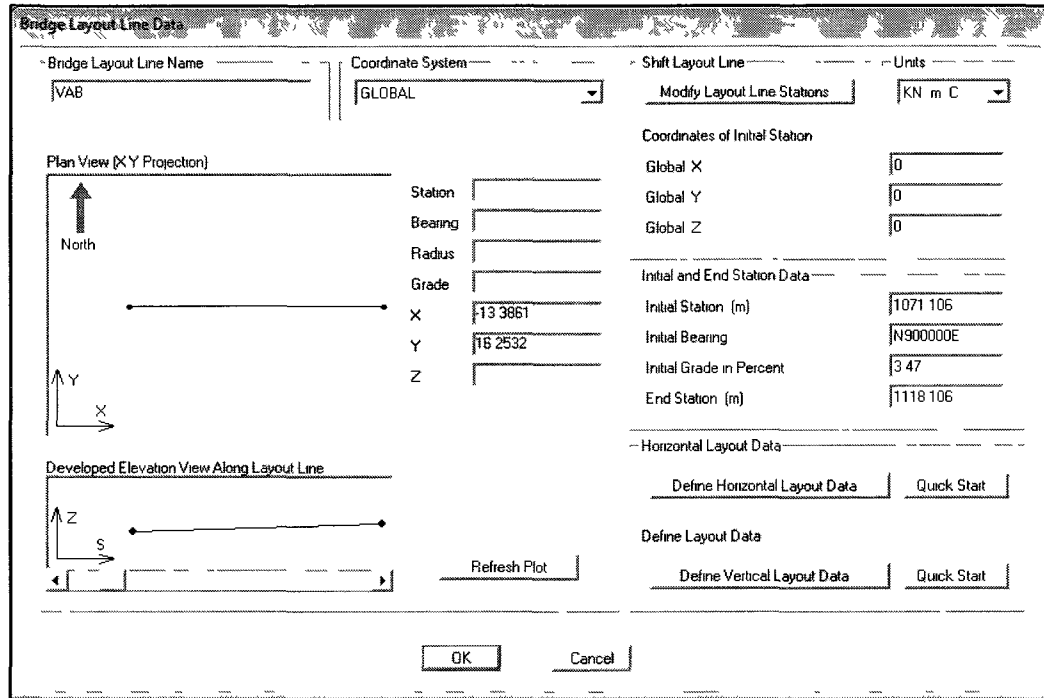






APPENDIX B: SCREENSHOTS OF STRUCTURAL MODEL

The VAB model was created in CSiBridge 15. Screenshots are provided in this section to aid in the recreation of the model.



Layout line input in the Bridge Wizard.

Material Property Data

General Data

Material Name and Display Color: Deck Concrete

Material Type: Concrete

Material Notes: Modify/Show Notes

Weight and Mass

Weight per Unit Volume: 21.917

Mass per Unit Volume: 22749

Units: KN m C

Isotropic Property Data

Modulus of Elasticity E: 26780000

Poisson's Ratio U: 0.2

Coefficient of Thermal Expansion A: 9.900E-06

Shear Modulus G: 11158333

Other Properties for Concrete Materials

Specified Concrete Compressive Strength f_c : 34725

Lightweight Concrete

Shear Strength Reduction Factor:

Switch To Advanced Property Display

OK Cancel

Material properties for the deck concrete.

Frame Properties

Properties

Find this property

W920X238

W36X232

W920X201

W920X263

Click to:

Import New Property

Add New Property

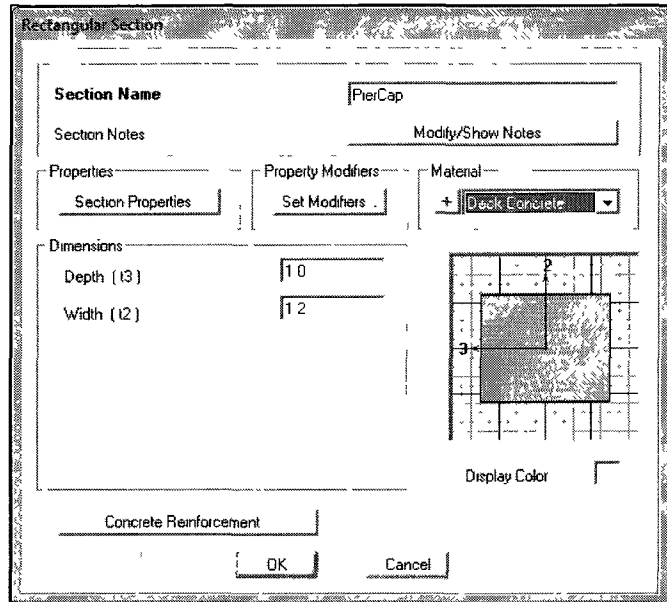
Add Copy of Property

Modify/Show Property

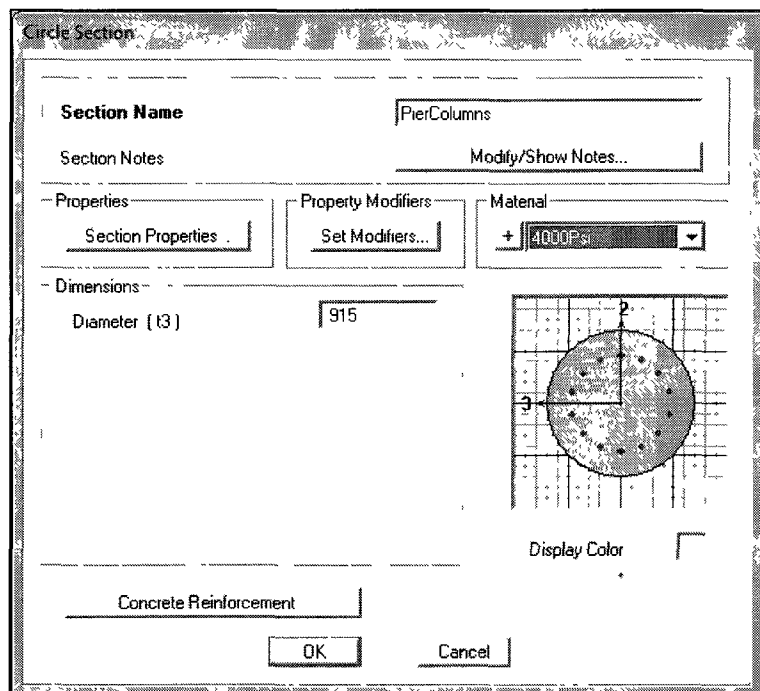
Delete Property

OK Cancel

Frame sections were entered into CSiBridge.



The concrete pier cap section were created in the Bridge Wizard.



The concrete pier column section were created in the Bridge Wizard.

Define Bridge Section Data - Steel Girder

Section Data

Item	Value
Bridge Section Name	SouthCenter
Slab Material Property	Deck Concrete
Number of Interior Girders	4
Total Width	12.715
Girder Longitudinal Layout	Along Layout Line
Constant Girder Spacing	No
Constant Girder Haunch Thickness (t2)	Yes
Constant Girder Frame Section	No
Girder Spacing Definition	
Girder Space S1	2.25
Girder Space S2	2.25
Girder Space S3	2.25
Girder Space S4	2.25
Girder Space S5	2.25
Slab Thickness	
Top Slab Thickness (t1)	0.203
Concrete Haunch + Flange Thickness (t2)	0.0508
Girder Section Properties	

Section is Legal

Girder Output

Girder Spacing

Modify/Show Properties Units:

Section properties for the south and center spans

Define Bridge Section Data - Steel Girder

Section Data

Item	Value
t1 Horizontal Dimension	0
t2 Horizontal Dimension	0
Left Overhang Data	
Left Overhang Length (L1)	0.7325
Left Overhang Distance to Fillet (L3)	0.2095
Left Overhang Outer Thickness (t5)	0.25
Right Overhang Data	
Right Overhang Length (L2)	0.7325
Right Overhang Distance to Fillet (L4)	0.2095
Right Overhang Outer Thickness (t6)	0.25
Live Load Curb Locations	
Distance To Inside Edge of Left Live Load Curb	0.495
Distance To Inside Edge of Right Live Load Curb	2.22
Distance To Centerline of Median Live Load Curb	0
Width of Median Live Load Curb	0
Insertion Point Location	
Offset X From Reference Point To Insertion Point	0
Offset Y From Reference Point To Insertion Point	0

Section is Legal

Girder Output

Girder Spacing

Modify/Show Properties Units:

Section properties for the south and center spans (cont.).

Define Bridge Section Data - Steel Girder

Section is Legal Show Section Details

Girder Output

Girder Spacing

Modify/Show Properties Units
 Materials: Units:

Section Data

Item	Value
General Data	
Bridge Section Name	North
Slab Material Property	Deck Concrete
Number of Interior Girders	6
Total Width	12.715
Girder Longitudinal Layout	Along Layout Line
Constant Girder Spacing	No
Constant Girder Haunch Thickness (t2)	Yes
Constant Girder Frame Section	No
Girder Spacing Definition	
Girder Space S1	0.45
Girder Space S2	2.25
Girder Space S3	2.25
Girder Space S4	2.25
Girder Space S5	2.25
Girder Space S6	2.25
Girder Space S7	0.45
Slab Thickness	

Section properties for the north span.

Define Bridge Section Data - Steel Girder

Section is Legal Show Section Details

Girder Output

Girder Spacing

Modify/Show Properties Units
 Materials: Units:

Section Data

Item	Value
t1 Horizontal Dimension	0
t2 Horizontal Dimension	0
Left Overhang Data	
Left Overhang Length (L1)	0.283
Left Overhang Distance to Fillet (L3)	0.2095
Left Overhang Outer Thickness (t5)	0.25
Right Overhang Data	
Right Overhang Length (L2)	0.283
Right Overhang Distance to Fillet (L4)	0.2095
Right Overhang Outer Thickness (t6)	0.25
Live Load Curb Locations	
Distance To Inside Edge of Left Live Load Curb	0.495
Distance To Inside Edge of Right Live Load Curb	2.22
Distance To Centerline of Median Live Load Curb	0
Width of Median Live Load Curb	0
Insertion Point Location	
Offset X From Reference Point To Insertion Point	0
Offset Y From Reference Point To Insertion Point	0

Section properties for the north span (cont).

Bridge Bearing Data

Bridge Bearing Name: Units:

Bridge Bearing Is Defined By:

Link/Support Property +

User Definition

User Bearing Properties

DOF/Direction	Release Type	Stiffness
Translation Vertical (U1)	Partial Fixity	560
Translation Normal to Layout Line (U2)	Fixed	
Translation Along Layout Line (U3)	Fixed	
Rotation About Vertical (R1)	Free	
Rotation About Normal to Layout Line (R2)	Partial Fixity	1765000
Rotation About Layout Line (R3)	Free	

OK Cancel

Bridge bearing data is entered using data from test documents.

Foundation Spring Data

Foundation Spring Name: Units:

Foundation Spring Is Defined By:

Link/Support Property +

User Definition

Property is Defined for This Length in a Line Spring:

Property is Defined for This Area in an Area Spring:

User Foundation Spring

DOF/Direction	Release Type	Stiffness
Translation Vertical (U1)	Fixed	
Translation Along Skew (U2)	Fixed	
Translation Normal to Skew (U3)	Fixed	
Rotation About Vertical (R1)	Fixed	
Rotation About Line Along Skew (R2)	Fixed	
Rotation About Line Normal to Skew (R3)	Fixed	

OK Cancel

Foundation springs were fixed.

Bridge Abutment Data

Bridge Abutment Name: Units:

Girder Support Condition

Integral

Connect to Girder Bottom Only

Substructure Type

Foundation Spring

Continuous Beam (Continuously Supported)

Section Property:

Beam Length:

Foundation Spring

Foundation Spring Property:

Note: When substructure type is grade beam foundation spring property represents a line spring

Bridge abutment properties were defined in the bridge abutment data section of the Bridge Wizard.

Bridge Bent Data

Bridge Bent Name: Units:

Girder Support Condition

Integral

Connect to Girder Bottom Only

Bent Data

Cap Beam Length:

Number of Columns:

Cap Beam Section:

Bent Type

Single Bearing Line (Continuous Superstructure)

Double Bearing Line (Discontinuous Superstructure)

Bents were defined in the Bridge Wizard.

Bridge Bent Column Data

Bridge Bent Name: Modify/Show Properties: Units:

Column Data

Column	Section	Distance	Height	Angle	Base Support
1	PierColumns	2	8	0	Fixed
2	PierColumns	6.25	8	0	Fixed
3	PierColumns	10.5	8	0	Fixed

Notes:

- 1 The distance is measured from the left end of the cap beam to the center of the column.
- 2 The column height is measured from the midheight of the cap beam to the bottom of the column.
- 3 The column angle is measured in degrees counterclockwise from a line parallel to the bent to the column local 2 axis.

Moment Releases at Top of Column

Column	R1 Release	R2 Release	R3 Release	R1 Stiffness	R2 Stiffness	R3 Stiffness
1	Fixed	Fixed	Fixed			
2	Fixed	Fixed	Fixed			
3	Fixed	Fixed	Fixed			

Bent columns are defined by choosing the section and location of each column.

Bridge Object Data

Bridge Object Name: Layout Line Name: Coordinate System: Units:

Define Bridge Object Reference Line

Span Label	Station m	Span Type
Start Abutment	1071.106	Start Abutment
Start Abutment	1071.106	Start Abutment
South Span	1082.86	Full Span to End Bent
Center Span	1106.36	Full Span to End Bent
North Span (a)	1109.24	Full Span to End Bent
North Span	1118.106	Full Span to End Abutment

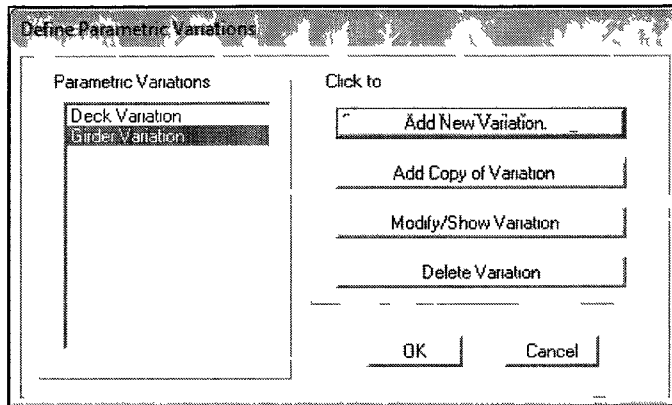
Modify/Show Assignments

- Spans
- User Discretization Points
- Abutments
- Bents**
- In Span Hinges (Expansion Jt)
- In Span Cross Diaphragms
- Superelevation
- Prestress Tendons
- Girder Rebar
- Staged Construction Groups
- Point Load Assigns
- Line Load Assigns

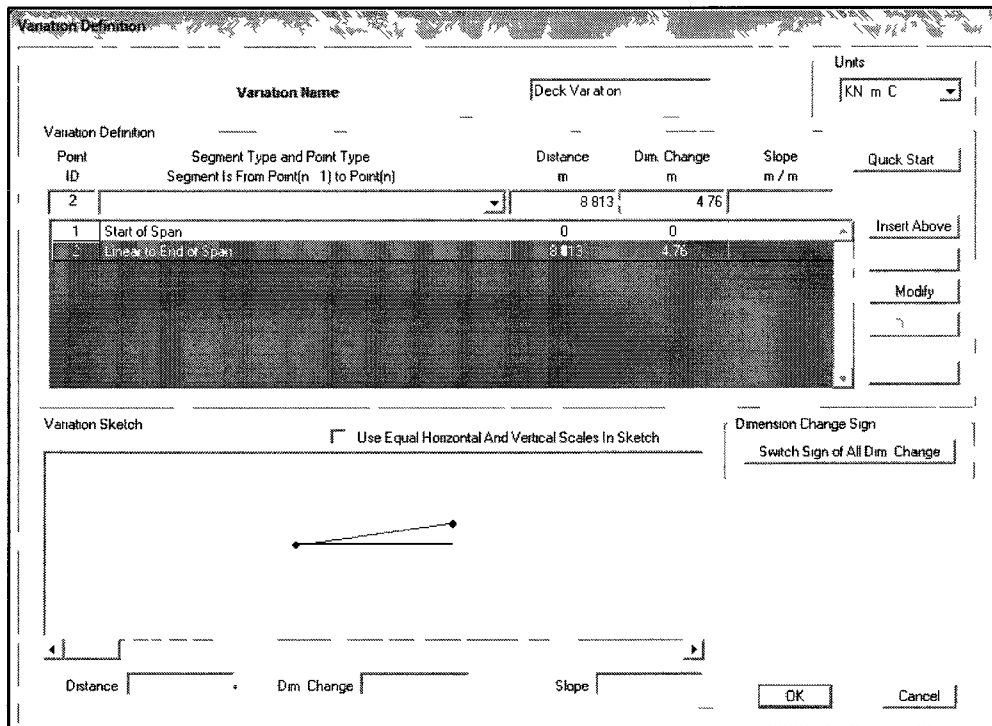
Note: Bridge object location based on bridge section intersection point following selected layout line.

Bridge Object Plan View (X-Y Projection)

Spans were defined in the Bridge Object Data window.



Two parametric variations needed to be applied to the north span of the bridge



The deck variation was created using the Bridge Wizard

Variation Definition

Variation Name: Units:

Variation Definition

Point ID	Segment Type and Point Type Segment Is From Point(n-1) to Point(n)	Distance m	Dim. Change m	Slope m/m	Quick Start
2		8.813	2.38		
1	Start of Span	0	0		Insert Above
2	Linear to End of Span	8.813	2.38		etc

Buttons: Modify, Delete, etc

Variation Sketch: Use Equal Horizontal And Vertical Scales In Sketch

Dimension Change Sign: Switch Sign of All Dim. Change

Distance: Dim. Change: Slope:

Buttons: OK, Cancel

The exterior girder spacing was varied using the Bridge Wizard.

Bridge Object Span Assignments

Bridge Object Name:

Span Definition

Span	Section	Section Varies
South Span	SouthCenter	No
Center Span	SouthCenter	No
North Span	SouthCenter	No
North Span	North	Yes

Modify/Show Section Variation Along Selected Span

Buttons: OK, Cancel

The bridge object span assignment windows allows the user to assign deck sections to individual spans.

Bridge Section Variation Definition

Bridge Object Name: VAB Bridge Object
 Span Label: North Span
 Base Bridge Section Property: North

Bridge Section Variation Is Defined By: User Definition Reference to Another Span

Display Section: Show Base Section Show Section Variation

Define/Show Variations: [Button] Show Section Variation: [Button]

- User Defined Variation For Steel Girder

Parameter	Variation
General Data	
Total Width	Deck Variation
Girder Spacing Definition	
Girder Space S1	Girder Variation
Girder Space S2	Constant
Girder Space S3	Constant
Girder Space S4	Constant
Girder Space S5	Constant
Girder Space S6	Constant
Girder Space S7	Girder Variation
Slab Thickness	
Top Slab Thickness (t1)	Constant
Concrete Haunch + Flange Thickness (t2)	Constant
Fillet Horizontal Dimension Data	
t1 Horizontal Dimension	Constant
t2 Horizontal Dimension	Constant

OK Cancel

The user is brought to this window to assign parametric variations to particular elements

Bridge Object In-Span Cross-Diaphragm Assignments

Bridge Object Name: VAB Bridge Object Units: KN m C

In Span Cross-Diaphragm Definition

Span	Diaphragm Property	Distance	Bearing	Location	
South Span	D1	0.3	Default	All Spaces	
South Span	D1	0.3	Default	All Spaces	Add
South Span	U1	2.9375	Default	Girder 4.5	Modify
South Span	D1	5.875	Default	Girder 2.3	Delete
South Span	D1	5.875	Default	Girder 3.4	
South Span	U2	5.875	Default	Girder 4.5	
South Span	D2	5.875	Default	Girder 5.6	
South Span	D2	5.875	Default	Girder 1.2	
South Span	U1	8.8125	Default	Girder 4.5	
South Span	D2	11.5	Default	Girder 1.2	
South Span	D1	11.5	Default	Girder 2.3	
South Span	D1	11.5	Default	Girder 3.4	
South Span	U2	11.5	Default	Girder 4.5	
South Span	D2	11.5	Default	Girder 5.6	
Center Span	U1	2.9375	Default	Girder 4.5	
Center Span	D1	5.875	Default	Girder 2.3	
Center Span	D1	5.875	Default	Girder 3.4	
Center Span	U2	5.875	Default	Girder 4.5	
Center Span	D2	5.875	Default	Girder 5.6	
Center Span	D2	5.875	Default	Girder 1.2	

OK Cancel

Diaphragm information was entered into the Bridge Wizard.

Update Bridge Structural Model

Select a Bridge Object and Action

Bridge Object: VAB Bridge Object Action: Update Linked Model

Modify/Show Selected Bridge Object.

Discretization Information

Maximum Segment Length for Deck Spans: 1

Maximum Segment Length for Bent Cap Beams: 1

Maximum Segment Length for Bent Columns: 1

Structural Model Options

Update as Spine Model Using Frame Objects

Update as Area Object Model
Preferred Maximum Submesh Size: 12

Update as Solid Object Model
Preferred Maximum Submesh Size:

OK Cancel

Mesh information is entered the bridge model updater.

Bridge Lane Data

Lane Name: Lane 1 Coordinate System: GLOBAL Units: KN m C

Maximum Lane Load Discretization Lengths

Along Lane: 1 Across Lane: 1

Additional Lane Load Discretization Parameters Along Lane

Discretization Length Not Greater Than 1/ 4 of Span Length

Discretization Length Not Greater Than 1/ 10 of Lane Length

Lane Data

Bridge Layout Line	Station m	Centerline Offset m	Lane Width m
VAB1	1118.106	4	3.6585
VAB1	1071.106	4	3.6585
VAB1	1118.106	4	3.6585

Move Lane: Add, Insert, Modify, Delete

Plan View (X Y Projection)

North ↑

Layout Line: _____

Station: _____

Bearing: _____

Radius: _____

Grade: _____

X: _____

Y: _____

Z: _____

Snap To Layout Line

Snap To Lane

Objects Loaded By Lane

Program Determined

Group: _____

Lane Edge Type

Left Edge: Interior

Right Edge: Interior

Display Color:

OK Cancel

Three lanes were created across the width of the bridge for the live load to be placed in

General Vehicle Data

Vehicle name: HL 93 Units: Kip ft F

- Floating Axle Loads

	Value	Width Type	Axle Width
For Lane Moments	0	One Point	
For Other Responses	0	One Point	

Double the Lane Moment Load when Calculating Negative Span Moments

- Usage **- Min Dist Allowed From Axle Load** **Length Effects**

Lane Negative Moments at Supports Lane Exterior Edge: 1 Axle: None

Interior Vertical Support Forces Lane Interior Edge: 2 Uniform: None

All other Responses

Loads

Load Length Type	Minimum Distance	Maximum Distance	Uniform Load	Uniform Width Type	Uniform Width	Axle Load	Axle Width Type	Axle Width
Leading Load	Infinite		0.64	Fixed Width	10	10.64	Two Points	6
Leading Load	Infinite		0.64	Fixed Width	10	10.64	Two Points	6
Fixed Length	14		0.64	Fixed Width	10	42.56	Two Points	6
Fixed Length	14		0.64	Fixed Width	10	42.56	Two Points	6

Add Insert Modify Delete

Vehicle Applies To Straddle (Adjacent) Lanes Only Straddle Reduction Factor: _____

Vehicle Remains Fully In Lane (In Lane Longitudinal Direction)

OK Cancel

The HL-93 live load case was defined consisting of axle point loads and a distributed live load

Multi Step Bridge Live Load Pattern Generation

Vehicle	Lane	Start Dist	Start Time	Direction	Speed	
HL 93	Lane 3	0	0	Forward	1	
HL 93	Lane 1	0	0	Forward	1	Add
HL 93	Lane 2	0	0	Forward	1	Modify
HL 93	Lane 3	0	0	Forward	1	Delete

Note: Vehicles that are defined using a uniform load will not be included in the program generated multi step load case. Click this note to see a list of vehicle defined using uniform load.

- Load Pattern Discretization Information **Units**

Duration of Loading is: 10 seconds KN m C

Discretize Load every: 0.1 seconds

OK Cancel

The HL-93 load pattern consisted of three HS-20 trucks travelling in its respective lane.

Load Case Data - Moving Load

Load Case Name: HL 93 Set Def Name Modify/Show Notes

Load Case Type: Moving Load Design

Stiffness to Use: Zero Initial Conditions Unstressed State Inputant Note: Loads from the Nonlinear Case are NOT included in the current case

Multilane Scale Factors

Number of Lanes Loaded	Reduction Scale Factor
1	1
2	1
3	1

Modify

Lanes Loaded for Assignment 1

Assign Number	Vehicle Class	Scale Factor	Min Loaded Lanes	Max Loaded Lanes	Lanes Loaded
1	HL 93 Veh	1.75	3	3	All

Add Modify Delete

List of Lane Definitions: Lane 1, Lane 2, Lane 3

Remove

OK Cancel

The HL-93 load case.

Bridge Area Load Distribution Definition Data

Load Name: PavementLoad Units: kN/m.C

Load Direction: Load Type: Force, Coordinate System: GLOBAL, Direction: Gravity

Load Value: Left Edge Value: 0.88, Right Edge Value: 0.88

Load Transverse Location: Left Reference Location: Left Edge of Deck, Left Load Distance from Left Ref Location: 0.495, Right Reference Location: Left Edge of Deck, Right Load Distance from Right Ref Location: 0.495

Load Vertical Location: Top Slab is Loaded at Midheight of its Thinnest Portion

OK Cancel

The wearing surface was created as an area load.

Bridge Area Load Distribution Definition Data

Load Name: Sidewalk Units: KN/m/C

Load Direction:

Load Type: Force

Coordinate System: GLOBAL

Direction: Gravity

Load Value:

Left Edge Value: 10.92

Right Edge Value: 10.92

Load Transverse Location:

Left Reference Location: Right Edge of Deck

Left Load Distance from Left Ref Location: 2.22

Right Reference Location: Right Edge of Deck

Right Load Distance from Right Ref Location: 0

Load Vertical Location:

Top Slab is Loaded at Midheight of its Thinnest Portion

OK Cancel

The sidewalk load was created as an area load. The wearing surface distributed load was created in a similar fashion

Area Load Assignments - VAB Bridge Object

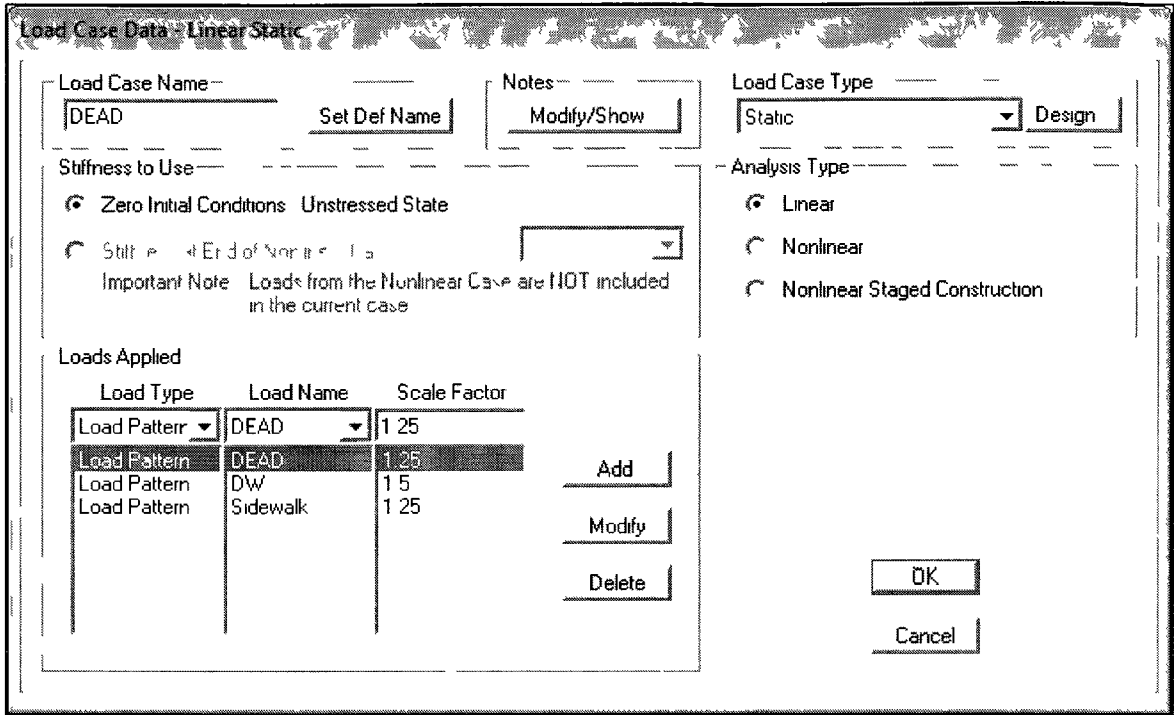
Area Load Data

Load Pattern	Load Distribution	Start Station m	End Station m	Left Edge Variation	Right Edge Variation
D/W	Pavement Load	1071.105	1118.106	None	None
Sidewalk	Sidewalk	1071.106	1118.106	None	None

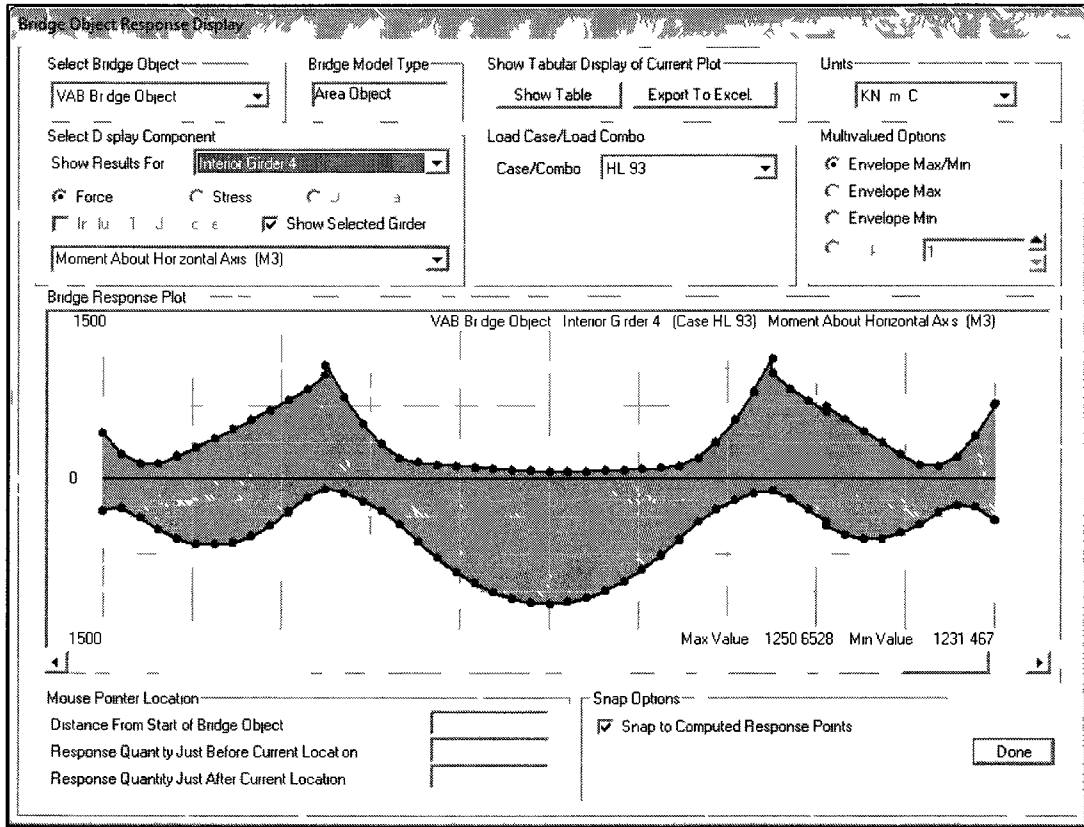
Units: KN/m/C

OK Cancel

The sidewalk and pavement loads were assigned to a load pattern



The dead load pattern, wearing surface load pattern, and sidewalk load pattern were assigned to the dead load case



Maximum moments were recorded from CSiBridge analysis results to formulate a load rating. This window shows the maximum/minimum moment envelope for an interior girder.

APPENDIX C: CALCULATION OF RATING FACTORS

C.1 Rating Factors Due to Negative Moment

Calculation of the plastic moment capacity, C, for use in load rating.

Interior Beam

W920x238	also known as	W36X160
$A_{int} := 30300\text{mm}^2$		$t_{f,int} := 25.9\text{mm}$
$d_{int} := .914\text{m} = 35.984\text{in}$		$I_{x,int} := 9760\text{in}^4$
$t_{w,int} := 16.5\text{mm}$		$\text{YieldStress}_{beam} := 50 \frac{\text{kip}}{\text{in}^2} = 3.447 \times 10^8 \text{ Pa}$
$b_{f,int} := 305\text{mm}$		$E_b := 29000\text{ksi}$
$\text{Length} := 47\text{m}$		

Exterior Beam

W920x345	also know as	W36X232
$A_{ext} := 43900\text{mm}^2$		$t_{f,ext} := .039878\text{m}$
$d_{ext} := .942\text{m}$		$I_{x,ext} := 15000\text{in}^4$
$t_{w,ext} := .022098\text{m}$		
$b_{f,ext} := .30734\text{m}$		

Concrete Deck

$\text{Deck}_{depth} := .2\text{m} = 7.874\text{in}$	$E_d := 3759\text{ksi}$
$f_c := 35\text{MPa} = 5.076\text{ksi}$	
$\text{Span}_{int} := 2.250\text{m} = 88.583\text{in}$	
$\text{Span}_{ext} := 1.704\text{m}$	

Haunch

Assume that haunch does not contribute to capacity.

$\text{Haunch}_{depth} := .045\text{m} = 1.772\text{in}$
--

$$\text{Capacity}_{\text{int}} := 2600 \text{ kip}\cdot\text{ft} = 3.525 \times 10^3 \cdot \text{kN}\cdot\text{m}$$

Table 3-2
AISC

$$\text{Capacity}_{\text{ext}} := 3900 \text{ kip}\cdot\text{ft} = 5.288 \times 10^3 \cdot \text{kN}\cdot\text{m}$$

Capacity Factors

$$\phi_c := 1.00 \quad \begin{array}{l} \text{Condition Factor - 6A.4.2.3} \\ \text{AASHTO MBE} \end{array}$$

$$\phi_s := 1.00 \quad \begin{array}{l} \text{System Factor - 6A.4.2.4} \\ \text{AASHTO MBE} \end{array}$$

$$\phi := 1.00 \quad \begin{array}{l} \text{LRFD Resistance Factor - 6A.4.2.2-1} \\ \text{AASHTO MBE} \end{array}$$

$$C_{\text{int}} := \text{Capacity}_{\text{int}} \cdot \phi_s \cdot \phi_c \cdot \phi = 3.525 \times 10^6 \cdot \text{N}\cdot\text{m}$$

$$C_{\text{ext}} := \text{Capacity}_{\text{ext}} \cdot \phi_s \cdot \phi_c \cdot \phi = 5.288 \times 10^3 \cdot \text{kN}\cdot\text{m}$$

$$M_{\text{nint}} := C_{\text{int}} = 3.525 \times 10^3 \cdot \text{kN}\cdot\text{m}$$

$$M_{\text{next}} := C_{\text{ext}} = 5.288 \times 10^3 \cdot \text{kN}\cdot\text{m}$$

Calculation of the dead load effect on a stringer - DC

Deck

$$\text{Deck} := \frac{1}{6} \left(12.715 \text{ m} \cdot \text{Deck}_{\text{depth}} + \text{Haunch}_{\text{depth}} \cdot t_{\text{f.int}} \right) \cdot 150 \frac{\text{lbf}}{\text{ft}^3} = 9.991 \frac{\text{kN}}{\text{m}}$$

Beams

$$\text{Beam}_{\text{int}} := 1.06 \left(A_{\text{int}} \cdot 490 \frac{\text{lbf}}{\text{ft}^3} \right) = 2.472 \frac{\text{kN}}{\text{m}} \quad \begin{array}{l} 1.06 \text{ was used to account for} \\ \text{misc. steel items} \end{array}$$

$$\text{Beam}_{\text{ext}} := 1.06 \left(A_{\text{ext}} \cdot 490 \frac{\text{lbf}}{\text{ft}^3} \right) = 3.582 \frac{\text{kN}}{\text{m}}$$

Diaphragms

$$\text{Diaphragms} := 1.06 \left(\frac{17.138 \text{ kgf}}{47 \text{ m}} \right) = 518.868 \frac{\text{N}}{\text{m}}$$

Curb & Sidewalk

$$\text{CurbSidewalk} := \frac{1}{6} \left(3.27 \frac{\text{kN}}{\text{m}} + 16.4 \frac{\text{kN}}{\text{m}} \right) = 3.278 \frac{\text{kN}}{\text{m}}$$

Calculation of the dead load effect on a stringer - DW

Pavement

$$\text{WearingSurface} := \frac{1}{6} 9\text{m} \cdot 40\text{mm} \cdot 140 \frac{\text{lb}}{\text{ft}^3} = 1.32 \frac{\text{kN}}{\text{m}}$$

Calculation of the dead load moment for an interior beam

The areas by which the loads are multiplied were calculated by an influence line spreadsheet.

$$\text{DC}_{\text{int}} := (\text{Deck} + \text{Beam}_{\text{int}} + \text{Diaphragms} + \text{CurbSidewalk}) \cdot (38.787\text{m}^2) = 630.709\text{kN}\cdot\text{m}$$

$$\text{DC}_{\text{ext}} := (\text{Deck} + \text{Beam}_{\text{ext}} + \text{Diaphragms} + \text{CurbSidewalk}) \cdot (38.787\text{m}^2) = 673.748\text{kN}\cdot\text{m}$$

$$\text{DW} := \text{WearingSurface} \cdot 38.787\text{m}^2 = 51.181\text{kN}\cdot\text{m}$$

Calculation of the LRFD distribution factor for an interior beam

$$S_{\text{int}} := 2.250\text{m} = 7.382\text{ft}$$

$$n := \frac{E_b}{E_d} = 7.715$$

$$L_{\text{int}} := 23.5\text{m} = 77.1\text{ft}$$

$$e_g := \frac{d_{\text{int}}}{2} + \frac{\text{Deck}_{\text{depth}}}{2} + \text{Haunch}_{\text{depth}} = 23.70\text{ft}$$

$$K_{g\text{int}} := n \cdot (I_{x,\text{int}} + A_{\text{int}} \cdot e_g^2) = 2.788 \times 10^5 \cdot \text{in}^4$$

$$m_{g\text{int}1\text{LRFD}} := .06 + \left(\frac{7.382}{14} \right)^4 \left(\frac{7.382}{77.1} \right)^3 \left(\frac{203500}{12.077 \cdot 10^3} \right)^1 = 0.412$$

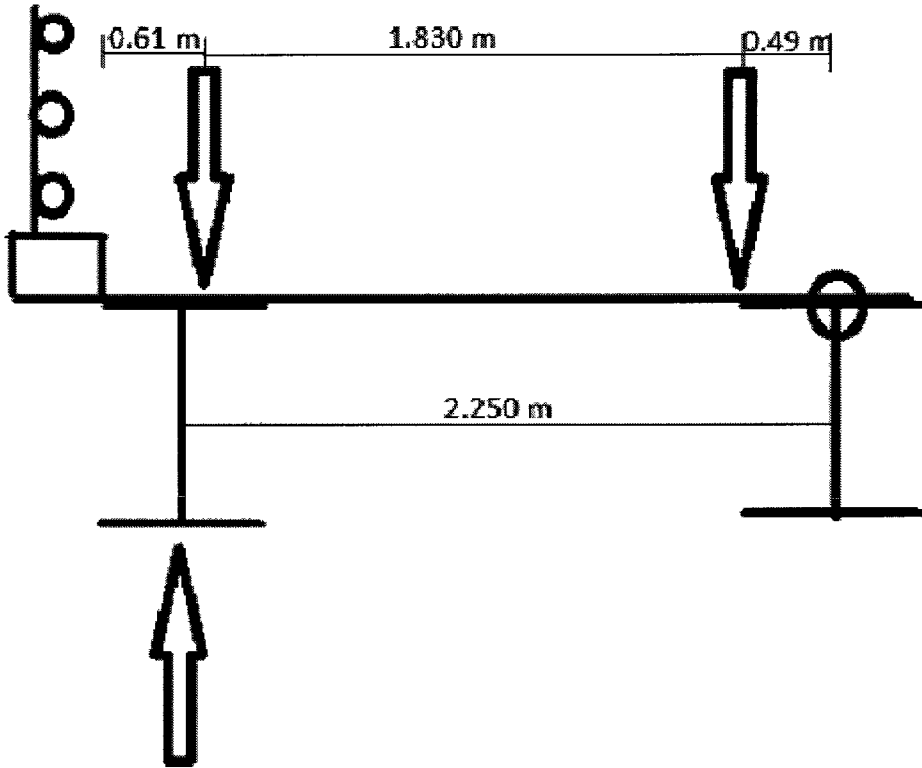
4.6.2.2
LRFD Bridge Design
Specifications

$$m_{g\text{int}2\text{LRFD}} := .075 + \left(\frac{7.382}{9.5} \right)^6 \left(\frac{7.382}{77.1} \right)^2 \left(\frac{203500}{12.077 \cdot 10^3} \right)^1 = 0.569$$

$$m_{g\text{intLRFD}} := \max(m_{g\text{int}1\text{LRFD}}, m_{g\text{int}2\text{LRFD}}) = 0.569$$

Calculation of the LRFD distribution factor for an exterior beam

Use the lever rule for one design lane loaded



$$m_{\text{ext1LRFD}} := .514$$

$$d_e := .779 \quad \text{ft}$$

$$e_{\text{ext}} := .77 + \frac{d_e}{9.1}$$

$$m_{\text{ext2LRFD}} := e_{\text{ext}} \cdot m_{\text{intLRFD}} = 0.487$$

$$m_{\text{extLRFD}} := \max(m_{\text{ext1LRFD}}, m_{\text{ext2LRFD}}) = 0.514$$

Calculation of the ASD & LFR distribution factor

$$mg_{intASD} := \frac{7.38}{5.5} = 1.342 \quad mg_{extASD} := \frac{7.38}{5.5} = 1.342$$

$$mg_{intLFD} := \frac{7.38}{5.5} = 1.342 \quad mg_{extLFD} := \frac{7.38}{5.5} = 1.342$$

$$mg_{DISPL} := .296$$

Live Load Calculations

$$laneload := 640 \frac{\text{lb}}{\text{ft}} = 9.34 \frac{\text{kN}}{\text{m}}$$

$$frontaxle := 8000 \text{ lb} = 35.586 \text{ kN}$$

$$rearaxle := 32000 \text{ lb} = 142.343 \text{ kN}$$

$$LL := 40.94 \text{ m}^2 (laneload) + 1.33 [2.4 \text{ m} (rearaxle) + 1.84 \text{ m} (rearaxle) + 2.03 \text{ m} (frontaxle)] = 1.283 \times 10^3 \cdot \text{kN} \cdot \text{m}$$

$$LL_{ASD} := [2.4 \text{ m} (rearaxle) + 1.84 \text{ m} (rearaxle) + 2.03 \text{ m} (frontaxle)] = 677.197 \text{ kN} \cdot \text{m}$$

$$LL_{LFR} := LL_{ASD}$$

LRFR Inventory Rating Factor (Based on AASHTO 2010)

$$\gamma_{DC} := 1.25 \quad \gamma_{DW} := 1.5 \quad \gamma_{LL} := 1.75$$

$$RF_{int} := \frac{M_{nint} - \gamma_{DC} \cdot DC_{int} - \gamma_{DW} \cdot DW}{(\gamma_{LL}) \cdot (LL \cdot mg_{intLRFD})} = 2.082 \quad RF_{ext} := \frac{M_{next} - \gamma_{DC} \cdot DC_{ext} - \gamma_{DW} \cdot DW}{(\gamma_{LL}) \cdot (LL \cdot mg_{extLRFD})} = 3.785$$

LRFR Operating Rating Factor (Based on AASHTO 2010)

$$\gamma_{DC} := 1.25 \quad \gamma_{DW} := 1.5 \quad \gamma_{LL} := 1.35$$

$$RF_{int} := \frac{M_{nint} - \gamma_{DC} \cdot DC_{int} - \gamma_{DW} \cdot DW}{(\gamma_{LL}) \cdot (LL \cdot mg_{intLRFD})} = 2.698 \quad RF_{ext} := \frac{M_{next} - \gamma_{DC} \cdot DC_{ext} - \gamma_{DW} \cdot DW}{(\gamma_{LL}) \cdot (LL \cdot mg_{extLRFD})} = 4.907$$

LFR Inventory Rating Factor (Based on AASHTO 2002)

$$A_1 := 1.30 \quad A_2 := 2.17$$

$$I := \frac{50}{77.08 + 125} = 0.247$$

$$RF_{int} := \frac{M_{nint} - A_1 \cdot (DC_{int} + DW)}{A_2 \cdot LL_{LFR} \cdot mg_{intLFD} (1 + I)} = 1.073 \quad RF_{ext} := \frac{M_{next} - A_1 \cdot (DC_{ext} + DW)}{A_2 \cdot LL_{LFR} \cdot mg_{extLFD} (1 + I)} = 1.767$$

LFR Operating Rating Factor (Based on AASHTO 2002)

$$A_{1w} := 1.30$$

$$A_{2w} := 1.3$$

$$I_w := \frac{50}{77.08 + 125} = 0.247$$

$$RF_{int} := \frac{M_{nint} - A_1 \cdot (DC_{int} + DW)}{A_2 \cdot LL_{LFR} \cdot mg_{intLFD} \cdot (1 + I)} = 1.791$$

$$RF_{ext} := \frac{M_{next} - A_1 \cdot (DC_{ext} + DW)}{A_2 \cdot LL_{LFR} \cdot mg_{extLFD} \cdot (1 + I)} = 2.949$$

ASR Exterior Beams

$$f_T := .55 \cdot \text{YieldStress}_{beam} = 1.896 \times 10^8 \text{ Pa}$$

$$I_w := \frac{50}{77.08 + 125} = 0.247$$

$$f_O := .75 \cdot \text{YieldStress}_{beam} = 2.586 \times 10^8 \text{ Pa}$$

$$S_{bL} := 15935619 \text{ mm}^3$$

$$S_{bDL} := 11706479 \text{ mm}^3$$

$$S_{bSDL} := 14262219 \text{ mm}^3$$

$$M_{RI} := f_T \cdot S_{bDL} = 2.22 \times 10^3 \cdot \text{kN} \cdot \text{m}$$

$$M_{RO} := f_O \cdot S_{bDL} = 3.027 \times 10^3 \cdot \text{kN} \cdot \text{m}$$

$$M_{DL} := 30.244 \text{ m}^2 (\text{Beam}_{ext} + \text{Diaphragms} + \text{Deck}) = 426.203 \text{ kN} \cdot \text{m}$$

$$M_{SDL} := 30.244 \text{ m}^2 (\text{WearingSurface} + \text{CurbSidewalk}) = 139.058 \text{ kN} \cdot \text{m}$$

$$M_{LL} := mg_{extASD} [LL_{ASD} + (LL_{ASD} \cdot I)] = 1.134 \times 10^3 \cdot \text{kN} \cdot \text{m}$$

ASR Inventory Rating Factor

$$RF_{ext} := \frac{M_{RI} - M_{DL} - M_{SDL}}{M_{LL}} = 1.46$$

ASR Operating Rating Factor

$$RF_{ext} := \frac{M_{RO} - M_{DL} - M_{SDL}}{M_{LL}} = 2.172$$

ASR Interior Beams

$$f_t := .55 \cdot \text{YieldStress}_{\text{beam}} = 1.896 \times 10^8 \text{ Pa}$$

$$I := \frac{50}{77.08 + 125} = 0.247$$

$$S_{bDL} := \frac{13254600 \text{ nm}^3}{.75 \cdot \text{YieldStress}_{\text{beam}}} = 2.586 \times 10^8 \text{ Pa}$$

$$S_{bDL} := 8735870 \text{ nm}^3$$

$$S_{bSDL} := 11956500 \text{ nm}^3$$

$$M_{RI} := f_t \cdot S_{bDL} = 1.656 \times 10^3 \cdot \text{kN} \cdot \text{m} \quad M_{RO} := f_o \cdot S_{bDL} = 2.259 \times 10^3 \cdot \text{kN} \cdot \text{m}$$

$$M_{DL} := 30.244 \text{ m}^2 (\text{Beam}_{\text{int}} + \text{Diaphragms} + \text{Deck}) = 392.643 \text{ kN} \cdot \text{m}$$

$$M_{SDL} := 30.244 \text{ m}^2 (\text{WearingSurface} + \text{CurbSidewalk}) = 139.058 \text{ kN} \cdot \text{m}$$

$$M_{LL} := mg_{\text{intASD}} [LL_{\text{ASD}} + (LL_{\text{ASD}} \cdot 1)] = 1.134 \times 10^3 \cdot \text{kN} \cdot \text{m}$$

ASR Inventory Rating Factor

$$RF_{\text{int}} := \frac{M_{RI} - M_{DL} - M_{SDL}}{M_{LL}} = 0.992$$

ASR Operating Rating Factor

$$RF_{\text{ext}} := \frac{M_{RO} - M_{DL} - M_{SDL}}{M_{LL}} = 1.524$$

LRFR based on moments from structural model

$$\text{Capacity}_{\text{int}} := M_{\text{int}} = 3.525 \times 10^3 \cdot \text{kN} \cdot \text{m}$$

$$\text{Capacity}_{\text{ext}} := M_{\text{next}} = 5.288 \times 10^3 \cdot \text{kN} \cdot \text{m} \quad \text{Max negative moments taken from model output}$$

$$DL_{\text{ext}} := \max(709 \text{ kN} \cdot \text{m}, 1379 \text{ kN} \cdot \text{m}) = 1.379 \times 10^3 \cdot \text{kN} \cdot \text{m}$$

$$DL_{\text{int}} := \max(650 \text{ kN} \cdot \text{m}, 715 \text{ kN} \cdot \text{m}, 803 \text{ kN} \cdot \text{m}, 952 \text{ kN} \cdot \text{m}) = 952 \text{ kN} \cdot \text{m}$$

$$LL_{\text{ext}} := \max(1319 \text{ kN} \cdot \text{m}, 1312 \text{ kN} \cdot \text{m}) = 1.319 \times 10^3 \cdot \text{kN} \cdot \text{m}$$

$$LL_{\text{int}} := \max(1196 \text{ kN} \cdot \text{m}, 1245 \text{ kN} \cdot \text{m}, 1245 \text{ kN} \cdot \text{m}, 1154 \text{ kN} \cdot \text{m}) = 1.245 \times 10^3 \cdot \text{kN} \cdot \text{m}$$

$$\underline{RF}_{int} := \frac{\text{Capacity}_{int} - DL_{int}}{LL_{int}} = 2.067$$

$$\underline{RF}_{ext} := \frac{\text{Capacity}_{ext} - DL_{ext}}{LL_{ext}} = 2.963$$

LRFR based on DF from displacements

Inventory

$$\underline{\gamma}_{DC} := 1.25$$

$$\underline{\gamma}_{DW} := 1.5$$

$$\underline{\gamma}_{LL} := 1.75$$

$$\underline{RF}_{int} := \frac{M_{nint} - \gamma_{DC} \cdot DC_{int} - \gamma_{DW} \cdot DW}{(\gamma_{LL}) \cdot (LL \cdot mg_{DISPL})} = 4.002$$

$$\underline{RF}_{ext} := \frac{M_{next} - \gamma_{DC} \cdot DC_{ext} - \gamma_{DW} \cdot DW}{(\gamma_{LL}) \cdot (LL \cdot mg_{DISPL})} = 6.573$$

Operating

$$\underline{\gamma}_{DC} := 1.25$$

$$\underline{\gamma}_{DW} := 1.5$$

$$\underline{\gamma}_{LL} := 1.35$$

$$\underline{RF}_{int} := \frac{M_{nint} - \gamma_{DC} \cdot DC_{int} - \gamma_{DW} \cdot DW}{(\gamma_{LL}) \cdot (LL \cdot mg_{DISPL})} = 5.188$$

$$\underline{RF}_{ext} := \frac{M_{next} - \gamma_{DC} \cdot DC_{ext} - \gamma_{DW} \cdot DW}{(\gamma_{LL}) \cdot (LL \cdot mg_{DISPL})} = 8.521$$

C.2 Rating Factors Due to Positive Moment

Calculation of the bridge capacity, dead load, live load, and rating factor

Interior Beam

W920x238	also known as	W36X160
$A_{int} := 30300\text{mm}^2$		$t_{f,int} := 25.9\text{mm}$
$d_{int} := .914\text{m}$		$I_{x,int} := 9760\text{in}^4$
$t_{w,int} := 16.5\text{mm}$		$\text{YieldStress}_{beam} := 50 \frac{\text{kip}}{\text{in}^2} = 3.447 \times 10^8 \text{ Pa}$
$b_{f,int} := 305\text{mm}$		$E_b := 29000\text{ksi}$
$\text{Length} := 47\text{m}$		

Exterior Beam

W920x345	also known as	W36X232
$A_{ext} := 43900\text{mm}^2$		$t_{f,ext} := .039878\text{m}$
$d_{ext} := .942\text{m}$		$I_{x,ext} := 15000\text{in}^4$
$t_{w,ext} := .022098\text{m}$		
$b_{f,ext} := .30734\text{m}$		

Concrete Deck

$\text{Deck}_{depth} := .2\text{m}$	$E_d := 3759\text{ksi}$
$f_c := 35\text{MPa} = 5.076\text{ksi}$	
$\text{Span}_{int} := 2.250\text{m} = 88.583\text{in}$	
$\text{Span}_{ext} := 1.704\text{m}$	

Haunch

Assume that haunch does not contribute to capacity.

$\text{Haunch}_{depth} := .045\text{m}$

Find the location of the neutral axis on the interior section

$$TFlange_{depth} := -1.560 \text{ lin} = -0.04 \text{ m}$$

$$Depth_{compression} := Deck_{depth} + Haunch_{depth} + TFlange_{depth} = 0.205 \text{ m}$$

$$a := .80 \cdot Depth_{compression} = 0.164 \text{ m}$$

$$Deck_{compression} := .80 \cdot f_c \cdot a \cdot Span_{int} = 1.035 \times 10^7 \text{ N}$$

$$TFlange_{compression} := \begin{cases} 0 & \text{if } TFlange_{depth} \leq 0 \\ (TFlange_{depth} \cdot b_{f,int} \cdot YieldStress_{beam}) & \text{if } TFlange_{depth} > 0 \end{cases}$$

$$TFlange_{Tension} := \begin{cases} 0 & \text{if } TFlange_{depth} \geq t_{f,int} \\ (t_{f,int} \cdot b_{f,int} \cdot YieldStress_{beam}) & \text{if } TFlange_{depth} \leq 0 \\ [(t_{f,int} - TFlange_{depth}) \cdot b_{f,int} \cdot YieldStress_{beam}] & \text{otherwise} \end{cases}$$

$$Web_{Tension} := (d_{int} - 2 \cdot t_{f,int}) \cdot t_{w,int} \cdot YieldStress_{beam} = 4.904 \times 10^6 \text{ N}$$

$$BFlange_{Tension} := t_{f,int} \cdot b_{f,int} \cdot YieldStress_{beam} = 2.723 \times 10^6 \text{ N}$$

$$Compression := Deck_{compression} + TFlange_{compression} = 1.035 \times 10^7 \text{ N}$$

$$Tension := TFlange_{Tension} + Web_{Tension} + BFlange_{Tension} = 1.035 \times 10^7 \text{ N}$$

$$Diff := Compression - Tension = -35.424 \text{ N}$$

$$PNA_{dist} := Depth_{compression} = 0.205 \text{ m}$$

$$C_c := \left(Depth_{compression} - \frac{Deck_{depth}}{2} \right) \cdot Deck_{compression} = 1.091 \times 10^6 \cdot \text{N} \cdot \text{m}$$

$$C_f := \frac{TFlange_{depth}}{2} \cdot TFlange_{compression} = 0 \cdot \text{N} \cdot \text{m}$$

$$T_{tf} := \frac{(t_{f,int} - TFlange_{depth})}{2} \cdot TFlange_{Tension} = 8.922 \times 10^4 \cdot \text{N} \cdot \text{m}$$

$$T_w := \left[\frac{(d_{int} - 2 \cdot t_{f,int})}{2} + (t_{f,int} - TFlange_{depth}) \right] \cdot Web_{Tension} = 2.436 \times 10^6 \cdot \text{N} \cdot \text{m}$$

$$T_{bf} := \left[\frac{t_{f,int}}{2} + (d_{int} - 2 \cdot t_{f,int}) + (t_{f,int} - TFlange_{depth}) \right] \cdot BFlange_{Tension} = 2.562 \times 10^6 \cdot \text{N} \cdot \text{m}$$

$$D_{\text{pint}} := \text{Depth}_{\text{compression}} = 0.205\text{m} \quad D_{\text{tint}} := \text{Deck}_{\text{depth}} + \text{Haunch}_{\text{depth}} + d_{\text{ext}} = 1.187\text{m}$$

$$\text{Capacity}_{\text{int}} := C_c + C_f + T_{\text{tf}} + T_w + T_{\text{bf}} = 6.177 \times 10^6 \cdot \text{N} \cdot \text{m}$$

Find the location of the neutral axis on the exterior section

$$\text{TFlange}_{\text{depth}} := .79266n = 0.02\text{m}$$

$$\text{Depth}_{\text{compression}} := \text{Deck}_{\text{depth}} + \text{Haunch}_{\text{depth}} + \text{TFlange}_{\text{depth}} = 0.265\text{m}$$

$$a := .85 \cdot \text{Depth}_{\text{compression}} = 0.225\text{m}$$

$$\text{Deck}_{\text{compression}} := .80 \cdot f_c \cdot a \cdot \text{Span}_{\text{ext}} = 1.075 \times 10^7 \text{N}$$

$$\text{TFlange}_{\text{compression}} := \begin{cases} 0 & \text{if } \text{TFlange}_{\text{depth}} \leq 0 \\ (\text{TFlange}_{\text{depth}} \cdot b_{\text{f,ext}} \cdot \text{YieldStress}_{\text{beam}}) & \text{if } \text{TFlange}_{\text{depth}} > 0 \end{cases}$$

$$\text{TFlange}_{\text{Tension}} := \begin{cases} 0 & \text{if } \text{TFlange}_{\text{depth}} \geq t_{\text{f,ext}} \\ (t_{\text{f,ext}} \cdot b_{\text{f,ext}} \cdot \text{YieldStress}_{\text{beam}}) & \text{if } \text{TFlange}_{\text{depth}} \leq 0 \\ [(t_{\text{f,ext}} - \text{TFlange}_{\text{depth}}) \cdot b_{\text{f,ext}} \cdot \text{YieldStress}_{\text{beam}}] & \text{otherwise} \end{cases}$$

$$\text{Web}_{\text{Tension}} := (d_{\text{ext}} - 2 \cdot t_{\text{f,ext}}) \cdot t_{\text{w,ext}} \cdot \text{YieldStress}_{\text{beam}} = 6.569 \times 10^6 \text{N}$$

$$\text{BFlange}_{\text{Tension}} := t_{\text{f,ext}} \cdot b_{\text{f,ext}} \cdot \text{YieldStress}_{\text{beam}} = 4.225 \times 10^6 \text{N}$$

$$\text{Compression} := \text{Deck}_{\text{compression}} + \text{TFlange}_{\text{compression}} = 1.289 \times 10^7 \text{N}$$

$$\text{Tension} := \text{TFlange}_{\text{Tension}} + \text{Web}_{\text{Tension}} + \text{BFlange}_{\text{Tension}} = 1.289 \times 10^7 \text{N}$$

$$\text{Diff} := \text{Compression} - \text{Tension} = 40.463\text{N}$$

$$\text{PNA}_{\text{dist}} := \text{Depth}_{\text{compression}} = 0.265\text{m}$$

$$C_{\text{w}} := \left(\text{Depth}_{\text{compression}} - \frac{\text{Deck}_{\text{depth}}}{2} \right) \cdot \text{Deck}_{\text{compression}} = 1.776 \times 10^6 \cdot \text{N} \cdot \text{m}$$

$$C_{\text{c}} := \frac{\text{TFlange}_{\text{depth}}}{2} \cdot \text{TFlange}_{\text{compression}} = 2.147 \times 10^4 \cdot \text{N} \cdot \text{m}$$

$$T_{\text{tf}} := \frac{(t_{\text{f,ext}} - \text{TFlange}_{\text{depth}})}{2} \cdot \text{TFlange}_{\text{Tension}} = 2.065 \times 10^4 \cdot \text{N} \cdot \text{m}$$

$$T_{\text{w}} := \left[\frac{(d_{\text{ext}} - 2 \cdot t_{\text{f,ext}})}{2} + (t_{\text{f,ext}} - \text{TFlange}_{\text{depth}}) \right] \cdot \text{Web}_{\text{Tension}} = 2.962 \times 10^6 \cdot \text{N} \cdot \text{m}$$

$$M_{ext} := \left[\frac{t_{f,ext}}{2} + (d_{ext} - 2 \cdot t_{f,ext}) + (t_{f,ext} - T_{Flange_depth}) \right] \cdot B_{Flange} \cdot Tension = 3.811 \times 10^6 \cdot N \cdot m$$

$$D_{pext} := Depth_{compression} = 0.265m \quad D_{text} := Deck_{depth} + Haunch_{depth} + d_{ext} = 1.187m$$

$$Capacity_{ext} := C_c + C_f + T_{tf} + T_w + T_{bf} = 8.59 \times 10^6 \cdot N \cdot m$$

Capacity Factors

$$\phi_c := 1.00 \quad \text{Condition Factor - 6A.4.2.3} \\ \text{AASHTO MBE}$$

$$\phi_s := 1.00 \quad \text{System Factor - 6A.4.2.4} \\ \text{AASHTO MBE}$$

$$\phi := 1.00 \quad \text{LRFD Resistance Factor - 6A.4.2.2-1} \\ \text{AASHTO MBE}$$

$$C_{int} := Capacity_{int} \cdot \phi_s \cdot \phi_c \cdot \phi = 6.177 \times 10^6 \cdot N \cdot m$$

$$C_{ext} := Capacity_{ext} \cdot \phi_s \cdot \phi_c \cdot \phi = 8.59 \times 10^3 \cdot kN \cdot m$$

$$M_{nint} := C_{int} \cdot \left[1.07 - .7 \left(\frac{D_{pint}}{D_{tint}} \right) \right] = 5.862 \times 10^3 \cdot kN \cdot m$$

$$M_{next} := C_{ext} \cdot \left[1.07 - .7 \left(\frac{D_{pext}}{D_{text}} \right) \right] = 7.848 \times 10^3 \cdot kN \cdot m$$

6.10.7.1.2
LRFD Bridge Design
Specifications

Calculation of the dead load effect on a stringer - DC

Deck

$$Deck := \frac{1}{6} \left(12.715m \cdot Deck_{depth} + Haunch_{depth} \cdot t_{f,int} \right) \cdot 150 \frac{lb_f}{ft^3} = 9.991 \frac{kN}{m}$$

Beams

$$Beam_{int} := 1.06 \left(A_{int} \cdot 490 \frac{lb_f}{ft^3} \right) = 2.472 \frac{kN}{m} \quad \text{1.06 was used to account for} \\ \text{misc. steel items}$$

$$Beam_{ext} := 1.06 \left(A_{ext} \cdot 490 \frac{lb_f}{ft^3} \right) = 3.582 \frac{kN}{m}$$

Diaphragms

$$Diaphragms := 1.06 \left(\frac{17.138kgf}{47m} \right) = 518.868 \frac{N}{m}$$

Curb & Sidewalk

$$CurbSidewalk := \frac{1}{6} \left(3.27 \frac{kN}{m} + 16.4 \frac{kN}{m} \right) = 3.278 \frac{kN}{m}$$

Calculation of the dead load effect on a stringer - DW

Pavement

$$\text{WearingSurface} := \frac{1}{6} \cdot 9\text{m} \cdot 40\text{mm} \cdot 140 \frac{\text{lb}}{\text{ft}^3} = 1.32 \frac{\text{kN}}{\text{m}}$$

Calculation of the dead load moment for an interior beam

The areas by which the loads are multiplied were calculated by an influence line spreadsheet.

$$\text{DC}_{\text{int}} := (\text{Deck} + \text{Beam}_{\text{int}} + \text{Diaphragms} + \text{CurbSidewalk}) \cdot (30.244\text{m}^2) = 491.792\text{kN}\cdot\text{m}$$

$$\text{DC}_{\text{ext}} := (\text{Deck} + \text{Beam}_{\text{ext}} + \text{Diaphragms} + \text{CurbSidewalk}) \cdot (30.244\text{m}^2) = 525.352\text{kN}\cdot\text{m}$$

$$\text{DW} := \text{WearingSurface} \cdot 30.244\text{m}^2 = 39.908\text{kN}\cdot\text{m}$$

Calculation of the LRFD distribution factor for an interior beam

4.6.2.2.2

LRFD Bridge Design

Specifications

$$S_{\text{int}} := 2.250\text{m} = 7.382\text{ft} \quad n := \frac{E_b}{E_d} = 7.715$$

$$L_{\text{int}} := 23.5\text{m} = 77.1\text{ft} \quad e_g := \frac{d_{\text{int}}}{2} + \frac{\text{Deck}_{\text{depth}}}{2} + \text{Haunch}_{\text{depth}} = 23.70\text{ft}$$

$$K_{g_{\text{int}}} := n \cdot (I_{x,\text{int}} + A_{\text{int}} \cdot e_g^2) = 2.788 \times 10^5 \cdot \text{in}^4$$

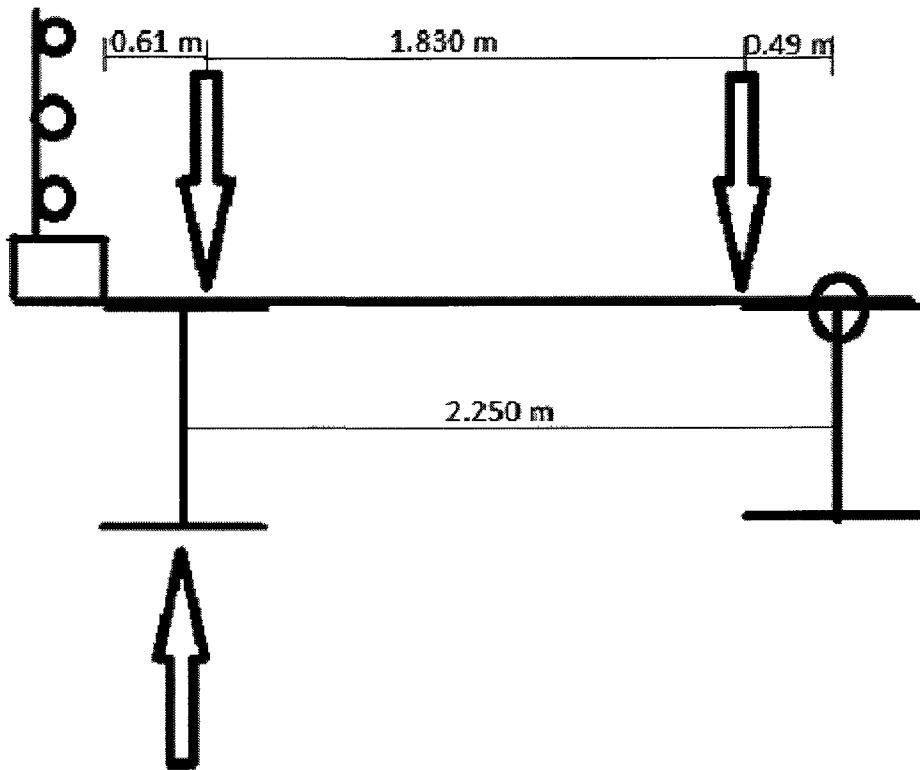
$$mg_{\text{int1LRFD}} := .06 + \left(\frac{7.382}{14}\right)^4 \left(\frac{7.382}{77.1}\right)^3 \left(\frac{203500}{12.077.1 \cdot 8^3}\right)^1 = 0.412$$

$$mg_{\text{int2LRFD}} := .075 + \left(\frac{7.382}{9.5}\right)^6 \left(\frac{7.382}{77.1}\right)^2 \left(\frac{203500}{12.077.1 \cdot 8^3}\right)^1 = 0.569$$

$$mg_{\text{intLRFD}} := \max(mg_{\text{int1LRFD}}, mg_{\text{int2LRFD}}) = 0.569$$

Calculation of the LRFD distribution factor for an exterior beam

Use the lever rule for one design lane loaded



$$m_{g_{ext1LRFD}} := .514$$

$$d_e := .779 \text{ ft}$$

$$e_{ext} := .77 + \frac{d_e}{9.1}$$

$$m_{g_{ext2LRFD}} := e_{ext} \cdot m_{g_{intLRFD}} = 0.487$$

$$m_{g_{extLRFD}} := \max(m_{g_{ext1LRFD}}, m_{g_{ext2LRFD}}) = 0.514$$

Calculation of the ASD & LFR distribution factor

$$mg_{intASD} := \frac{7.38}{5.5} = 1.342 \quad mg_{extASD} := \frac{7.38}{5.5} = 1.342$$

$$mg_{intLFD} := \frac{7.38}{5.5} = 1.342 \quad mg_{extLFD} := \frac{7.38}{5.5} = 1.342$$

$$mg_{DISPL} := .296$$

Live Load Calculations

$$laneload := 640 \frac{lbf}{ft} = 9.34 \frac{kN}{m}$$

$$frontaxle := 8000lbf = 35.586kN$$

$$rearaxle := 32000lbf = 142.343kN$$

$$LL := 34.554m^2(laneload) + 1.33[3.67m(rearaxle) + 1.84m(rearaxle) + 1.84m(frontaxle)] = 1.453 \times 10^3 \cdot kN \cdot m$$

$$LL_{ASD} := [3.67m(rearaxle) + 1.84m(rearaxle) + 1.84m(frontaxle)] = 849.788kN \cdot m$$

$$LL_{LFR} := LL_{ASD}$$

LRFR Inventory Rating Factor (Based on AASHTO 2010)

$$\gamma_{DC} := 1.25$$

$$\gamma_{DW} := 1.5$$

$$\gamma_{LL} := 1.75$$

$$RF_{int} := \frac{M_{nint} - \gamma_{DC} \cdot DC_{int} - \gamma_{DW} \cdot DW}{(\gamma_{LL}) \cdot (LL \cdot mg_{intLRFD})} = 3.585 \quad RF_{ext} := \frac{M_{next} - \gamma_{DC} \cdot DC_{ext} - \gamma_{DW} \cdot DW}{(\gamma_{LL}) \cdot (LL \cdot mg_{extLRFD})} = 5.457$$

LRFR Operating Rating Factor (Based on AASHTO 2010)

$$\gamma_{DC} := 1.25$$

$$\gamma_{DW} := 1.5$$

$$\gamma_{LL} := 1.35$$

$$RF_{int} := \frac{M_{nint} - \gamma_{DC} \cdot DC_{int} - \gamma_{DW} \cdot DW}{(\gamma_{LL}) \cdot (LL \cdot mg_{intLRFD})} = 4.647 \quad RF_{ext} := \frac{M_{next} - \gamma_{DC} \cdot DC_{ext} - \gamma_{DW} \cdot DW}{(\gamma_{LL}) \cdot (LL \cdot mg_{extLRFD})} = 7.074$$

LFR Inventory Rating Factor (Based on AASHTO 2002)

$$A_1 := 1.30 \quad A_2 := 2.17 \quad I := \frac{50}{77.08 + 125} = 0.247$$

$$RF_{int} := \frac{M_{nint} - A_1 \cdot (DC_{int} + DW)}{A_2 \cdot LL_{LFR} \cdot mg_{intLFD} \cdot (1 + I)} = 1.675 \quad RF_{ext} := \frac{M_{next} - A_1 \cdot (DC_{ext} + DW)}{A_2 \cdot LL_{LFR} \cdot mg_{extLFD} \cdot (1 + I)} = 2.305$$

LFR Operating Rating Factor (Based on AASHTO 2002)

$$A_w := 1.30 \quad A_{ow} := 1.3 \quad I_w := \frac{50}{77.08 + 125} = 0.247$$

$$RF_{int} := \frac{M_{nint} - A_1 \cdot (DC_{int} + DW)}{A_2 \cdot LL_{LFR} \cdot mg_{intLFD} \cdot (1 + I)} = 2.796 \quad RF_{ext} := \frac{M_{next} - A_1 \cdot (DC_{ext} + DW)}{A_2 \cdot LL_{LFR} \cdot mg_{extLFD} \cdot (1 + I)} = 3.847$$

ASR Exterior Beams

$$f_I := .55 \cdot \text{YieldStress}_{beam} = 1.896 \times 10^8 \text{ Pa} \quad I_w := \frac{50}{77.08 + 125} = 0.247$$

$$f_O := .75 \cdot \text{YieldStress}_{beam} = 2.586 \times 10^8 \text{ Pa}$$

$$S_{bL} := 15935619 \text{ mm}^3$$

$$S_{bDL} := 11706479 \text{ mm}^3$$

$$S_{bSDL} := 14262219 \text{ mm}^3$$

$$M_{RI} := f_I \cdot S_{bL} = 3.021 \times 10^3 \cdot \text{kN} \cdot \text{m} \quad M_{RO} := f_O \cdot S_{bL} = 4.12 \times 10^3 \cdot \text{kN} \cdot \text{m}$$

$$M_{DL} := 30.244 \text{ m}^2 (\text{Beam}_{ext} + \text{Diaphragms} + \text{Deck}) = 426.203 \text{ kN} \cdot \text{m}$$

$$M_{SDL} := 30.244 \text{ m}^2 (\text{WearingSurface} + \text{CurbSidewalk}) = 139.058 \text{ kN} \cdot \text{m}$$

$$M_{LL} := mg_{extASD} [LL_{ASD} + (LL_{ASD} \cdot I)] = 1.422 \times 10^3 \cdot \text{kN} \cdot \text{m}$$

ASR Inventory Rating Factor

$$RF_{\text{ext}} := \frac{M_{RI} - M_{DL} \cdot \frac{S_{bL}}{S_{bDL}} - M_{SDL} \cdot \frac{S_{bL}}{S_{bSDL}}}{M_{LL}} = 1.607$$

ASR Operating Rating Factor

$$RF_{\text{ext}} := \frac{M_{RO} - M_{DL} \cdot \frac{S_{bL}}{S_{bDL}} - M_{SDL} \cdot \frac{S_{bL}}{S_{bSDL}}}{M_{LL}} = 2.38$$

ASR Interior Beams

$$f_t := .55 \cdot \text{YieldStress}_{\text{beam}} = 1.896 \times 10^8 \text{ Pa} \quad \lambda := \frac{50}{77.08 + 125} = 0.247$$

$$f_c := .75 \cdot \text{YieldStress}_{\text{beam}} = 2.586 \times 10^8 \text{ Pa}$$

$$S_{bL} := 13254600 \text{ nm}^3$$

$$S_{bDL} := 8735870 \text{ nm}^3$$

$$S_{bSDL} := 11956500 \text{ nm}^3$$

$$M_{RI} := f_t \cdot S_{bL} = 2.513 \times 10^3 \cdot \text{kN} \cdot \text{m} \quad M_{RO} := f_c \cdot S_{bL} = 3.427 \times 10^3 \cdot \text{kN} \cdot \text{m}$$

$$M_{DL} := 30.244 \text{ m}^2 (\text{Beam}_{\text{int}} + \text{Diaphragms} + \text{Deck}) = 392.643 \text{ kN} \cdot \text{m}$$

$$M_{SDL} := 30.244 \text{ m}^2 (\text{WearingSurface} + \text{CurbSidewalk}) = 139.058 \text{ kN} \cdot \text{m}$$

$$M_{LL} := m_{\text{intASD}} \cdot [LL_{\text{ASD}} + (LL_{\text{ASD}} \cdot \lambda)] = 1.422 \times 10^3 \cdot \text{kN} \cdot \text{m}$$

ASR Inventory Rating Factor

$$RF_{\text{int}} := \frac{M_{RI} - M_{DL} \cdot \frac{S_{bL}}{S_{bDL}} - M_{SDL} \cdot \frac{S_{bL}}{S_{bSDL}}}{M_{LL}} = 1.24$$

ASR Operating Rating Factor

$$RF_{\text{int}} := \frac{M_{RO} - M_{DL} \cdot \frac{S_{bL}}{S_{bDL}} - M_{SDL} \cdot \frac{S_{bL}}{S_{bSDL}}}{M_{LL}} = 1.882$$

LRFR based on moments from structural model

$$\text{Capacity}_{\text{int}} := M_{\text{nint}} = 5.862 \times 10^3 \cdot \text{kN}\cdot\text{m}$$

$$\text{Capacity}_{\text{ext}} := M_{\text{next}} = 7.848 \times 10^3 \cdot \text{kN}\cdot\text{m}$$

$$\text{DL}_{\text{ext}} := \max(568 \text{ kN}\cdot\text{m}, 1108 \text{ kN}\cdot\text{m}) = 1.108 \times 10^3 \cdot \text{kN}\cdot\text{m}$$

$$\text{DL}_{\text{int}} := \max(517 \text{ kN}\cdot\text{m}, 599 \text{ kN}\cdot\text{m}, 682 \text{ kN}\cdot\text{m}, 771 \text{ kN}\cdot\text{m}) = 771 \cdot \text{kN}\cdot\text{m}$$

$$\text{LL}_{\text{ext}} := \max(1445 \text{ kN}\cdot\text{m}, 1452 \text{ kN}\cdot\text{m}) = 1.452 \times 10^3 \cdot \text{kN}\cdot\text{m}$$

$$\text{LL}_{\text{int}} := \max(1238 \text{ kN}\cdot\text{m}, 1289 \text{ kN}\cdot\text{m}, 1306 \text{ kN}\cdot\text{m}, 1211 \text{ kN}\cdot\text{m}) = 1.306 \times 10^3 \cdot \text{kN}\cdot\text{m}$$

$$\text{RF}_{\text{int}} := \frac{\text{Capacity}_{\text{int}} - \text{DL}_{\text{int}}}{\text{LL}_{\text{int}}} = 3.898$$

$$\text{RF}_{\text{ext}} := \frac{\text{Capacity}_{\text{ext}} - \text{DL}_{\text{ext}}}{\text{LL}_{\text{ext}}} = 4.642$$

LRFR based on DF from displacements

Inventory

$$\gamma_{\text{DC}} := 1.25$$

$$\gamma_{\text{DW}} := 1.5$$

$$\gamma_{\text{LL}} := 1.75$$

$$\text{RF}_{\text{int}} := \frac{M_{\text{nint}} - \gamma_{\text{DC}} \cdot \text{DC}_{\text{int}} - \gamma_{\text{DW}} \cdot \text{DW}}{(\gamma_{\text{LL}}) \cdot (\text{LLmg}_{\text{DISPL}})} = 6.892$$

$$\text{RF}_{\text{ext}} := \frac{M_{\text{next}} - \gamma_{\text{DC}} \cdot \text{DC}_{\text{ext}} - \gamma_{\text{DW}} \cdot \text{DW}}{(\gamma_{\text{LL}}) \cdot (\text{LLmg}_{\text{DISPL}})} = 9.476$$

Operating

$$\gamma_{\text{DC}} := 1.25$$

$$\gamma_{\text{DW}} := 1.5$$

$$\gamma_{\text{LL}} := 1.35$$

$$\text{RF}_{\text{int}} := \frac{M_{\text{nint}} - \gamma_{\text{DC}} \cdot \text{DC}_{\text{int}} - \gamma_{\text{DW}} \cdot \text{DW}}{(\gamma_{\text{LL}}) \cdot (\text{LLmg}_{\text{DISPL}})} = 8.934$$

$$\text{RF}_{\text{ext}} := \frac{M_{\text{next}} - \gamma_{\text{DC}} \cdot \text{DC}_{\text{ext}} - \gamma_{\text{DW}} \cdot \text{DW}}{(\gamma_{\text{LL}}) \cdot (\text{LLmg}_{\text{DISPL}})} = 12.283$$